

CONTROLS AND OCCURRENCE OF INTERFLOW OVER A RESTRICTIVE ARGILLIC
HORIZON IN A LOW GRADIENT HILLSLOPE

by

JAMES L. GRECO III

(Under the Direction of C. Rhett Jackson)

ABSTRACT

Interflow (throughflow or lateral flow), is shallow lateral subsurface flow that moves over a horizon that restricts percolation. Interflow is important for a number of reasons. First, rapid saturated interflow through macropores can travel to streams and alluvial aquifers with high celerity. Also, experimental studies have shown that interflow can be an important source of baseflow and stormflow. Because interflow travels through a biologically active region of soil with roots and relatively high OM content, the final outcome is the potential contamination of surface water bodies from subsurface water. Many of the soils in the southeastern US are characterized by an argillic, or clay horizon, that largely parallels the soil surface at depths ranging from a few centimeters to hundreds of centimeters. The degree to which these argillic horizons alter subsurface movement of infiltrated water is not well known. This research investigates how often and under what conditions a relatively deep (20-150⁺cm) argillic horizon on low slope (2-12%) hillsides causes interflow to occur. Research was conducted at the Savannah River Site, Aiken, South Carolina, on a small (38 ha) zero-order watershed. In the first phase of this research, a high resolution topographic map of the horizon was developed. This map was used to instrument designated “low” spots with 65 max-rise piezometers in order to

determine the controls these low spots impart on subsurface flow. In situ hydraulic conductivities of the argillic layer and the surface horizons were measured using an Amoozegar meter, soil cores were taken to develop moisture release curves and estimate bulk density. Along with soil topographic measurements, 13 data-logging piezometers were installed to measure the piezometric head above, in, and below the argillic horizon. The stream that drains the catchment was instrumented with a 2-foot (61cm) H-flume with a data-logged pressure transducer. Climate data including precipitation, barometric pressure, and temperature, was continuously collected in an open area approximately ¼ mile (300m) from the study site. Combining the shallow surface and subsurface piezometric heads with stream flow rates, it was possible to determine if and when the horizon could contribute to streamflow. Results from the study indicate a thin transient water table occurred at some locations across the hillslope for a few storm events. This water table is thought to be attributed to the water restrictive argillic horizon. Relatively warm weather and dry conditions that characterized the monitoring period likely limited observations of saturated conditions above the argillic horizon.

INDEX WORDS: Hillslope, Interflow, Zero-order hillslope, Argillic

CONTROLS AND OCCURRENCE OF INTERFLOW OVER A RESTRICTIVE ARGILLIC
HORIZON IN A LOW GRADIENT HILLSLOPE

by

CONTROLS AND OCCURRENCE OF INTERFLOW OVER A RESTRICTIVE ARGILLIC
HORIZON IN A LOW GRADIENT HILLSLOPE

by

JAMES L. GRECO III

BSA, The University of Georgia, 2004

A Thesis Submitted to the Graduate Faculty of The University of Georgia in Partial Fulfillment
of the Requirements for the Degree

MASTER OF SCIENCE

ATHENS, GEORGIA

2008

© 2008

James L. Greco III

All Rights Reserved

CONTROLS AND OCCURRENCE OF INTERFLOW OVER A RESTRICTIVE ARGILLIC
HORIZON IN A LOW GRADIENT HILLSLOPE

by

JAMES L. GRECO III

Major Professor: C. Rhett Jackson

Committee: Todd C. Rasmussen
Larry T. West

Electronic Version Approved:

Maureen Grasso
Dean of the Graduate School
The University of Georgia
May 2008

DEDICATION

I would like to dedicate my work to my ever-supportive family and friends. Without their support and prayers I would have never made it through. To my father, thank you for always pushing me to succeed in my academic career, reassuring me that an education is something no one can take away from me and whenever I got down for always asking me; “James, are we having fun yet?”. To my mother, thank you for all your support both mentally and spiritually. To my sister, brother-in law and nephew, thank you for listening to me and always welcoming me back when I would come home for visits. To the rest of my friends and family who are too numerous to mention here, thank you for all the support you provided over the years. I cannot forget my Brittany Spaniel pup, Johnny Cash, who always greeted me with licks and tail wagging no matter what kind of day it had been. It’s been a long road. Finally, I would like to thank God, for guiding me through this entire process.

ACKNOWLEDGEMENTS

I would like to thank each and every person who helped me with this project along the way. First, I would like to thank Rhett Jackson for accepting me as his student, it has been an exciting and knowledge filled path. I would like to thank Todd Rasmussen for being my initial advisor and encouraging me to stick with hydrology and guiding me towards this project. Larry West, for being the soil wizard he is, and answering all my crazy questions. John Dowd, for his unrelenting commitment to excellence and ethics in data acquisition and processing, oh and for the time and headaches he devoted to creating “Slope Commander”.

For all my friends who helped me with field, lab, and computer work (Noah Fraser, Chris Holliday, Jaime Paul, Mike Crooks, Ken Bradshaw, Kelli Coleman, Scott Terrell, Rajith Mukundan, Tony Greco, and everyone else I may have forgotten to mention). Also, I could not have wrapped this project up without the help of my ever faithful and always prepared technician and friend Thomas Middlebrooks ‘Brooks’ Camp. Thank you all for your help.

Finally, I would like to thank the SRS and USFS for providing the grant money for this project and the financing of my master’s program at UGA.

TABLE OF CONTENTS

	Page
ACKNOWLEDGEMENTS	v
LIST OF TABLES	viii
LIST OF FIGURES	ix
CHAPTER	
1 Introduction.....	1
1.1 Problem Statement	1
1.2 Background	2
1.3 Research Questions, Related Hypotheses, and Approaches.....	4
1.4 Justification	6
2 Literature Review.....	7
3 Materials and Methods.....	23
3.1 The Savannah River Site	23
3.2 Shallow Groundwater and Streamflow Measurements	26
3.3 Site Visit Intervals	29
3.4 Surface and Subsurface Topography Classification.....	29
3.5 Soil Data	31

3.6	Climate Data.....	34
3.7	Hillslope Model Description	35
4	Results and Discussion	37
4.1	Soil Results.....	37
4.2	Hydrologic Results	61
4.3	Model Results.....	76
5	Conclusion	78
6	Recommendations for Continued Investigation.....	80
	Literature Cited.....	82
	APPENDICES	86
A	Piezometer Notes	86
B	Sand Column Particle Size Distribution	91
C	Soil Descriptions.....	92
D	Particle Size Distribution Pippette Method.....	95
E	Maximum Rise Piezometer Data	97
F	HYDRUS Results	100

LIST OF TABLES

	Page
Table 1: Lithostratigraphic and Hydrostratigraphic Units of SRS.....	25
Table 2: PSD SRS 1	41
Table 3: PSD SRS 2	41
Table 4: PSD SRS 3	41
Table 5: In-Situ Ks.....	42
Table 6: Moisture Release Data. Core 35	44
Table 7: Moisture Release Data. Core 457	45
Table 8: Moisture Release Data. Core 334	46
Table 9: Moisture Release Data. Core 118	47
Table 10: Moisture Release Data. Core 319	48
Table 11: Moisture Release Data. Core 391	49
Table 12: Moisture Release Data. Core 453	50
Table 13: XS Soil Sampling Grid (depth to argillic)	53
Table 14: XN Soil Sampling Grid (depth to argillic)	54
Table 15: YS Soil Sampling Grid (depth to argillic)	54
Table 16: YN Soil Sampling Grid (depth to argillic)	55

LIST OF FIGURES

	Page
Figure 1: Hillslope Flow Processes.....	8
Figure 2: Schematic of Newman’s Lateral Subsurface Flow Trench.....	11
Figure 3: Schematic of Meerveld and McDonnell’s Fill and Spill Hypothesis.....	17
Figure 4: Map of Southeastern United States, SRS, and Study Watershed.....	26
Figure 5: Plan View Schematic of Recording Piezometer Nests.....	27
Figure 6: 2 Foot H-flume	28
Figure 7: Piezometer Nest Cross Section View	29
Figure 8: Tile Probe	30
Figure 9: CCHP Diagram From A. Amoozegar 1989	32
Figure 10: 1:1 Comparison of Measured Precipitation at Augusta vs. Precipitation Measured at SRS Climate Station.....	35
Figure 11: Exposed Soil at SRS Trench Face.....	38
Figure 12: Exposed Trench Face at SRS, Showing Dead Pine.....	39
Figure 13: In-Situ Ks	43
Figure 14: Moisture Release (sand)	51
Figure 15: Moisture Release (argillic)	52
Figure 16: Map of Depth to Argillic with Soil Sample Points	56
Figure 17: Map of Depth to Argillic Horizon.....	57
Figure 18: Map of Argillic Topography with Piezometer Nests and Trench	58

Figure 19: Surface Topography	59
Figure 20: Plan View Schematic of Depth to Argillic Along Trench (Lines 0 and 52)	60
Figure 21: Plan View Schematic of Depth to Argillic Along Trench (Lines 8 and 36)	60
Figure 22: Long Term Average Monthly Precipitation and SRS Monthly Precipitation	61
Figure 23: Cumulative Precipitation Deviation From Average	62
Figure 24: Graph of Piezometer Nest 1. Entire Study Period.....	63
Figure 25: Graph of Piezometer Nest 2. Entire Study Period.....	64
Figure 26: Graph of Piezometer Nest 3. Entire Study Period.....	65
Figure 27: Graph of Piezometer Nest 4. Entire Study Period.....	66
Figure 28: Alluvial Flood Plain Piezometer and Stream Discharge. Entire Study Period	67
Figure 29: Piezometer Nest 1. 12/25/2006 Perching Event.....	68
Figure 30: Piezometer Nest 3. 7/26/2006 Perching Event.....	69
Figure 31: Piezometer Nest 3. 12/25/2006 Perching Event.....	70
Figure 32: Piezometer Nest 3. 3/2/2007 Perching Event.....	70
Figure 33: Piezometer Nest 4. 12/25/2006 Perching Event.....	71
Figure 34: Piezometer Nest 4. 3/2/2007 Perching Event.....	71
Figure 35: All IC Piezometers Perching Events. Entire Study Period.....	72
Figure 36: PET and Stream Q. Entire Study Period	73
Figure 37: PET and Stream Q. 8/23/2006 to 9/25/2006	73

Chapter 1: Introduction

1.1 Problem Statement:

Interflow is defined many ways and has alternate names including throughflow, or shallow lateral flow. Interflow is defined variously as: “water that infiltrates into the soil and moves laterally through the upper soil horizons until it returns to the surface, often in a stream channel” (Ward and Trimble, 2004); “an intermediate component of runoff, between overland flow and groundwater flow, made up of subsurface flow which returns to form surface runoff without reaching the water table before arriving at the watershed outlet” (Kirkby, 1991); “lateral subsurface flow or subsurface storm flow is the lateral flow of water through near-surface soils, regolith, and bedrock” (Newman et al., 1998); “downslope flow of water occurring physically within the soil profile, usually under unsaturated conditions except those close to flowing streams, occurring where permeability decreases with depth” (Kirkby, 1991). Dingman incorporates interflow and throughflow into one definition and further expands on other theories with the same meaning, “downslope flow occurring between the ground surface and a perched or regional water table is called interflow or throughflow. It is sometimes described as unsaturated Darcian flow in the soil matrix, sometimes as saturated pipe flow in macropores that largely bypasses the soil matrix, and sometimes as flow in saturated zones of very limited vertical extent caused by soil horizons that impede vertical percolation” (Dingman, 1994). For the purposes of this study, interflow is defined as shallow lateral subsurface flow that moves over a horizon that restricts percolation.

It is important to gain an understanding of the processes that cause shallow subsurface water movement because of the many chemical transformations that can occur in shallow soil

water, such as nutrient cycling and contaminant mobilization and the subsequent movement of these chemicals across the landscape in subsurface water. Interflow can reduce residence time (the amount of time a molecule of water spends in the soil) which has implications for both water chemistry and streamflow response. With respect to groundwater flow to a stream, interflow can shorten residence time from years or decades to hours or months.

Most intensive studies of hillslope hydrologic processes have looked at steep hillslopes in mountainous environments (e.g. studies at Panola Mountain, GA. USA, Mai Mai, New Zealand, and the Hitachi Ohta Experimental Watershed, Japan). These mountainous regions are characterized by shallow soils underlain by low permeability bedrock or semi-permeable saprolite. Very little work has been done to describe water flow pathways on moderate slopes (2-10%) lacking bedrock but featuring soil layering. For example, where sandy soils overlay an argillic horizon that might impede percolation and cause water to perch due to a lower saturated hydraulic conductivity (K_s). Such a water restricting layer (1-2⁺m) (argillic horizon) with irregular topography could contribute to interflow as much as the impermeable surfaces in steep mountainous environments. We have investigated interflow in a low-gradient hillslope having deep surface soils over a water restricting argillic horizon, where the argillic horizon has varying (K_s) values and topography compared to surface soils.

1.2 Background:

The relative importance of different hillslope flow processes varies with many factors including slope, soil layering, soil texture, soil depth, macropore distribution, and subsurface topography.

Many of the soils in the southeastern US are characterized by a water restrictive horizon (argillic), that largely parallels the soil surface at depths ranging from a few to 100⁺ centimeters. This project investigated interflow on a zero-order hillslope hollow. A zero-order hillslope or hollow is an unchanneled hillslope described by a general bowl shape (Tsuboyama et al., 2000). We detailed the subsurface topography of the argillic horizon and identify “low” spots with a high-resolution topographic map across the hillslope.

While it is widely known that significant interflow of subsurface water through soil cannot occur unless there is an impermeable or semi-impermeable layer in a sloping soil (Jackson, 1992), most of the research on interflow in hillslopes has focused on relatively steep slopes overlying bedrock. Earlier hillslope hydrology studies focused on characterizing anisotropy in soils with respect to saturated hydraulic conductivity (Ks) and soil layering (Zaslavsky and Rogowski 1969, Weyman 1973, Zaslavsky and Sinai 1981a, Zaslavsky and Sinai 1981b, Wallach and Zaslavsky 1991, and Jackson, 1992).

Interflow can occur as either saturated or unsaturated flow. Saturated conditions are defined by a positive soil water pressure (soil pores are filled with water), while unsaturated conditions are those in which the soil has a negative pressure (tension) creating a suction (soil pores air filled). In New Mexico, a study concluded that most interflow occurred as unsaturated macropore network flow within the clay horizon (Newman et al., 1998). In the Upper Coastal Plain of Georgia, Shaw et al. (2001) investigated the importance of interflow in irrigation management where soils creating impedance to vertical flow could require less irrigation versus soils without a vertical flow restriction. Shaw et al. found that soil pedogenic processes can create horizons, such as argillic horizons, within the soil profile that affect transient water flow in the unsaturated zone (Shaw et al., 2001). The authors noted particle size inconsistencies can

create soil interfaces that mimic impermeable lenses. Lenses at soil horizons with increasing clay content can restrict vertical movement of water when infiltration is faster than percolation through an argillic horizon (Shaw et al., 2001).

More recently, investigators have taken an interest in the role of subsurface topographic variation of flow development (Freer et al. 1997 and Meerveld and McDonnell 2006.) These studies, conducted at Panola Mountain, GA, involved shallow soils over granite bedrock having highly variable subsurface topography on a planar hillslope (a hillslope with a constant slope in transverse and longitudinal directions) with very minor variance in surface topography. From that study, a “fill and spill” concept of saturated interflow development was proposed (Meerveld and McDonnell, 2006). However, these studies noted the topographical differences between the soil and bedrock interfaces, and there have been no equivalent studies of the differences in surface and subsoil topography. This project included an investigation of the topography of the argillic surface with respect to the soil surface.

1.3 Research Questions, Related Hypotheses, and Approaches:

Below are outlined three main questions that guide this research. Each question is associated with one or more hypotheses.

1. Do saturated conditions occur above the argillic horizon and under what conditions?

Our first hypothesis is that hydraulic properties of surface soils (topsoils) and subsurface soils (the argillic horizon) differ significantly. Our second hypothesis is that because of hydraulic differences in surface and subsurface soils, specifically reduced hydraulic conductivity

in the argillic horizon, perching is expected to occur during larger storm events. A third related hypothesis is that perching events will occur in concert with larger stream flow events.

Continuous water level data from an orthogonal piezometer network was used to characterize daily, seasonal, and storm variation in saturated hydraulic head above, below, and within the argillic horizon. These data incorporated with stream flow and soil hydraulic data helped determine the occurrence, duration, and conditions of saturated conditions above the argillic horizon. Of particular interest was whether perched saturated conditions occur above the argillic horizon. From this data we can determine whether the water above the argillic horizon was ponded due to differences in K_s at horizon interfaces, or if the water was forced up from below due to differences in K_s and h (total hydraulic head, $h = z + p$ where z = elevation; measured with total station; p = pressure head; measured by piezometers).

2. Are saturated conditions more common in argillic low points?

Our fourth hypothesis is that argillic horizon topography will differ from surface topography and perching is more likely in low points in the subsurface topography.

A high-resolution (4 x 2m) topographic map of the horizon over an area of about 6500 m², was used to determine the low points and spatial variability of the horizon. Low points identified on this map were equipped with max-rise piezometers to determine maximum water levels at each point. The expectation was that these low points will have higher piezometric heads for sustained time periods, when compared to areas with higher elevation.

3. Under what circumstances does HYDRUS 2D predict the occurrence of interflow on downslope slices of the hillslope?

Our fifth and final hypothesis is that perching events can be modeled with the HYDRUS 2D finite element model of Richards' equation for saturated and unsaturated flow (HYDRUS 2D User Manual).

HYDRUS 2D was applied to 3 model domains, where each model domain uses the same boundary conditions and soil hydraulic properties. Each model domain was different in terms of size (x,z) or length x depth coordinates. The first model incorporated the entire hillslope (380m x 60m), another domain was a soil "slice" (2m x 10m), and the final domain was a smaller scale of the entire hillslope domain (30m x 5m). These simulations should help demonstrate what kind precipitation and soil hydraulic conditions lead to the generation of interflow above the argillic horizon.

1.4 Justification:

This research provided information regarding subsurface flow processes in a low-gradient hillslope, it is important because to date no equivalent studies have been conducted on low-gradient hillslopes in temperate humid environments. This study could elucidate how subsurface storm flow is generated on low-gradient hillslopes, yielding information that has the potential inform many efforts to come. Hydrology, as a science, looks to both expand and simplify the catalog of hillslope flow processes. This study served to help write the first chapter.

Chapter 2: Literature Review

Hillslope hydrology has long been challenged with determining the flow path water takes after it rains. This paper focuses on one hillslope flow path - interflow. Here the scientific literature is reviewed to evaluate the question, “what are the dominant controls of interflow on a hillslope (eg. K_s , h , soil texture/structure, and topography)?” Interflow defined by Flügel (1993) as “the portion of rainfall which infiltrates on the hillslope and percolates through the soil till it reaches less permeable layers on which it flows in saturated and unsaturated conditions downslope, seeping either directly or via the groundwater aquifer into the river” (Flügel and Smith, 1999). The concept of interflow has a few terms with very similar meaning, such as lateral flow, “lateral subsurface flow or subsurface storm flow is the lateral flow of water through near-surface soils, regolith, and bedrock” (Newman et al., 1998). Throughflow defined by Hutchinson and Moore (2000), “is soil water that moves laterally downslope. It typically occurs where a relatively permeable soil overlies a less permeable layer, which promotes the development of a perched water table and flow parallel to the upper surface of the basal confining layer” (Hutchinson and Moore, 2000). While yet another term for which interflow can be related to is subsurface storm flow (SSF). SSF is the fast lateral subsurface movement of water in hillslopes and has been “observed to contribute substantially to direct runoff (eg. Hewlett and Hibbert, 1967; Freeze 1972; Anderson and Burt, 1990; Scherrer, 1997; Jones and Connelley, 2002; Weiler *et al.*, 2006) (Keinzler and Naef, in Press.). Past and present studies have used field and lab data, as well as computer models and numerical solutions to describe interflow.

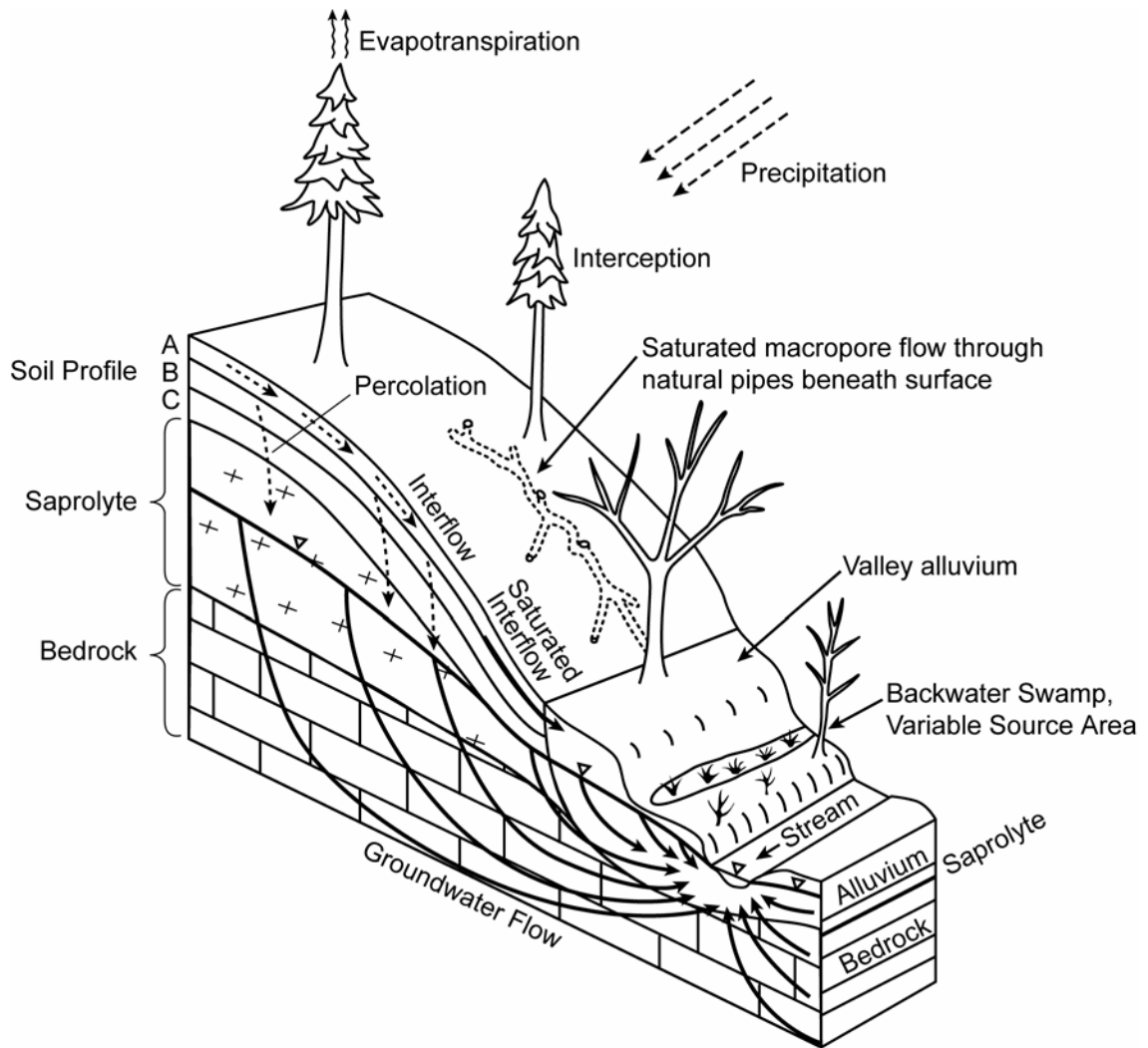


Figure 1. Hillslope Flow Processes.

Image From: Jackson, C.R. 2006. Wetland Hydrology. In Ecology of Freshwater and Estuarine Wetlands, D.P. Batzer and R.R. Sharitz, Eds. University of California Press. Adapted from: Atkinson, T.C. 1978. Techniques for measuring subsurface flow on hillslopes. In Hillslope Hydrology, M.J. Kirkby, Ed. John Wiley and Sons. Adapted by C.R. Jackson

Robert Horton first recognized the significance of water infiltration into soil. (Horton, 1933) Horton came up with a maximum and minimum infiltration capacity for specific soils. If the soil could not allow the water to infiltrate at a rate high enough to offset the amount of rainfall, Hortonian overland flow or runoff would occur. This idea was central to the hydrological realm until Hewlett and Hibbert (1963) shed new light on the subject and proposed that water infiltrates into the soil and that it can flow laterally in the subsurface to the stream (Hewlett and Hibbert, 1963). Early work by Hewlett and Hibbert (1963) yields the idea of a “dynamic storage” region that is separated from the groundwater zone. In steep watersheds unsaturated flow should not be ignored when determining hydrographic information, as these areas (below the vadose zone and above the water table) can contribute to base flows of a stream long after the cessation of a precipitation event (Hewlett and Hibbert, 1963). However, measurements of lateral subsurface flow have proven difficult to achieve. While several methods have been used, no single method seems to be the agreed upon style for the different experiments carried out both past and present. Hewlett and Hibbert, used an inclining trough measuring 3 x 3 x 45-foot with a 40 percent slope (Hewlett and Hibbert, 1963). The problem with using a trough like this is getting the native soil from the hillslope into the trough without disrupting soil structure. Consequently, there is no way to dig up a soil profile, put it in a trough and maintain the natural form of the soil. To alleviate the need to dig up soil it was common practice to pack the trough with different layers of soil (i.e. sand, loam, loamy sand) to simulate layering in the field. However, sand would be used to fill the entire trough creating a uniform layer and soil horizons would not be present. Nieber and Walter (1981), again used a simulated hillslope to measure two dimensional moisture flow; but as was common in most hillslope reconstructions; they used a uniform sand soil (Nieber and Walter, 1981).

Ragan set up an underground “vault” with a depth of thirty inches and had collection pans at depth intervals from three to ten inches. The vault was equipped with collection troughs at each depth which drained into a volumetric collection tank (Ragan, 1967). Also in this vault was an observation well used to monitor ground water levels situated below the deepest soil collection trough. Ragan’s set up used a relatively uniform soil which was essentially different colored sands and probably had similar hydraulic conductivities. Ragan’s trough was used in the field but probably gave a better estimate of a lowland or floodplain area. However, the design is excellent and can be used in other scenarios (i.e. backslope, toeslope or any other area on the hillslope). A variation of Ragan’s trough was Newman’s lateral subsurface flow collection trench (Fig. 2), which made use of three natural soil horizons (A, B, and R bandelier tuff) and could be evaluated for heterogeneity in hydraulic conductivities (Newman *et al.*, 1998).

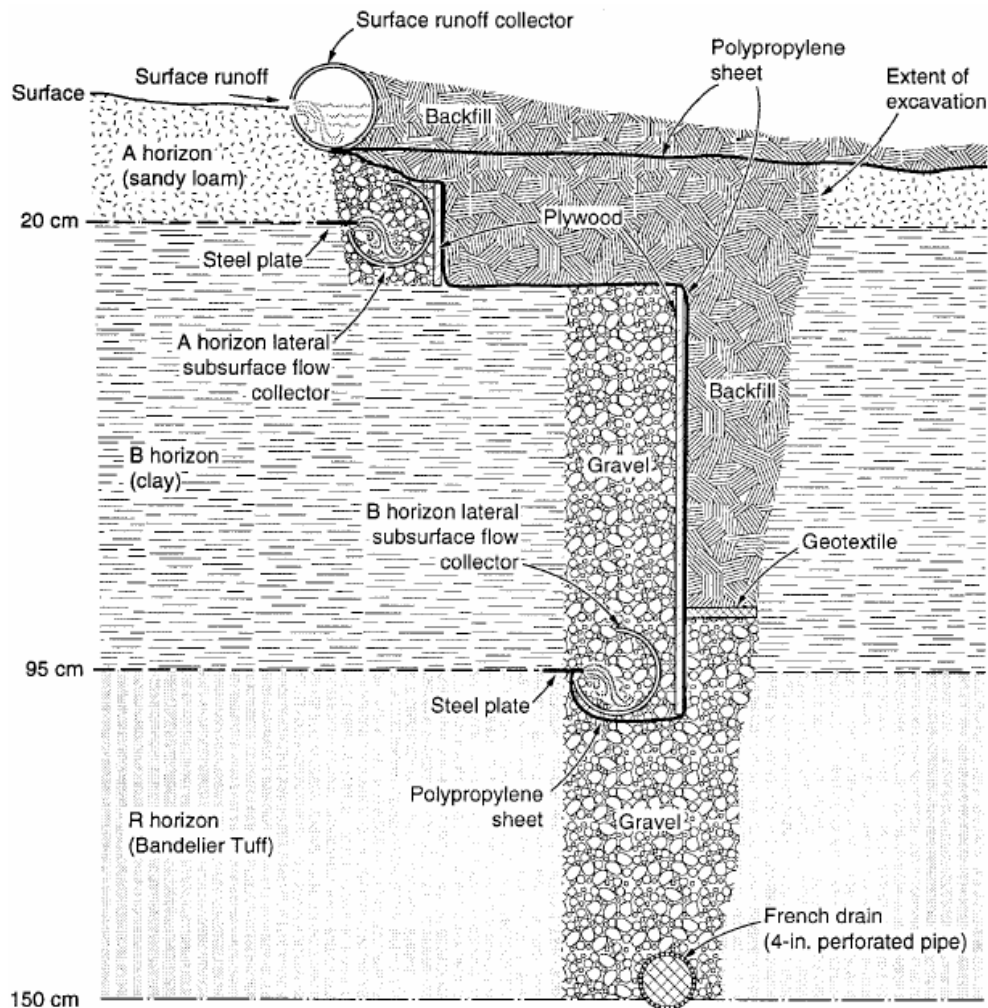


Figure 2. Schematic of Newman's Lateral Subsurface Flow Trench.

Looking into the concept of anisotropy, Zaslavsky and Rogowski (1969), show how infiltrating water can have an effect on soil profile development in the upper slope positions, where infiltration is not limited to a vertical direction. The main argument of this paper is lateral flow producing soil profile development, with anisotropy being the causative agent of lateral flow. Consequently, lateral flow will increase with an increasing amount of anisotropy. Soil profile development due to infiltration was found to be at much higher rates on concave portions of the hillslope. Concave portions of hillslopes experience an increase in flux density, allowing more infiltration, which creates soil profile development from increased water flow. This paper

shows how a soil profile can develop due to water infiltration and anisotropic soil and hydraulic conditions. Due to anisotropic hydraulic conditions water will flow in a lateral direction, which will be confined predominantly to concave portions of the hillslope. Furthermore, lateral flow due to anisotropy will allow water to be carried further horizontally, preventing water from infiltrating deep into the soil profile. A build up in the B layer of a soil profile upslope of a flood plain is evidence of lateral water flow causing soil profile development, which negates alluvial deposition as a source of soil profile development in the up slope region (Zazlavsky and Rogowski, 1969).

Weyman (1973) studied the hydraulics of flow with particular interest paid to breaks in vertical permeability of the soil. The paper asks several important questions of which the following directly pertain to interflow: does lateral flow occur within any soil, or are distinct soil horizons or impermeable bedrock necessary for its initiation? Does lateral flow occur within both saturated and unsaturated soil and if so, does one soil state dominate the hillslope hydrograph? Weyman (1973), points out that to date there was extensive literature on the topic of interflow, but most investigation had been in laboratory settings or computer models, while there is a deficiency in field experiments. As such, Weyman conducted field investigations and came up with similar results to Hewlett and Hibbert (1963), but determined much more as to how the hillslope responds under saturated conditions. The response of the hillslope to rainfall was dominated by surface infiltration capacity of the soil and saturated through flow within the mineral soil.

Zazlavsky and Sinai (1981a), investigated soil layering, leading to unsaturated lateral flow of water parallel to soil layers in the upper portion of the soil profile. This paper detailed anisotropic conditions where a soil has two distinct K_s values causing water to flow laterally.

Lateral movement of water was seen in both concave and convex hillslope segments, as well as in concave and convex structures in the soil profile. Concave structures were sources of moisture accumulation, while convex structures were shown to prevent pollutants from leaching down into the water table. Convex structures acted as a “thatch roof” allowing a horizontal water flow with minimal infiltration into the soil profile. The paper also cites anisotropic conditions were of primary importance, where the coefficient of anisotropy is directly related to the differences in conductivity between two soil layers. A point to be noted was the conductivity pressure head of two soils intersect at a point leading to lateral flow of water (probably due to slope degree), not vertical because there are no pressure head gradients at the point of intersection (Zazlavsky and Sinai, 1981a).

In a companion paper Zazlavsky and Sinai (1981b), presented a numerical solution to the problem of lateral flow through a transition layer. A transition layer was found between two horizons or within a horizon in a soil profile, and the thickness and K_s will vary largely with soil type and land use. Central points of this paper were the changes in K_s within a profile with depth, and the amount of discharge and saturation of the transition layer was directly related to the thickness of the layer and rainfall amount. A thin transition layer may not reach saturation due to high K_s and insufficient rainfall. Conversely, a thick transition layer might reach saturation at some point in time, with the thickness of the layer being directly proportional to the depth of rainfall necessary to produce saturated conditions. A soil without a transition layer will not produce a lateral flow of enough magnitude to consider viable. However, soil with a transition layer could produce virtually all the lateral flow of the slope. The paper clearly shows how water flowed through a transition layer, producing unsaturated lateral flow in the upper portion of the soil profile. A transition layer has the potential to act as a gradient of the water

due to the slope degree, thickness, rainfall amount, and differences in K_s (anisotropy) of the layer (Zaslavsky and Sinai, 1981b).

McDonnell (1990) used soil moisture energy conditions at different topographic locations within a catchment. The paper describes how isotopically old water is transported rapidly to the stream channel during rainfall events via preferential flow paths (macropores, pipes, and cracks in the shallow subsurface mineral soil). This study revisits Mosely's (1979) conclusion where soil pipes exist at the interface of the mineral soil and bedrock, unable to penetrate the bedrock, creating a lateral flow path (McDonnell, 1990). Water was observed flowing through soil pipes at the banks of stream channels and was substantiated by rapid increases of hillslope runoff in the downstream direction. Another interesting find, was the idea of "by-pass" flow, where vertical movement of free water along continuous cracks from the mineral soil to the bedrock interface, through an unsaturated or partially saturated soil. The final point of this paper related to interflow development is the idea of a transient water table at the soil-bedrock interface (McDonnell, 1990). Transient water table development at points along the hillslope can lead to lateral flow of water downslope due to differences in hydraulic gradient.

A similar study at the Maimai, M8 catchment, presents a case study of shallow flow generation in a steep unchanneled catchment (McDonnell, et al., 1991). This study reinforces the gap in detailed field observations of a single hillslope, complementing a prior statement by Rodhe (1981). Data from the paper show tensiometer and throughflow effect for two precipitation events, supported by a previous study by Mosely (1979), but leads to a new interpretation that describes a "large portion" of runoff flowing above the B horizon, without any saturation of the mineral soil or substantial change in soil tension (ψ) (McDonnell et al., 1991). Using two natural precipitation events, this study refutes the aforementioned study (McDonnell,

1990), stating that through flow in the basin was formed from saturated flow in the litter and OH horizons, where water perches at the interface of the OH and B2 horizons due to differences in permeability (McDonnell et al., 1991). Using a 30L artificial application of water to the site, the study shows that tensiometric response was negligible, reinforcing previous isotopic data. For the artificial event, water flowed at the shallow subsurface interface of the OH and B2 horizons, not through the soil matrix. This flow path was termed “Pseudo-overland flow” (McDonnell et al., 1991). This study does not explicitly define flow as interflow, but it is apparent that water is not being delivered to the stream via soil cracks or pipes, rather delivered to down slope regions laterally at an interface, whereby water does not flow through the soil matrix.

Freer et al. (1997) studied the dynamics of topography at the hillslope scale and compared the findings between two hydrologically distinct catchments. The familiar Maimai M8 catchment was compared to the Panola Mountain Research Watershed, GA. Catchment size at Panola was greater (41-ha compared to 10-ha), however, the findings of the paper present an idea that will be used for many future investigations on the controls of subsurface topography with respect to flow paths. Using the topographic index $\ln(\alpha/\tan \beta)$ of Kirkby (1976), where α is upslope accumulated area and β is the local slope angle, the index proposes that surface and subsurface topography are similar where saturation at a point will increase with increasing values of the index (Freer et al. 1997). This study addresses the importance of acknowledging the dominant downslope hydraulic gradients at the hillslope scale which could differ from surface topography, by answering the question, is it appropriate to describe flow paths by surface topography or is it more important to describe hydraulic controls based on the subsurface topography of a hydrologically impeding layer? This idea works well for hillslopes where there is a deviation of surface and subsurface topography, as evidenced at the Panola hillslope, while

Kirkby's index works well at sites like Maimai where surface and subsurface flow paths are highly correlated (Freer et al. 1997).

The "fill and spill" hypothesis presented by Tromp-van Meerveld and McDonnell, 2006b, further refines the idea of hillslope response to rainfall. In this companion paper, authors relate a threshold amount of rainfall to hillslope response, where increasing amounts of rainfall cause low points in the hillslope to fill up and spill over to the next low point, essentially connecting low points within the hillslope. The threshold response was shown where a certain amount of rainfall was required to hydraulically connect the entire hillslope (summit to toe slope). This paper served as a basis to move hillslope hydrology past the classic "point-based" descriptions, to an entire hillslope response. Furthermore, the threshold detection system can be a way to boil down information from complex hillslopes and eventually categorize similar processes of different hillslopes.

The "fill and spill" hypothesis states that saturation first occurs in shallow soils in the upper portion of the slope due to less moisture deficit when compared to areas at the lower slope with deeper soils. Once saturation occurs at the soil-bedrock interface, water flows laterally over the bedrock to a central depression in the hillslope (Tromp-van Meerveld and McDonnell, 2006b). The proposed "fill and spill" hypothesis is an explanation of the threshold response in subsurface storm flow as reported in Tromp-van Meerveld and McDonnell (2006a), showing that bedrock microtopography can control "slope-scale connectivity" of subsurface saturation and "hillslope flow contributions at the catchment scale" (Tromp-van Meerveld and McDonnell, 2006b).

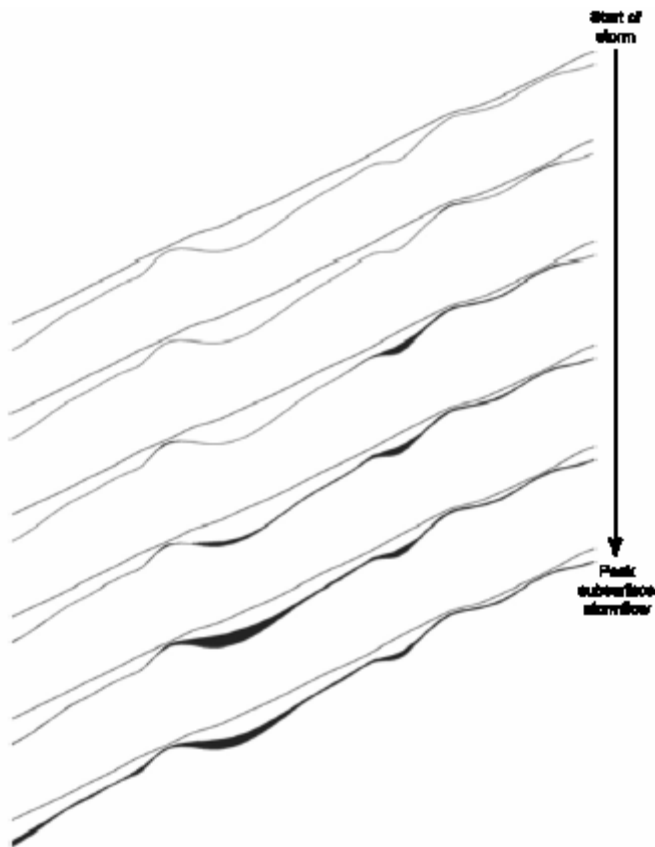


Figure 3. Schematic of Meerveld and McDonnell's Fill and Spill Hypothesis.

The paper shows that once local “low” points become saturated, they spill over and flow laterally to the next “low” point (Fig. 3). Large storms enable more of the hillslope to be hydrologically connected. Once the threshold response is fulfilled and a large area of the hillslope is connected, the hillslope will contribute to subsurface storm flow over the connected area (Tromp-van Meerveld and McDonnell, 2006b).

Most recent hillslope investigations to this point have used hydrometric data coupled with trench outflow to inform numerical model efforts. This study investigates the contribution of a zero-order basin to discharge from a 1st order catchment by combining piezometric response, soil temperature, and runoff (Tsuboyama et al. 2000). They studied hydrologic processes on a 0.25 ha unchanneled hollow at the Hitachi Ohta Experimental watershed, Japan. A primary assumption of the study is that rainwater temperature is higher than soil water temperature and

thermal responses in soil water (increase) can be attributed to percolating rainfall (Tsuboyama et al., 2000). The authors used three soil temperature measuring stations two in the upper and lower soil profile, where upper and lower stations – (placed at the most upslope portion of the hillslope) - have thermisters at the soil surface, just below, and at soil/bedrock interfaces, and the outlet has one thermister at the surface interface and were used to measure changes in soil water temperature, potentially linking these changes to different flow paths. Piezometric data was obtained with piezometers across the hillslope at the soil/bedrock interface.

For small storms ($\geq 6\text{mm/hr}$), the study shows a rapid increase in soil temperature at the outlet, indicating that rainwater was percolating to the measured depth (20cm). However, there is a decline in temperature measured at the outlet, indicating a change in the dominant flow direction from vertical to lateral (Tsuboyama et al., 2000). This allows the interpretation that a rapid lateral flow of water is initiated within and flows through the shallow subsurface at the lower and middle sections of the hollow (consequently there are no thermisters mid slope). Piezometric data is not conclusive for small storm events, but did show a time lag, compared with larger rainfall events (small lag is about 12 days, large lag 7 days).

Large storms ($\geq 40\text{mm/hr}$), show a much different response. The initial temperature rise in the upper soil profile and piezometric response comprise an initial peak of subsurface storm flow (Tsuboyama et al., 2000). Soil temperatures deeper in the profile showed small fluctuations in temperature. Again soil temperatures in the upper soil profile were attributed to percolating rainwater, but the rapid increase at the outlet compared to up slope positions suggest that rapid movement of water occurred laterally within the shallow subsurface from middle to lower hillslope segments (Tsuboyama et al. 2000). Further support for the time lag of subsurface storm flow is evidenced by the delayed piezometric response at lower slope positions (near the outlet

thermister), and as stated earlier, the time lag in piezometer response is much less during large rain events (Tsuboyama et al., 2000). An interesting find of this paper relating to Tromp-van Meerveld and McDonnell (2006b), are the thresholds of rainfall inputs, compared to piezometric response time (small vs. large events). The authors conclude that soil temperature fluctuations during large rainstorms indicate that piezometric response was caused by subsurface water flowing from upslope positions, via convergent flow (Tsuboyama et al., 2000).

Almost all studies of interflow have been conducted in humid/temperate climates on steep slopes with shallow soils overlying bedrock. The following two studies investigate interflow in a semi-arid environment, New Mexico, with relatively deep layered soils (95cm) overlying bedrock and Southwest Georgia with deep layered soils (445cm).

In New Mexico, the study found that interflow was dynamic and occurred largely as saturated conditions prevailed from snow melt and spring rain events (Newman et al., 1998). An interesting point is that about 80% of the water flowed through the B horizon with the rest flowing through the A horizon, this assertion is backed up by stable isotope and chloride data. Also, lateral flow showed larger volumes and greater durations in the B horizon 400L/day compared to 190 L/day in the A horizon at each respective peak. Newman et al. (1998), cite the work of McDonnell (1990, 1991), stating the minimum condition for water to flow through macropores is a “flux density” of precipitation in excess of soil matrix hydraulic conductivity, thus water inputs are greater than the infiltration capacity of the matrix, creating macropore flow (Newman et al., 1998). The conclusions based on Ks, stable isotope, and chloride data, determine that unsaturated lateral flow in New Mexico is primarily controlled by preferential flow paths (macropore flow), where most of the flow is conducted through the B horizon leading to a rapid flow regardless of low soil hydraulic conductivities (Newman et al., 1998). During

snow melt, when saturated conditions prevail (volumetric water content > 33%), both A and B horizons contribute to lateral flow creating a two domain system, evidenced by a substantial rise in chloride, organic carbon, and other aqueous chemicals carried by the lateral migration of water (Newman et al., 1998).

Shaw et al. (2001), investigated several upper coastal plain soils in South Georgia, with water restrictive horizons and gained knowledge for the importance of interflow in irrigation management where soils creating impedance to vertical flow could require less irrigation versus soils without a vertical flow restriction. The authors cite that soil pedogenic processes can create horizons, for example an argillic clay horizon within the soil profile affecting transient water flow in the unsaturated zone (Shaw et al., 2001). Also, pointing out that particle size inconsistency can lead to soil interfaces mimicking impermeable lenses. Lenses at soil horizons with increasing clay content can restrict vertical movement of water when infiltration is faster than percolation through an argillic horizon (Shaw et al., 2001). If enough restriction to vertical percolation exists, water can flow laterally above or within zones of less permeability. The study compared two soil pedons. Pedons (NW and SE) were named according to their coordinates at the site and had different results with respect to interflow at each pedon. The NW pedon showed two locations of water build up, one in the E2 horizon and one in the Bt2 (argillic) horizon. At the SE pedon there was one location of water build up, in the Bt4 horizon creating impedance to vertical flow with decreased tension above this horizon. The accumulation of water in the Bt4 horizon is attributed to lower Ks, even when the data suggests no significant difference of Ks within the Bt horizon (Shaw et al. 2001). A slight amount of lateral movement of water was detected at 60 and 90 cm in the SE pedon, which is dissimilar to the NW pedon, because the depths do not relate to maximum matric potential or minimal Ks (Shaw et al., 2001).

Germann and Zimmerman (2005), show orders of magnitude difference in surface and subsurface K_s , and state that any morphologically different soil layers with presumed lower K_s , for instance compacted soils, soil horizons with increased densities and lower porosities, or perched water table development, could be capable of diverting flow from vertical to lateral. Also, in hillslope soils preferential flow is presumed to change from a vertical to lateral direction at layers of reduced permeability (Germann and Zimmerman, 2005).

In a more recent study by Retter et al.(2006), references Weyman's study (1973), further detailing the direction and occurrence of subsurface flow, incorporating Weyman's theory that infiltration is gravity driven where the dominate flow paths in slopes are unsaturated and move vertically towards the base of the profile (Retter et al., 2006). Using TDR nests, the authors measure direction and velocity of flow in a heterogeneous soil. Their study concludes that water movement in a heterogeneous soil is not truly down, i.e. not truly in the z-direction. The authors show a "bending of flow" where flow paths can deviate up to 67° from the z-axis to a lateral flow direction, thus creating lateral flow, and a delay with respect to infiltration (Retter et al., 2006). The authors show how breaks in the vertical permeability of the soil generate lateral subsurface flow, stating, upon saturation, lateral flow should occur due to equipotential lines within the saturated zone being "nearly orthogonal" to the slope gradient (Retter et al., 2006). Also, the runoff response of the hillslope to rainfall inputs will be delayed as it takes considerable time for water to move laterally to the base of the soil profile, but once at the base lateral flow commences and dictates the magnitude of the hillslope response (Retter et al., 2006).

It should be noted while we have investigated flow paths extensively, to date hillslope flow paths are not well understood despite many efforts beyond the early work of Hewlett in the 1960's (Freer et al., 1997). Also, Germann and Zimmerman (2005) report, physical processes

that control runoff generation resulting from rainfall inputs are still in a developmental phase (Beven, 2001).

Hydrology has made great strides to catalog hillslopes across the world, and while it would be nice to relate hillslopes in a similar region, it is not feasible. There are too many variables to account for at each site. Many similarities exist between hillslopes of certain physiographic regions, and computer models should be able to account for these differences and describe flow processes. However, as the literature shows, process definitions and descriptions can be used at each hillslope, but this does not mean we can have a uniform set of equations or explanations to describe and compare all hillslopes.

Chapter 3: Materials and Methods

3.1 The Savannah River Site:

The hillslope under investigation is located within the Savannah River Site (SRS) Federal nuclear reservation (Figure 1), 33°N latitude 82°W longitude, consisting of parts of Aiken, Barnwell and Allendale Counties, South Carolina (Kilgo and Blake, 2005). The SRS comprises approximately 802-km², and was bought by the United States Government and constructed to facilitate the needs of the cold war in the 1950's to produce nuclear weapons, with the primary materials being tritium and plutonium-239 (<http://www.srs.gov>). In 1972, the SRS was converted to the nation's first National Environmental Research Park (Rogers, 1990). Presently the SRS serves as a nuclear waste facility.

To develop the site the United States government displaced nearly 1,500 families, most of which used the land for farming (cattle, hog, chicken, and timber) and agricultural (cotton and corn) (Rogers, 1990). The land subsequently reverted to forest cover. The SRS is included in the Southeastern Evergreen Forest Region, defined by Braun (1950) (Jones *et. al.*, 1984). Land use ranges from 60 to 70 percent woodland, mainly pine and hardwood, where most stands were planted as natural longleaf pine (*Pinus palustris*), while mature longleaf pine were used to harvest terpentine (Rogers, 1990).

Climate

The climate at SRS is warm (moist) temperate, winter daily average temperature is 9 degrees Celcius (°C) and daily minimum is 3°C. Summer daily average temperature is 26°C and the average daily maximum is 32°C. Total annual precipitation is 1214mm, distributed relatively

uniform throughout the year, however April, May, October, and November tend to be drier than other months (Rogers, 1990; Kilgo and Blake 2005). Evapotranspiration (ET), the amount of water being removed from the system via evaporation and transpiration from plants, is an important factor to determine when conducting any hydrologic study.

Annual pan evapotranspiration (PET) at SRS is about 1448 mm. This data was collected over a 29-year period (1963-1992) at Sandville, SC (Kilgo and Blake, 2005). Using a pan coefficient (Cp) of 0.7, actual evapotranspiration (AET) is 1013 mm. Compared to data from the mixed waste site at SRS, this data is adequate, where PET over a one-year period was 1517 mm, and using a Cp of 0.7, AET was 1062 mm.

Soils and Geology

The SRS is within the Upper Coastal Plain subprovince of the Atlantic Coastal Plain physiographic province (Collings and Montgomery, 1957), and is divided into two geographic divisions: with the northern part in the Aiken Plateau and the southern part within the coastal terraces also known as the “low country” (Kilgo and Blake, 2005). Around 40 percent of the SRS lies in the Aiken Plateau (Cooke, 1936), with elevations ranging from 82 to 122 m, this area is also termed the upland, with Paleudult soils (Jones et al., 1984; Kilgo and Blake 2005). The coastal terraces division occupy the other 60 percent of the SRS, where the terraces were formed by advance and retreat of the Pliocene sea (Jones et al., 1984). Seven abandoned shorelines have been detected along the Atlantic coast, four of which have been shown to occur within the SRS, with elevation ranging from 24 m at the Savannah River to 82 m (Cooke, 1936). Soils of the low flats and floodplains are Humaquepts and Dystrochrepts while Paleudults are restricted to well-drained uplands (Jones et al., 1984).

Table 1. Lithostratigraphic and Hydrostratigraphic Units of SRS.

Age	Lithostratigraphy		Hydrostratigraphy			
Miocene	Hawthorn	Altamaha (Upland Unit)		Surficial Aquifer		
Eocene	Barnwell	Tobacco Road		Upper Three Runs Aquifer		
		Dry Branch	Irwinton Sand			
			Twiggs Clay		Tan Clay Aquitard	
			Griffins Landing		Barnwell-McBean Aquifer	
		Clinchfield				
	Orangeburg	Tinker/Santee			Green Clay Aquitard	
		Warley Hill				
		Congaree				Gordon Aquifer
	Black Mingo	Fishburne/Fourmile				
		Snapp/Williamsburg			Crouch Branch Aquitard	
Ellenton						
Cretaceous	Lumbee	Steel Creek/Peedee		Crouch Branch Aquifer		
		Black Creek				
Paleocene	Black Mingo	Crouch Branch Aquitard		Meyers Branch Confining System		
Cretaceous	Lumbee	Dublin-Midville Aquifer System		Dublin-Midville Aquifer System		

Table 1 presents the Litho and Hydrostratigraphy, from Rasmussen and Mote (2007). The upper most unconfined aquifer (Surficial Aquifer), is probably the aquifer draining to the seepage face of the perennial stream (Fig. 4). The aquifer is part of the Upper Three Runs Aquifer within the Floridan Aquifer System.

Hillslope and SubWatershed description

The research site is a small (38 ha) zero-order watershed (Fig.4) located at 33° 15' 53.61"N and 81° 38' 8.44"W. Vegetation on the site is typical of most forested areas in the Southeast, with mixed conifer and hardwoods in upslope areas (Pine, Oak, Southern Waxmyrtle)

where hardwoods (Oak, Sweet Gum, Yellow Poplar) and river cane dominate the lower slope regions. Approximately 150-200m northeast of the hillslope is a small stream (blue line, Fig.4) that drains the watershed.

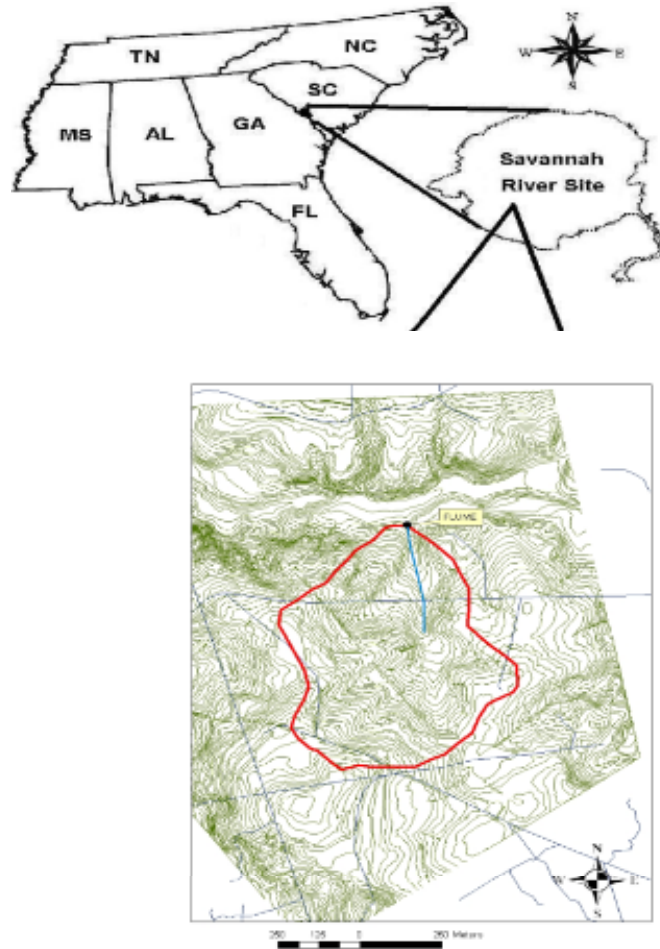


Figure 4. Map of Southeastern United States, SRS, and Study Watershed.

3.2 Shallow Groundwater and Streamflow Measurements:

Four piezometer nests (Fig. 5) consisting of three piezometers where one is placed above (A), within (IC) and below (D) the argillic horizon (Fig. 7), were installed across the hillslope in an orthogonal network.

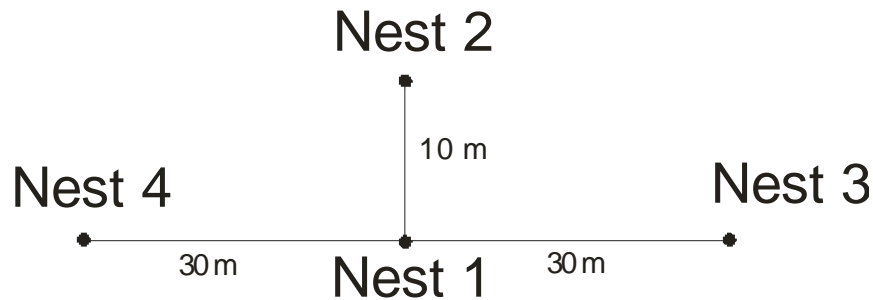


Figure 5. Plan View Schematic of Recording Piezometer Nests.

Figure 7, illustrates a cross section of each piezometer installed across the hillslope. Also, a piezometer (Alluvial FP) was installed in the floodplain of the intermittent stream channel, about 150 to 200 m downslope of the nests. An orthogonal network is a schematic placement of the piezometers at right angles to one another (Fig. 5). All piezometers in this network as well as the alluvial piezometer were outfitted with data loggers to continuously monitor shallow ground water fluctuations. A piezometer is defined as “an open-ended, solid walled pipe inserted in a water-bearing stratum holds water at the height to which the water pressure in the stratum holds it, whereby the upper surface defined by a piezometer is the piezometric surface” (Black, 1996). All data recording piezometers were constructed from schedule 40 polyvinyl chloride (PVC) pipe from Boart Longyear, with PVC slotted screen interval screwed into the bottom. Data were recorded at 15-minute intervals in all piezometers. Piezometers above and in the argillic horizon were outfitted with Odyssey Capacitance probes (Dataflow Systems LTD PTY), where water contacts a vented Teflon cable, enabling the logger to read and record a depth of water due to the electrical contact between the water and cable. Deep piezometers were outfitted with either HOB[®] or SOLINST[®] pressure transducers, where a thin glass plate, open to the water or air measures absolute pressure, where the pressure exerted

by a column of fresh water is directly proportional to the height of water in the piezometer. Notes on each piezometer installation can be found in Appendix A.

A small stream that drains the hillslope was instrumented with a 2' H-flume (Fig. 6). The flume has enabled us to determine stream flow based on the specific stage discharge relationship of the flume. That is, at a specific stage (height of water in the stream continuously measured by the pressure transducer), a calculated amount of water (discharge in units of volume/time i.e. L/s) was flowing through the spout of the flume. The flume stilling well was where flowed from inlets on the side of the flume, thus water flows into the stilling well and stream stage readings were obtained. A SOLINST[®] pressure transducer (data-logger) mounted within the stilling well continuously monitors fluctuations in stream stage (at 5 minute intervals), ultimately enabled us to calculate stream flow.

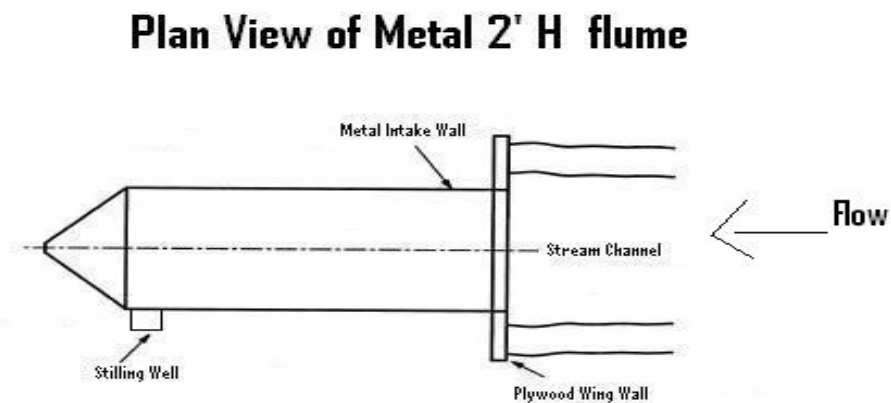


Figure 6. 2 Foot H-Flume. Original image <http://www.icrisat.org/gt-aes/oned/measurements.htm>. Image edited by: James L. Greco III 3-24-2006

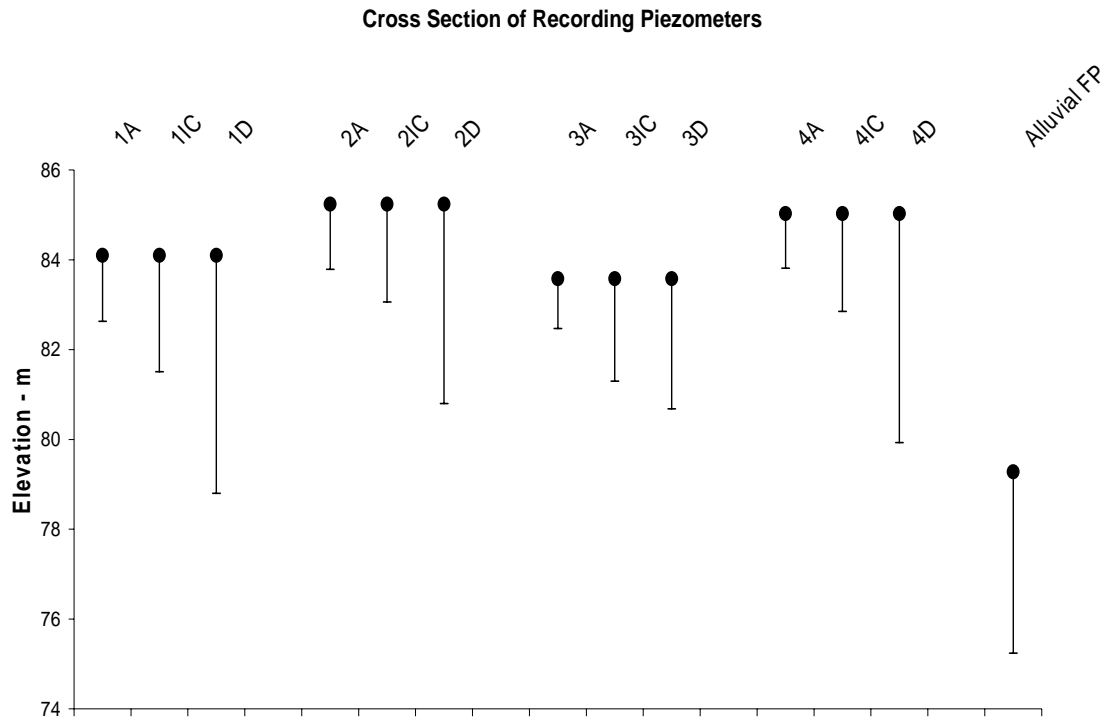


Figure 7. Piezometer Nest Cross Section View. The black dot at the top represents the top of the piezometer casing as ground surface elevation, the line is the length of the PVC casing, and the horizontal line at the bottom represents the bottom of the piezometer where the data-logger was placed.

3.3 Site Visit Intervals:

Data was extracted from all data loggers every three weeks. Other fieldwork was done on an as needed basis. All data loggers continuously collected data at set time intervals, while certain data (check gage, max-rise piezometer, and stream stage) were taken manually and recorded during each site visit.

3.4 Surface and Subsurface Topography Classification:

Surface topography was obtained using United States Geological Survey (USGS) 2' contour topographic maps. USGS maps used in conjunction with surveyed or ground truth

points were imported into ArcMap, using the Kriging function to create a visual image of the surface topography.

Subsurface topography of the argillic horizon was obtained by setting up a 4m x 2m grid system across the hillslope. The grid area comprised about 6500 m² of the upper hillslope and was laid out carefully and accurately using a Sokkisha BT20 theodolite, an instrument commonly used in surveying to ensure precise angles and straight lines are placed across a defined space.



Figure 8. Tile Probe. Image from: <http://www.benmeadows.com/store/item/221055/>

Depth to the top of argillic horizon was measured at each point on the grid. Depth to the top of argillic horizon was measured using a tile probe (Fig 8.), which can travel easily through sand, but will not penetrate a horizon of differing bulk density (such as an argillic layer). At each point three measurements were made to ensure accuracy (the probe did not hit a root, rock, or other subsoil obstruction), and the deepest of three measurements was recorded. The depth to top of argillic horizon dataset was imported into ArcMap, where Kriging was again used to create a visual of the variability of depth to the top of the argillic horizon. Using this map and the surface topography map, a function in ArcMap known as “math” was used to subtract the depth to the top of argillic horizon from the surface map and create a subsurface topography map

essentially producing a visualization of the subsurface argillic topography as if it were at the surface.

After creating the subsurface topography map, “low” points in the argillic horizon or points where the argillic horizon creates a subsurface valley were instrumented with max-rise piezometers. Max-rise piezometers (MRp) are a cheap and effective water level measurement tool, where a ½” diameter piece of PVC pipe and cork dust are placed within a larger piece of PVC. Water rises in the piezometer with cork dust floating with the water, which is then deposited onto the internal pipe. Pulling the small pipe out and measuring from the bottom to where the cork dust settles onto the pipe enabled us to measure water level fluctuations at each site visit. Since max-rise piezometers are two pieces of PVC, one inside the other, no mechanical maintenance was involved. However, at each site visit where data is collected from the MRp, the cork dust will need to be replenished.

3.5 Soil Data:

Field Ks

Soil hydraulic properties for surface, mid-depth and water-restrictive horizons were determined in-situ. In-situ Ks was determined using a compact constant head permeameter (CCHP) developed by Aziz Amoozegar (Fig. 9). A CCHP has two main functions (1) to maintain a constant head at the bottom of a cylindrical borehole and (2) determine the flow of water from the borehole into the soil (Amoozegar, 1989). Once flow data were obtained, Ks was calculated using the Glover solution, a complete description of the Glover solution and its application to the CCHP has been fully reviewed and validated by Aziz Amoozegar (Amoozegar, 1989).

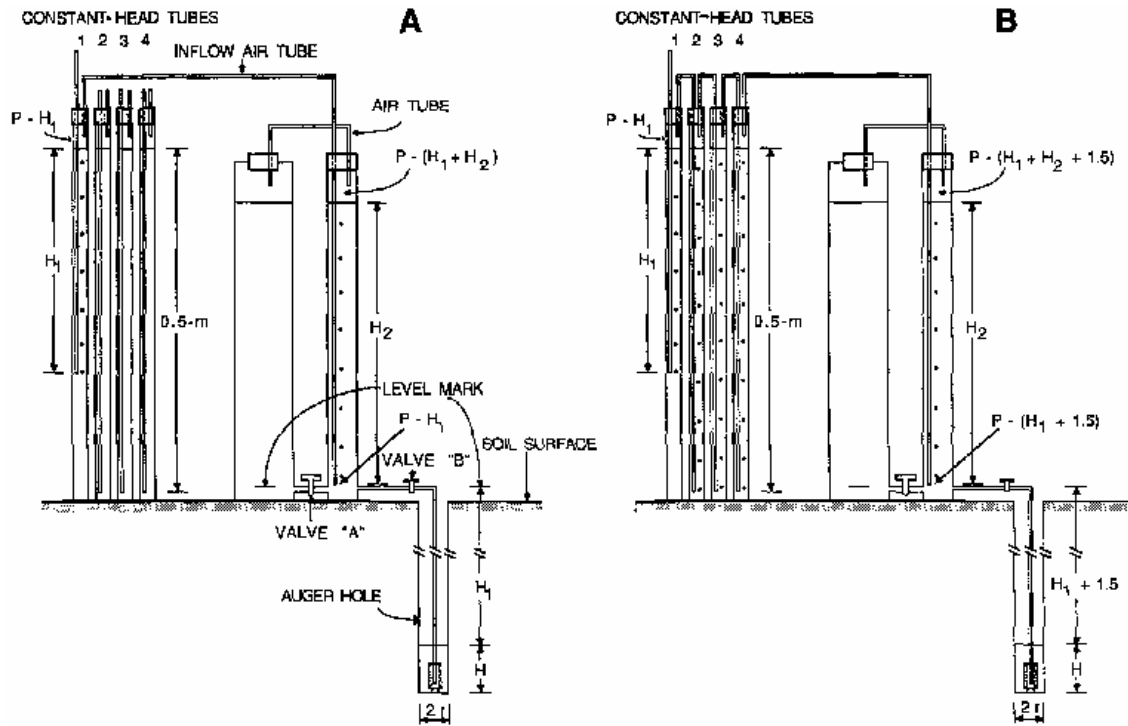


Figure 9. CCHP Diagram from A. Amoozegar 1989.

Soil moisture release curve

Two soil moisture release curves were determined for surface (sand) and subsurface (argillic) horizons. A moisture release curve yields data about how the soil will respond to a drying cycle (i.e. high negative pressure head or tension). A common practice to develop a moisture release curve is to obtain in-situ soil samples using a soil core.

Soil cores were taken from each horizon using a soil core of the following dimensions: 8 cm internal diameter x 7.7 cm deep. The cores were driven into the ground and carefully dug out to ensure a uniform amount of soil in each core (both the top and bottom of each core had a level amount of soil which corresponded with the lip of the core). All cores were sprayed with a fine mist of water, wrapped in cheese cloth and placed carefully into a zip-lock bag to ensure the core did not dry out during transport.

A sand column was used to place three to four cores on top of and induce negative pressure heads from (-10 to -90 cm) and maintain a set pressure head until each soil core reached equilibrium. Pressure head was spaced into 10 cm intervals over the entire range of negative pressure heads (saturated to -90 cm). Equilibrium was reached once the tube draining the sand column was no longer dripping, indicative of a cessation of water movement from the soil core(s) through the sand column. The sand column was filled with uniform sand (62.80% coarse sand and 36.22% medium sand; corresponding to a particle sizes of 0.5 mm to 1 mm and 0.25 mm to 0.5 mm respectively) and having the following dimensions: 30.5 cm inside diameter x 179 cm tall (note: height was taken from the outlet tube used to drain the column for each tension adjustment). Particle size of the sand in the sand column was done using the dry sieve method, where a set amount of soil (sand) is weighed and shaken through a sieve set, and each fraction of sand remaining in each sieve is weighed, and a per-cent of particle size can be determined from the weight of soil in each sieve (PSD of material in sand column in Appendix B).

Particle Size Distribution

An important factor that has been shown to affect the flow of water and K_s of soil is the particle size distribution (PSD). PSDs were obtained by collecting soil samples from each horizon at three random sites (SRS1, SRS2, SRS3 a full description and classification of each site is presented in Appendix C), while mapping and classifying the soils of the hillslope. Soil samples were air dried, weighed, crushed, and coarse particles were removed by dry sieving through a 2 mm sieve. PSDs were determined for all sites using the pipette method, after surface horizon organic matter was removed with H_2O_2 and fine particles were dispersed with sodium hexameta-phosphate. A complete description of the pipette method for PSD can be found in, Kilmer and Alexander (1949), the procedure used in this investigation can be found Appendix D.

3.6 Climate Data:

Climate data from the site was obtained via a weather station about ¼ mile from the study site. The station consisted of an air pressure transducer, tipping bucket rain gage, and a manual rain gage (All Weather Rain Gauge). Barometric pressure (BP) and air temperature were used to compensate for observed fluctuations in shallow ground and surface water due to BP. Rainfall was measured via a HOBO® tipping bucket rain gage, where there are two “buckets” that fill with rain water, each tip corresponding to 1/100” of accumulated rainfall. Total precipitation was checked using an All Weather Rain Gauge (Productive Alternatives, INC. Fergus Falls, MN). This station was set-up in mid September 2006, this was due to an apparent lack of precipitation data from SRS. The gap in precipitation data was filled in using data from a rain-gage in Augusta Georgia. A 1:1 comparison of SRS to Augusta precipitation is presented in Figure 10, notice the deviation between the two sites is minimal and can be considered accurate.

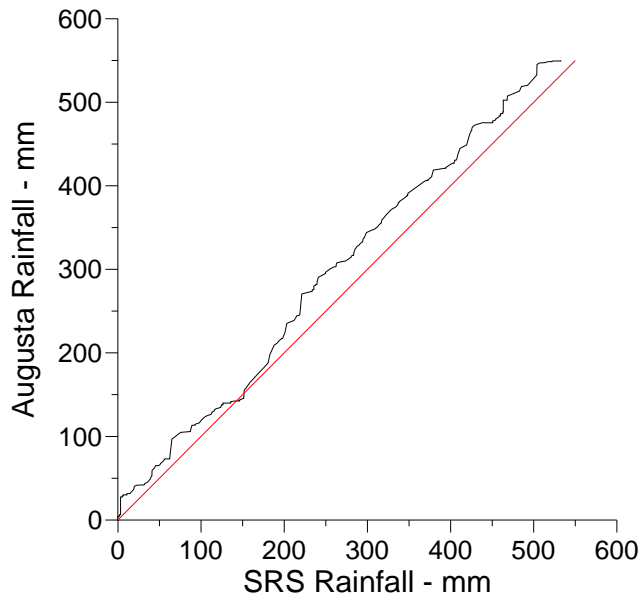


Figure 10. 1:1 Comparison of Measured Precipitation at Augusta vs. Measured Precipitation at SRS Climate Station.

3.7 Hillslope Model Description:

Hillslope characterization data was used to design a 60 m deep x 380 m long computation grid and parameterize the HYDRUS 2-D model, a finite element model based on the Richards equation that was used to simulate hillslope flow processes. Initial model setup was completed without calibration using the soil hydraulic information determined from field samples and lab testing as well as one year of observed data (this data was read into the model as “time variable boundary conditions”, where an atmospheric boundary was used across the surface of the domain, and stream stage as measured at the flume was used as a “variable head boundary” at the stream, everywhere else was a “no flow boundary” (Appendix F). The model was also used to determine simulated conditions i.e. lowering or increasing K_s , changing the highly irregular subsurface topography of the argillic horizon to linear, and decreasing the entire domain size.

Alternative model domains included: creating a slice of soil that was 2 m wide by 10 m deep, and decreasing the domain size to 5 m deep x 40 m long. From model results, a monitoring program was developed to further refine and calibrate the model, providing a framework for continuation of the study, which may include more instrumentation being installed at the site.

Chapter 4: Results and Discussion

4.1 Soil Results:

Soil Characterization

The pedological definition of soil is: “the collection of natural bodies on the earth’s surface containing living matter and supporting or capable of supporting plants out of doors” (West, 2006). Soil is made up of a group of horizons, where each horizon is determined by color, texture and structure. Soils were characterized by visually examining the trench face at the site, and taking auger samples at three random points across the hillslope. While walking across the trench face, it was immediately apparent that the soils were highly variable both in topography and texture, for example the exposed trench face showed an argillic horizon that was very close to the soil surface, and then appeared to dip down when walking along the trench, as shown in Fig.11. Also note the color changes along the trench face, a soil horizon is determined by a color, texture or structure change, this further supports the idea that soil horizons have large variation across the hillslope.

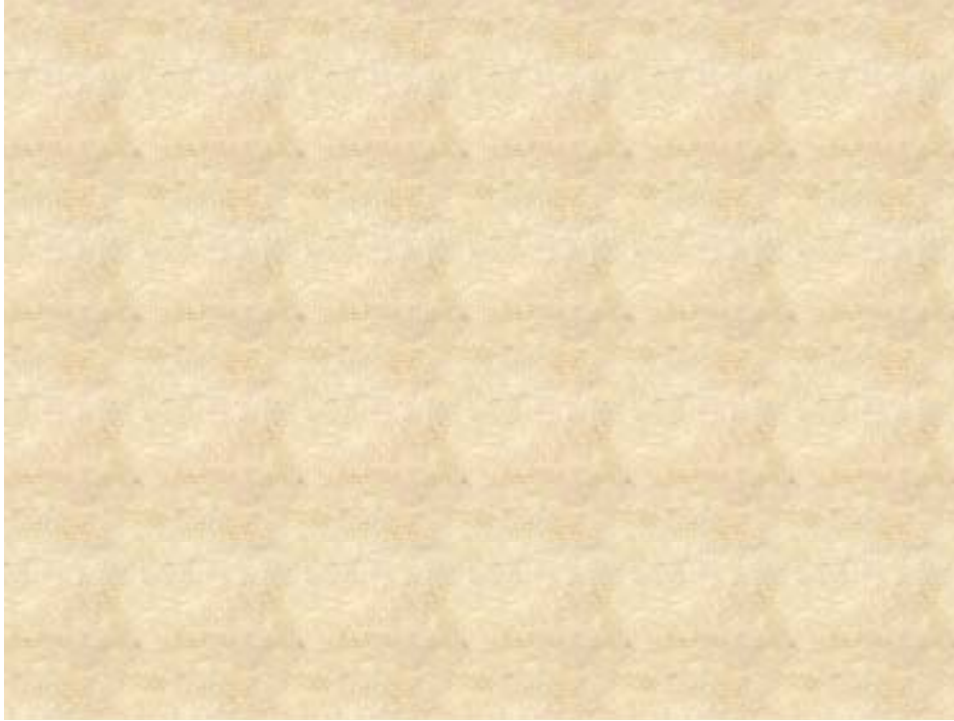


Figure 11. Exposed Soil at SRS Trench Face.

The exposed trench face (Fig's. 11-12) also showed what has been observed at the site, which are loblolly pine roots extending into and through the argillic horizon. Loblolly pine utilizes a tap root which is a large root that extends deep into the soil and explores for water and nutrients. This taproot has the ability to penetrate the argillic horizon and whether natural causes or harvesting removes the top of the tree, the removal of the tree top leaves the taproot to die creating large macropores or soil pipes, which can lead to the rapid flow of water through these created macropores and pipes.



Figure 12. Exposed Trench Face at SRS, Showing Dead Pine.

Samples were obtained at each horizon and particle size distribution (PSD) analysis was performed in the lab, as described in the methods section. PSD of each soil texture (sand, silt and clay) is as follows, where each particle size is in (millimeters) mm.

Sand: Very Coarse (VC) = 2.0 – 1.0 mm; Coarse (C) = 1.0 – 0.5 mm; Medium (M) = 0.5 – 0.25 mm; Fine (F) = 0.25 – 0.10 mm; Very Fine (VF) = 0.10 – 0.05 mm Total (TS) = 2.0 – 0.05 mm.

Silt: 0.05 – 0.002 mm.

Clay: <0.002 mm

PSDs revealed that surface soils and subsurface soils were very different with respect to texture. Surface soils ranged in texture from sand to loamy sand ranging from 85 to 90% TS,

and an average particle size of 86.2% TS (STD = 3.7%) Avg. Bulk Density = 1.78 g/cm³ (STD = 0.08), porosity = 0.33, and a color range of 10YR 4/4 brown to 10YR 5/6 light yellowish brown. Subsurface soils had a texture range of sandy loam to clay, ranging from 10 to 63% clay and an average of 32.1% clay (STD = 19.4%) Avg. Bulk Density = 1.76 g/cm³ (STD = 0.06), porosity = 0.34, and a color range of 2.5YR 5/6 reddish brown to 10YR 5/6 light yellowish brown. A complete field description of the soils can be found in Appendix C.

While some of the Bt or argillic horizons are very low in clay, the above eluvial horizon at this specific site (SRS3) has less than 15% clay, therefore, the increase in clay content in the Bt horizon directly below has to be 3%. Thus the low clay percentages at the site still classify the horizon as an argillic horizon. An argillic horizon is very common in the southeast and is an indication of a very old stable landscape (around the Pliocene age). This is an example of just how variable the textures at the site truly are. Interestingly enough, both texture and subsurface topography of the argillic horizon make this site a very difficult site to characterize in terms of the soil's influence on interflow.

Large discrepancies in PSD for each horizon could be an artifact of depositional events, as there are a few different parent material types for the soils at the site. Parent materials ranged from fluvio-marine and marine, to alluvial and eolian.

Soils were classified based upon PSD and field observations. Each site (SRS1, SRS2 and SRS3) (Tables 2-4) was classified and consequently had very different soil series and classifications. According to the NRCS soil classification system, which can be found at <http://www2.ftw.nrcs.usda.gov/osd>, soils at the site are classified as:

SRS1: Ailey series; The Ailey series is classified as being in the loamy, kaolinitic, thermic, Arenic Kanhapludults.

SRS2: Goldsboro taxadjunct; The Goldsboro series is classified as being in the fine-loamy, kaolinitic, thermic, Aquic Kandiudults.

SRS3: Lucknow series; The Lucknow Series is classified as being in the loamy, kaolinitic, thermic, Grossarenic Kandiudults.

Table 2. PSD SRS 1.

		PARTICLE SIZE DISTRIBUTION (MM)									
		-----SAND-----									
SITE	HORIZON	DEPTH	VC	C	M	F	VF	TOTAL	SILT	CLAY	TEXTURE
		(CM)	(2.0-1.0)	(1.0-0.5)	(0.5-0.25)	(0.25-0.10)	(0.10-0.05)	(2.0-0.05)	(0.05-0.002)	(< 0.002)	CLASS
		-----%-----									
SRS-1											
	A	0-5	5.8	14.0	24.1	31.6	12.2	87.8	10.9	1.4	sand
	E	5-61.0	10.3	19.0	26.2	23.4	7.3	86.1	12.3	1.6	sand
	Bt1	61-84	4.0	19.9	26.4	13.0	4.0	67.4	9.7	22.9	sandy clay loam
	Bt2	84-96	2.4	20.8	23.4	5.3	1.4	53.3	6.6	40.1	sandy clay
	BC1	96-120	3.7	28.3	23.1	4.3	1.0	60.3	5.5	34.2	sandy clay loam
	BC2	120-145+	6.8	30.1	23.9	5.4	1.3	67.5	6.1	26.4	sandy clay loam

Table 3. PSD SRS 2.

		PARTICLE SIZE DISTRIBUTION (MM)									
		-----SAND-----									
SITE	HORIZON	DEPTH	VC	C	M	F	VF	TOTAL	SILT	CLAY	TEXTURE
		(CM)	(2.0-1.0)	(1.0-0.5)	(0.5-0.25)	(0.25-0.10)	(0.10-0.05)	(2.0-0.05)	(0.05-0.002)	(< 0.002)	CLASS
		-----%-----									
SRS-2											
	A	0-15	10.0	24.3	29.4	17.5	4.7	85.8	11.1	3.1	loamy sand
	BA	15-41	9.5	20.2	26.5	16.7	4.7	77.6	13.4	9.0	sandy loam
	Bt1	41-74	7.3	17.1	20.4	12.3	3.6	60.7	11.0	28.3	sandy clay loam
	Bt2	74-137+	3.4	10.8	9.7	3.5	1.1	28.4	7.8	63.8	clay

Table 4. PSD SRS 3.

		PARTICLE SIZE DISTRIBUTION (MM)									
		-----SAND-----									
SITE	HORIZON	DEPTH	VC	C	M	F	VF	TOTAL	SILT	CLAY	TEXTURE
		(CM)	(2.0-1.0)	(1.0-0.5)	(0.5-0.25)	(0.25-0.10)	(0.10-0.05)	(2.0-0.05)	(0.05-0.002)	(< 0.002)	CLASS
		-----%-----									
SRS-3											
	A	0-20	11.4	29.2	27.1	17.6	4.9	90.2	8.0	1.8	sand
	E1	20-83	9.6	29.8	25.3	16.3	5.2	86.2	11.5	2.4	loamy sand
	E2	83-100	21.5	29.3	21.0	13.0	3.9	88.6	10.6	0.8	sand
	E3	100-115	20.6	32.3	20.1	10.5	3.5	87.0	9.9	3.1	sand
	Bt1	115-141	11.2	25.4	22.7	15.2	4.9	79.3	10.9	9.8	sandy loam

Soil hydraulic results

Field data were collected at 16 random locations across the hillslope to determine in-situ Ks of the surface (sand), subsurface (middle-sand and deep-argillic) horizons. As is evidenced by the graph (Fig. 13), Ks of the surface and mid horizons are very similar. However, the

subsurface argillic horizon Ks is markedly lower. Table 5 presents in-situ Ks determined using the static Glover solution.

Table 5. In-Situ Ks.

Horizon	Depth	Ks
	Cm	cm/h
Surface	22	20.084
Surface	23	26.310
Surface	29	20.458
Surface	20	6.548
Surface	22.5	5.800
Surface	22	4.154
Mid	50	14.385
Mid	60	12.471
Mid	35	7.126
Mid	52	7.311
Mid	57	5.839
Argillic	80	0.043
Argillic	88	0.043
Argillic	140	4.372
Argillic	105	0.066
Argillic	141	0.512
Argillic	112	0.247609
Argillic	100	0.008528
Argillic	88	0.197366
Argillic	147	0

Data from this table were used to create the following graph of in-situ Ks. It is interesting to note that surface and mid Ks values are very similar, this is not surprising as both depths (surface and mid) have the same soil texture (sand). However, the argillic horizon Ks values are strikingly different, with values one to three orders of magnitude lower than both surface and mid horizons. The argillic horizon does have one value that stands out amongst the rest, that is the reading at a depth of 140 cm where Ks = 4.372 cm/h (Table. 5). This reading is very different than the rest of the readings from the argillic horizon and is consequently similar to some of the readings in the surface and mid horizons (i.e. depths of 22.5 and 22 cm in the surface horizon and 57 cm in the mid horizon).

Table 6. Moisture Release Data. Core 35.

Core 35 Sand

Pressure Head (cm)	Total Mass soil+core+water (g)	Mass water (g)	Theta G (g/g)	Theta V (cm ³ /cm ³)
0	918.2	98.0	0.149	0.282
-10	906.2	86.0	0.130	0.247
-20	897.4	77.2	0.117	0.222
-30	878.8	58.6	0.089	0.169
-40	865.3	45.1	0.068	0.130
-50	855.6	35.4	0.054	0.102
-60	838.6	18.4	0.028	0.053
-70	833.9	13.7	0.021	0.039
-80	832.0	11.8	0.018	0.034
-90	830.9	10.7	0.016	0.031

Mass Oven Dry (g)	820.2
Mass Soil Core (g)	160.68
Mass Soil (g)	659.52
Volume (cm ³)	347.49
Bulk Density (g/cm ³)	1.90

Table 7. Moisture Release Data. Core 457.

Core 457 Sand

Pressure Head (cm)	Mass soil+core+water (g)	Mass water (g)	Theta G (g/g)	Theta V (cm ³ / cm ³)
0	874.1	90.2	0.14	0.26
-10	859.5	75.6	0.12	0.22
-20	849.3	65.4	0.10	0.19
-30	829.8	45.9	0.07	0.13
-40	811.2	27.3	0.04	0.08
-50	800.8	16.9	0.03	0.05
-60	794.1	10.2	0.02	0.03
-70	791.4	7.5	0.01	0.02
-80	790.0	6.1	0.01	0.02
-90	789.7	5.8	0.01	0.02

Mass Oven Dry (g)	783.86
Mass Soil Core (g)	156.63
Mass Soil (g)	627.23
Volume (cm ³)	347.49
Bulk Density (g/cm ³)	1.81

Table 8. Moisture Release Data. Core 334.

Core 334 Sand

Pressure Head (cm)	Mass soil+core+water (g)	Mass water (g)	Theta G (g/g)	Theta V (cm ³ / cm ³)
0	872.8	94.2	0.15	0.27
-10	856.2	77.6	0.12	0.22
-20	835.0	56.4	0.09	0.16
-30	820.0	41.4	0.07	0.12
-40	806.7	28.1	0.05	0.08
-50	800.3	21.7	0.03	0.06
-60	788.3	9.6	0.02	0.03
-70	784.9	6.3	0.01	0.02
-80	783.7	5.1	0.01	0.01
-90	783.7	5.1	0.01	0.01

Mass Oven Dry (g)	778.65
Mass Soil Core (g)	156.08
Mass Soil (g)	622.57
Volume (cm ³)	347.49
Bulk Density (g/cm ³)	1.79

Table 9. Moisture Release Data. Core 118.

Core 118 Argillic

Pressure Head (cm)	Total Mass soil+core+water (g)	Mass water (g)	Theta G (g/g)	Theta V (cm ³ /cm ³)
0	885.8	116.4	0.19	0.33
-10	873.3	103.9	0.17	0.30
-20	874.8	105.4	0.17	0.30
-30	874.3	104.9	0.17	0.30
-40	874.0	104.6	0.17	0.30
-50	873.3	103.9	0.17	0.30
-60	859.0	89.6	0.15	0.26
-70	858.7	89.3	0.15	0.26
-80	858.4	89.0	0.15	0.26
-90	858.3	88.9	0.14	0.26

Mass Oven Dry (g)	769.43
Mass Soil Core (g)	156.35
Mass Soil (g)	613.08
Volume (cm ³)	347.49
Bulk Density (g/cm ³)	1.76

Table 10. Moisture Release Data. Core 319.

Core 319 Argillic

Pressure Head (cm)	Total Mass soil+core+water (g)	Mass water (g)	Theta G (g/g)	Theta V (cm ³ /cm ³)
0	870.1	114.2	0.19	0.33
-10	858.0	102.1	0.17	0.29
-20	857.6	101.7	0.17	0.29
-30	857.4	101.5	0.17	0.29
-40	856.6	100.7	0.17	0.29
-50	855.6	99.7	0.17	0.29
-60	839.4	83.5	0.14	0.24
-70	838.9	83.0	0.14	0.24
-80	838.1	82.2	0.14	0.24
-90	838.0	82.1	0.14	0.24

Mass Oven Dry (g)	755.86
Mass Soil Core (g)	156.69
Mass Soil (g)	599.17
Volume (cm ³)	347.49
Bulk Density (g/cm ³)	1.72

Table 11. Moisture Release Data. Core 391.

Core 391 Argillic

Pressure Head (cm)	Mass soil+core+water (g)	Mass water (g)	Theta G (g/g)	Theta V (cm ³ / cm ³)
0	883.1	124.2	0.21	0.36
-10	868.9	110.0	0.18	0.32
-20	868.0	109.1	0.18	0.31
-30	867.9	109.0	0.18	0.31
-40	866.7	107.8	0.18	0.31
-50	865.9	107.0	0.18	0.31
-60	843.1	84.2	0.14	0.24
-70	840.7	81.8	0.14	0.24
-80	840.1	81.2	0.13	0.23
-90	839.4	80.5	0.13	0.23

Mass Oven Dry (g)	758.89
Mass Soil Core (g)	156.71
Mass Soil (g)	602.18
Volume (cm ³)	347.49
Bulk Density (g/cm ³)	1.73

Table 12. Moisture Release Data. Core 453.

Core 453 Argillic

Pressure Head (cm)	Mass soil+core+water (g)	Mass water (g)	Theta G (g/g)	Theta V (cm ³ / cm ³)
0	923.3	125.4	0.20	0.36
-10	909.7	111.8	0.17	0.32
-20	910.7	112.8	0.18	0.32
-30	909.9	112.0	0.17	0.32
-40	909.2	111.3	0.17	0.32
-50	908.6	110.7	0.17	0.32
-60	890.0	92.1	0.14	0.27
-70	889.1	91.2	0.14	0.26
-80	889.1	91.2	0.14	0.26
-90	888.4	90.5	0.14	0.26

Mass Oven Dry (g)	797.87
Mass Soil Core (g)	156.21
Mass Soil (g)	641.66
Volume (cm ³)	347.49
Bulk Density (g/cm ³)	1.85

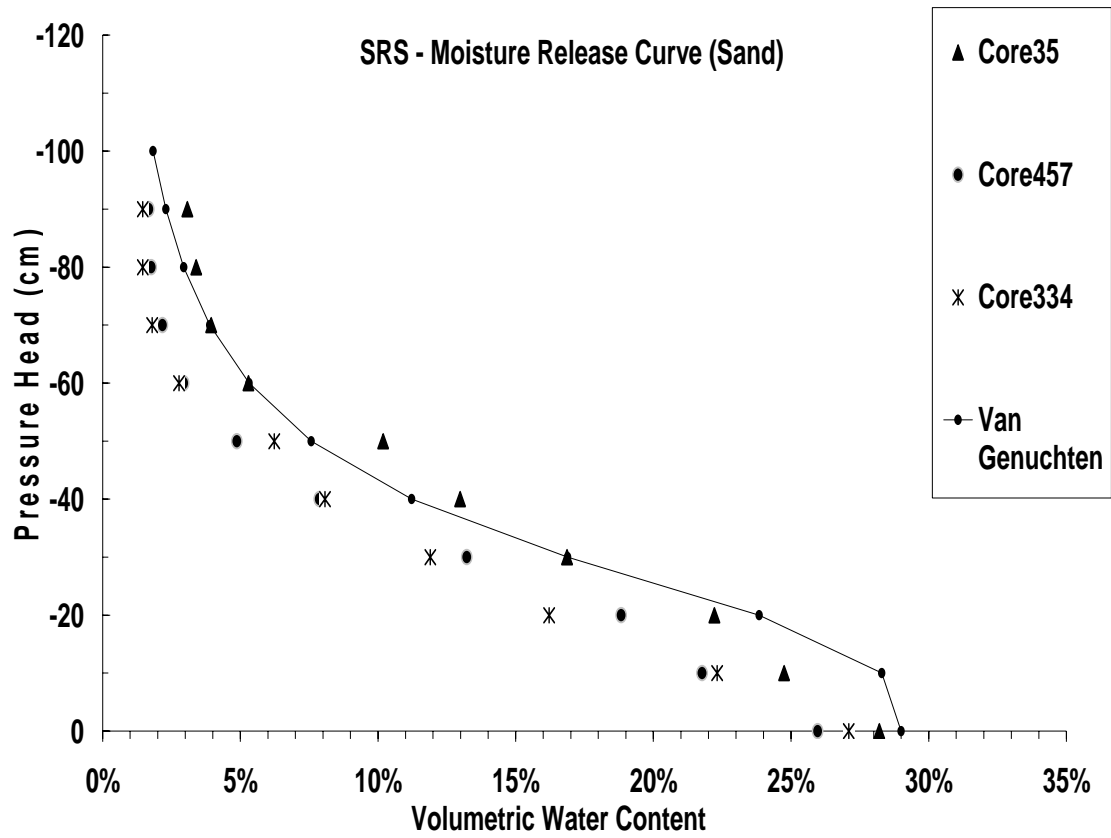


Figure 14. Moisture Release (sand).

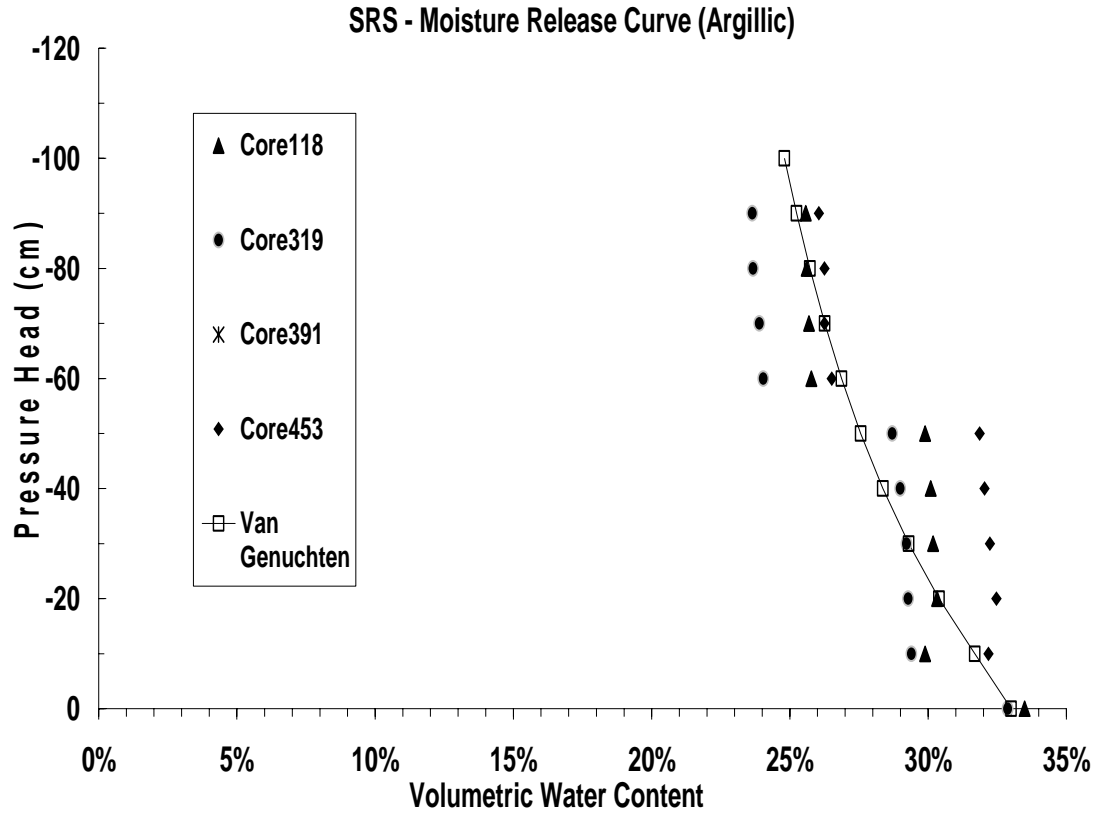


Figure 15. Moisture Release (argillic).

Tables 13-16 present data collected from the sampling grid detailed in the materials and methods section. Each X and Y coordinate have both north (N) and south (S) aspects, which correspond to the direction away from the X or Y line that data points were collected from, it should also be noted that spacing in the X or Y direction is 4 m, while N and S aspect spacing every 2 m each value represents depth (cm) to the top of argillic horizon.

Table 13. XS Soil Sampling Grid (depth to argillic). The table represents “X” line positions from 0 to 52 m across and “S” or south sampling points within the sampling grid. Data within the table are depth to argillic as measured with the tile probe, where the deepest of three measurements was recorded.

	X 0	X 4	X 8	X 12	X 16	X 20	X 24	X 28	X 32	X 36	X 40	X 44	X 48	X 52
S 0	150	138	115	107	108	101	74	88	118	50	75	58	90	87.5
S 1	120	150	125	96	91	85.5	95	121	96	83	85	61	105.5	96
S 2	137	130	86	102	91	101	97	76	105	67	65	72	97	84
S 3	113	131	93	102	116	97	100	115	77	70.5	77	89	98.5	104
S 4	112	90	94	106	102	80	139	88.5	105	85.5	75	92	103.5	123.5
S 5	115	139	135	138	120	58	94.5	94	97	104.5	79	97	126	110
S 6	124	114	137	103.5	117	94	89	114	136	61	88	91.5	93	90
S 7	141	143	136	101	93.5	88.5	82	101	74	84	93	88	143	91.5
S 8	143	144	111	132	87	80.5	125	86.5	105.5	74	89	102	83.5	150
S 9	134.5	124	125	102	96	62	76	104	78	105	150	76	143	150
S 10	113	111.5	116	105	128	89.5	98.5	74	98.5	75	83.5	142	118.5	123
S 11	114	135	129.5	78	140	125	104	102	108	95.5	81	121	136	150
S 12	85	109	127	115	126	89	98	98.5	108	109.5	107	150	135	66
S 13	109	140	91	112	93	94	90	116	114	75.5	62	127	134.5	97
S 14	130	90	107	121	85	73.5	103.5	110	119	110	122	66	108.5	128
S 15		99	86	113	89	73	100	104	65	63	61	60.5	122	56
S 16		81	98.5	124	96.5	67	69	106.5	95.5	135.5	103	93	114	104
S 17					76.5	108	39	70	67	80.5	75	88	108	98
S 18					73		89	46	101	79	99	71	103	66
S 19							117.5	126	102	136.5	77.5	95	113	103
S 20							58	99.5	132	71.5	105	82	76	107.5
S 21										128	107	80	127	109.5
S 22										108	75	97.5	122	101
S 23										130	86	82	88	88
S 24													116	68
S 25														80

Table 14. XN Soil Sampling Grid (depth to argillic). The table represents “X” line positions from 0 to 52 m across and “N” or north sampling points within the sampling grid. Data within the table are depth to argillic as measure with the tile probe, where the deepest of three measurements was recorded.

	X 0	X 4	X 8	X 12	X 16	X 20	X 24	X 28	X 32	X 36	X 40	X 44	X 48	X 52
N 0	150	138	115	107	108	101	74	88	118	80.3	76.3	104.6	105.6	107.9
N 1	81	86	71.5	65	80	28.5	60	63	70.1	63	150	101.4	96.3	118.5
N 2	50	103	54	74	82	39.4	57.5	47.5	55	40	84.5	100.4	121	112.6
N 3	50	70	35	48	72	25.4	49	50	38.1	28	97	96.3	108.6	105
N 4	62	75	66	54	51	19.5	30.3	32	35	36.4	98.8	87.3	107.4	105
N 5	98	57	73.5	46	48	18.5	24.4	46	24.4	21.6	73.6	87.5	104	93.4
N 6	60	50	118	41	46	19.3	25	23	26	23	77.5	109.6	102.3	91.4
N 7	53	56	53			28	22	19		33.6	62.4	106.6	93	105
N 8	72.5	49	53				29.5	21		23.5	114	80.2	105	99.5
N 9	60	61	57				24.5	23		20.6	63.5	96	89.6	98.7
N 10	71	68	69							20	60.3			103.2
N 11										30	93.8			

Table 15. YS Soil Sampling Grid (depth to argillic). The table represents “Y” line positions from 0 to 52 m across and “S” or south sampling points within the sampling grid. Data within the table are depth to argillic as measure with the tile probe, where the deepest of three measurements was recorded.

	Y 0	Y 4	Y 8	Y 12	Y 16	Y 20	Y 24	Y 28	Y 32	Y 36	Y 40	Y 44	Y 48.45
S 0	32.0	41.0	24.0	63.1	73.0	43.0	104.1	76.8	21.4	48.4	77.9	83.5	118.5
S 1	22.0	40.0	21.0	24.0	20.0	62.0	100.8	98.8	33.4	20.5	80.0	72.6	117.7
S 2	17.0	24.0	52.0	65.5	52.0	83.0	85.0	77.3	30.0	21.5	93.7	59.8	87.3
S 3	33.0	39.0	32.0	46.0	43.5	84.0	120.4	100.5	40.8	38.4	86.5	79.0	64.4
S 4	16.0	26.0	51.0	41.0	63.0	54.0	79.5	76.6	58.4	43.9	50.5	77.5	84.2
S 5	31.0	23.0	25.0	38.0	68.0	62.0	89.0	122.2	42.6	30.8	61.1	72.0	78.0
S 6	24.0	51.0	40.0	43.0	76.0	71.0	91.8	87.5	36.8	31.0	63.8	96.4	94.2
S 7	29.0	45.0	23.5	61.0	150.0	69.0	102.0	119.4	21.2	21.0	55.4	80.6	84.0
S 8	23.0	25.5	49.0	84.0	97.0	86.0	150.0	117.0	69.8	19.4	65.0	81.0	78.0
S 9	20.5	19.5	41.5	88.0	63.0	103.2	150.0	114.6	75.3	33.0	62.9	75.4	60.4
S 10	40.0	19.5	42.0	44.0	72.0	95.8	103.5	107.1	49.7	20.0	77.5	72.6	70.0
S 11			64.0	54.0	87.0	84.6	129.9	129.5	19.6		61.4		
S 12			57.0	93.0	95.0	101.4	116.0	70.0	75.2				
S 13			56.0	75.0		103.6	84.8	63.5					
S 14				32.0		63.0							
S 15				52.0		51.6							

Table 16. YN Soil Sampling Grid (depth to argillic). The table represents “Y” line positions from 0 to 52 m across and “N” or north sampling points within the sampling grid. Data within the table are depth to argillic as measure with the tile probe, where the deepest of three measurements was recorded.

	Y 0	Y 4	Y 8	Y 12	Y 16	Y 20	Y 24	Y 28	Y 32	Y 36	Y 40	Y 44	Y 48.45
N 0	32	41	24	63.1	73	21	46	26	24	19.5	21.4	16.6	59.3
N 1	61	81	28	72.1	61.6	22	58	44.8	26	62.4	31.3	25.4	47
N 2	35	71	72.5	75.4	80	19	23	47.4	41	24	60.3	35.3	49.6
N 3	51	77	68.5	74.3	81.5	18	40.5	37	38.3	38.5	29.5	64.5	58.5
N 4	82	87	82	65.9	69	26	49	47	51.5	50	35.5	60.6	92.9
N 5	25.5	34.5	53	97	96	15	45	53	50	55	52.6	53.4	65.4
N 6	50.8	32	48	91	68.4	41	58	34	47.4	49	55.6	70	63
N 7	43	68.5	38	70	57.6	45	27	36	19	52.3	55.9	58	81
N 8	40	52	62	58	24.5	46	26	42.5	27	52.5	61	25	101.3
N 9	113	39	74	60	53.4	31	31.5	19	36	65.5	57	85.9	79.6
N 10	30	59	21.5	58.5	54.4	37	20	17	53.4	62.7	50	91	81.3
N 11	54.5	58.5	24	70	45.5	27	33	40.5	58				
N 12	66	56	17	63	45.8	33	29						
N 13	38	51.5	22	41	59.7	31							
N 14		24	55	80	58.3								

The following maps (Figs.16-18) and plan view graphs (Figs. 20-21) (line 0 and 52; and 8 and 36), were created from tables 13 through 16. One should note the first map, ‘Depth to Argillic’ has all the sampling points that were used across the hillslope, showing the precise and uniform grid system. Also, the depth to argillic is highly variable in both N and S directions, as well as across lines X and Y. Plan view graphs (Fig. 20 and 21) of the depth to clay across the trench also show a highly variable depth to clay, each graph was creating by taking four random “lines” (0, 8, 36, and 52) from the grid set up on the hillslope. While depth to clay is highly variable, there appears to be a few distinct subsurface channels, in the middle of the hillslope (referencing across the trench the horizon dips creating what looks like subsurface channels at or around 20 m, 40 m, 60 m, and 80 m), with multiple sections of the hillslope contributing to this channel.

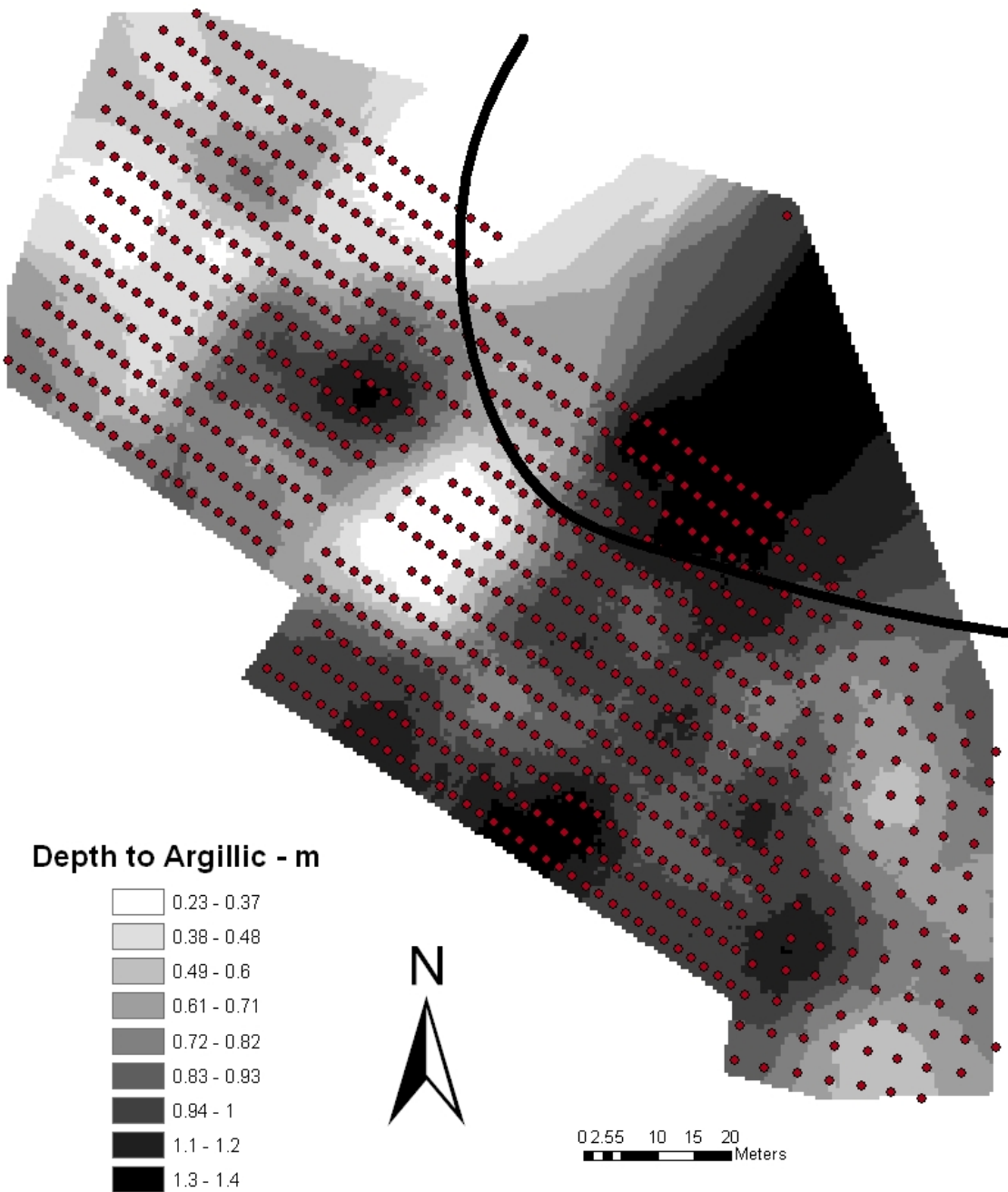


Figure 16. Map of Depth to Argillic with Soil Sample Points. The trench line roughed in (black line), was drawn in with previous surveyed points. The actual trench at the site, is a few meters southwest of line shown here. This is true for all maps with trench drawn in.

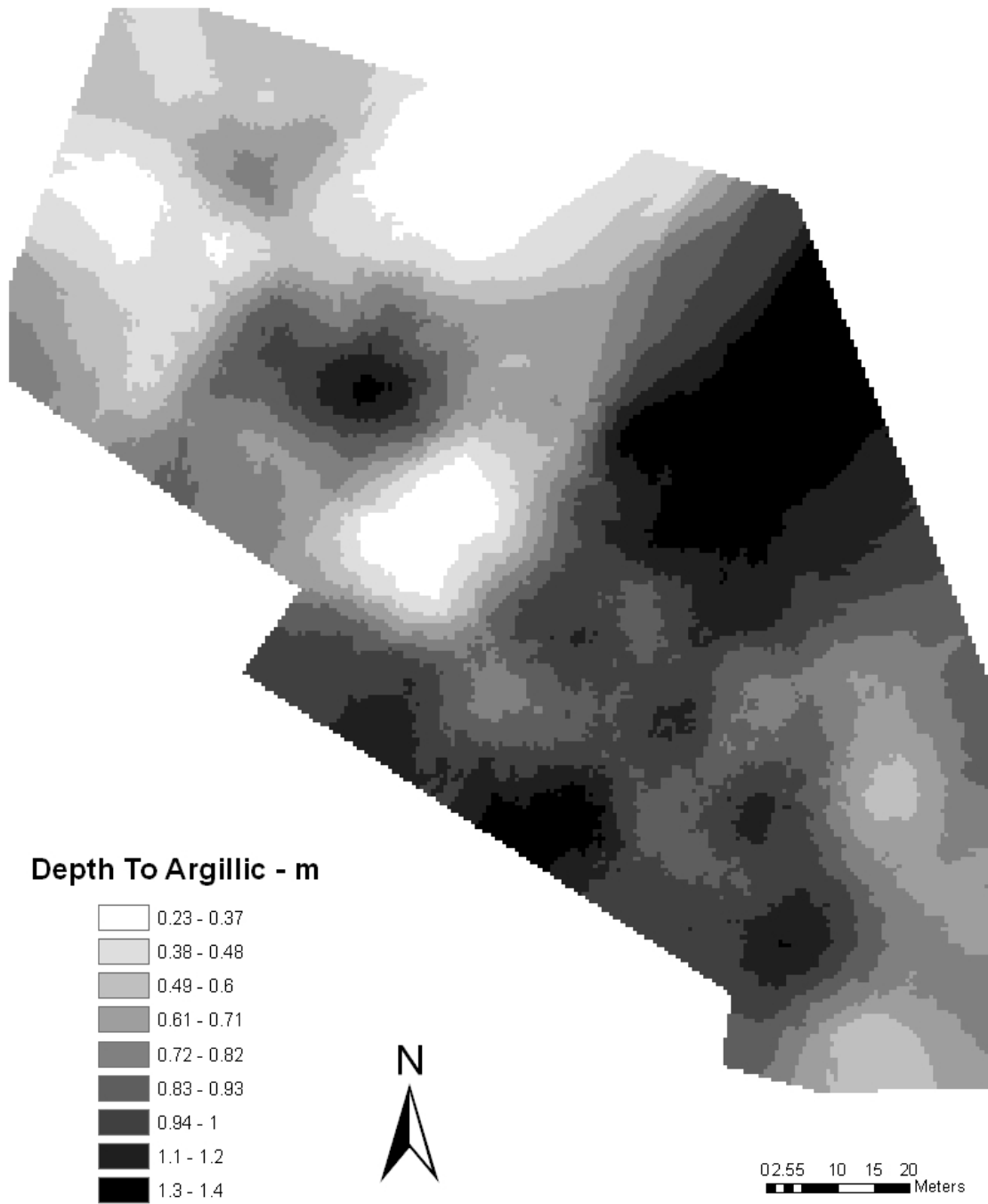
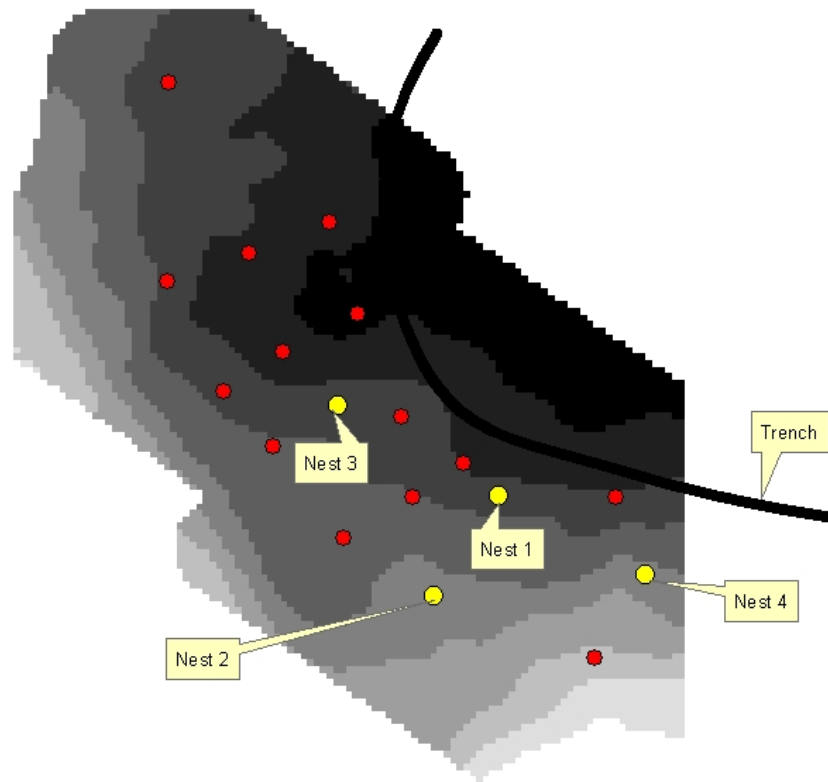
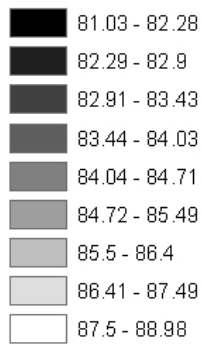


Figure 17. Map of Depth to Argillic Horizon.



Argillic Topograhly - m



- Max Rise Piezometer
- Piezometer Nest

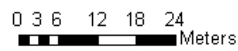
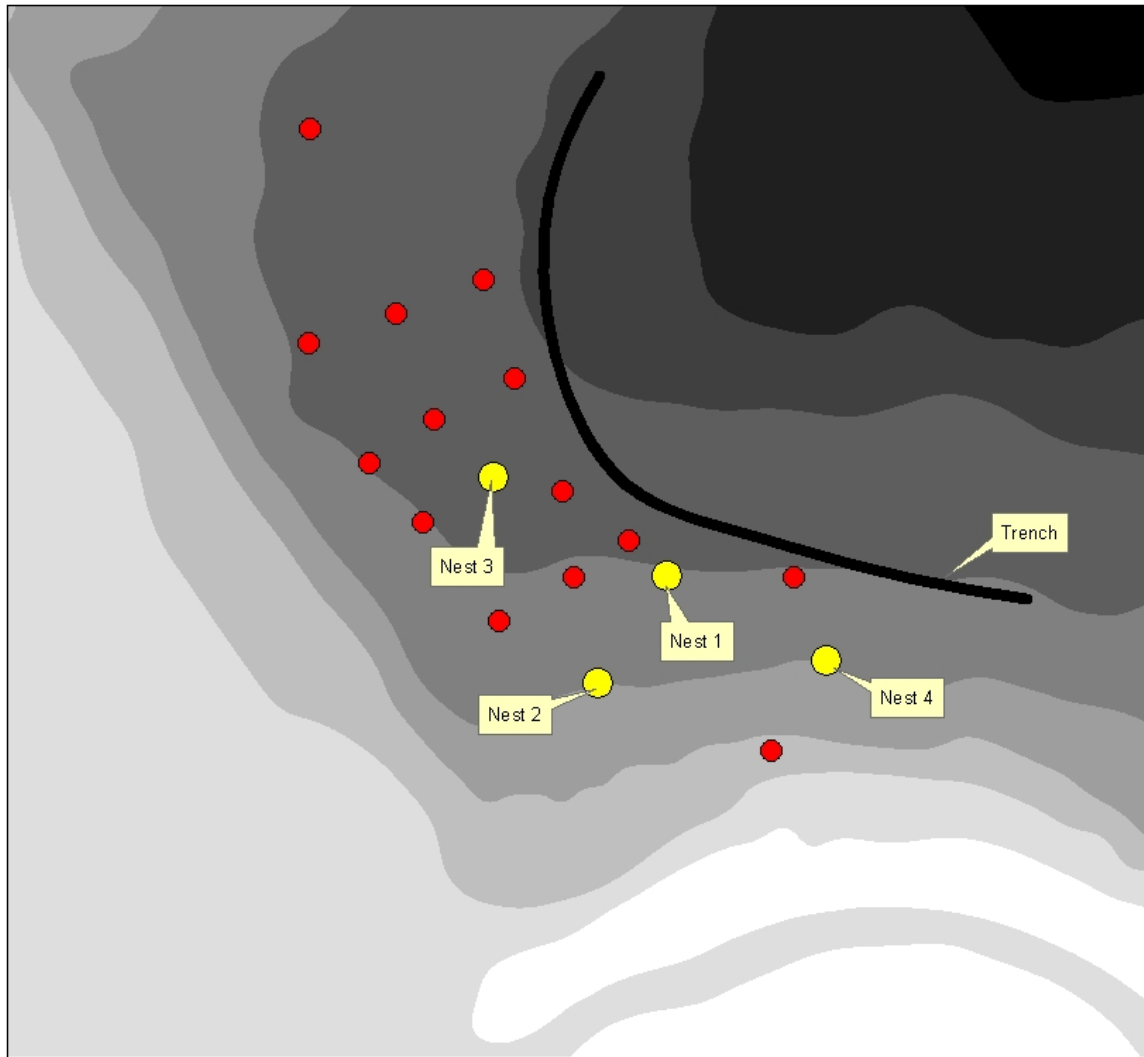
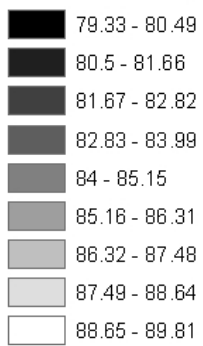


Figure 18. Map of Argillic Topography with Piezometer Nests and Trench.



Surface Topography - m



● Max Rise Piezometer

● Piezometer Nest

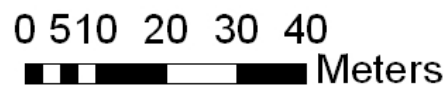


Figure 19. Surface Topography.

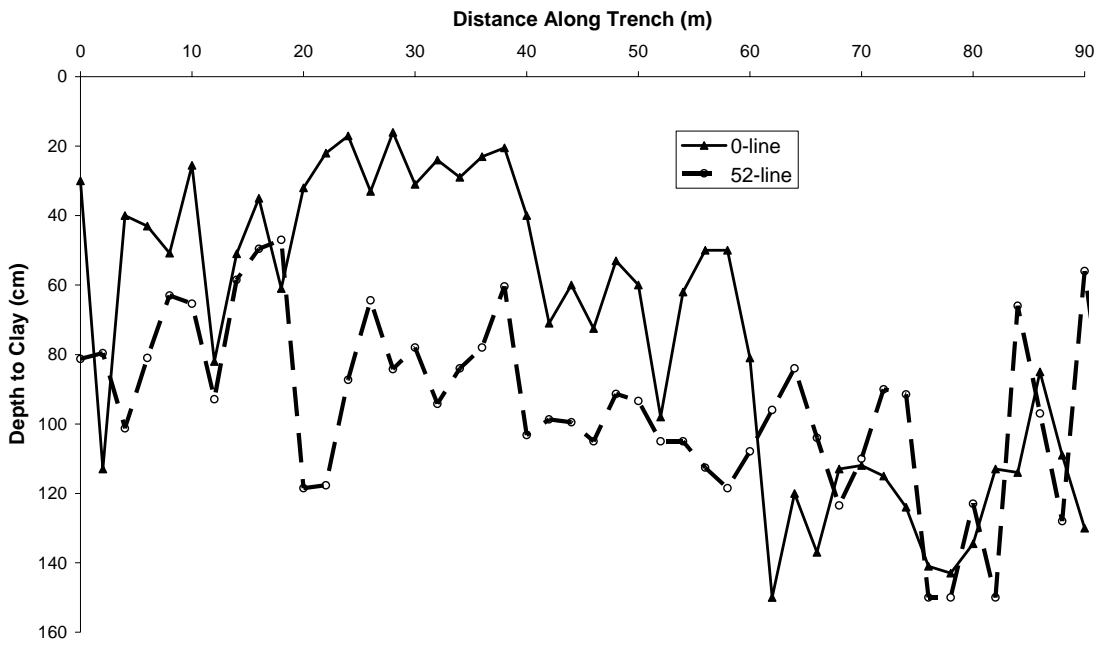


Figure 20. Plan View Schematic of Depth to Argillic Along Trench (Lines 0 and 52).

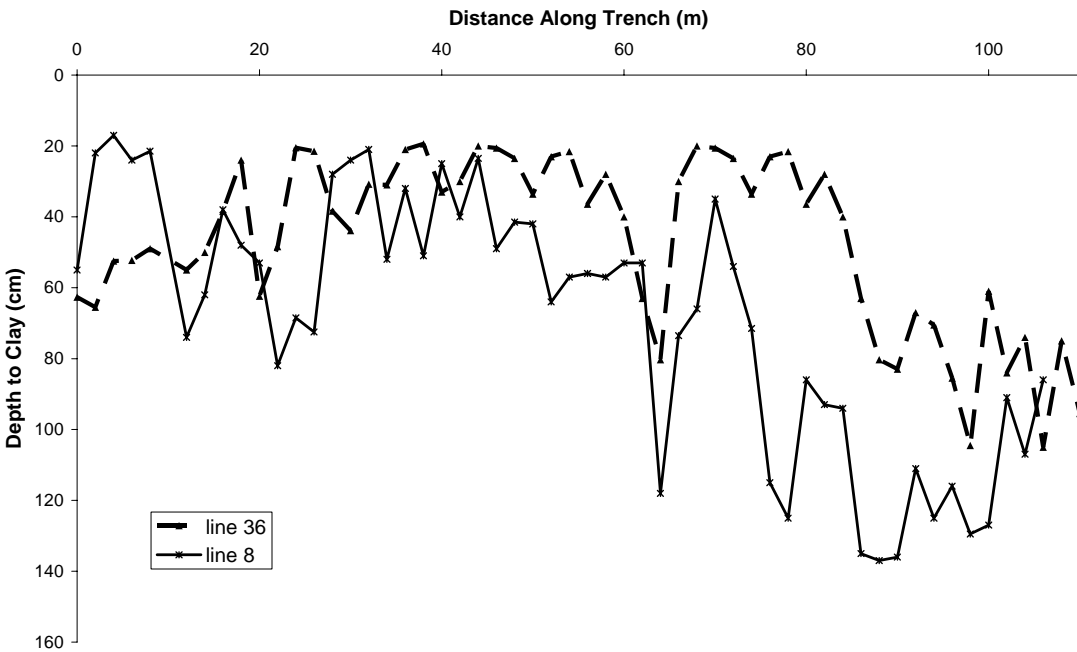


Figure 21. Plan View Schematic of Depth to Argillic Along Trench (Lines 8 and 36).

4.2 Hydrologic Results:

The period of record (6-29-06 to 7-2-07), was considered a drought year, as precipitation was about 287 mm less than normal. Figure 22 is a comparison of long term monthly average precipitation from 1948 to 2007 measured at a rain-gage in Aiken, SC. vs. the precipitation measured at the site.

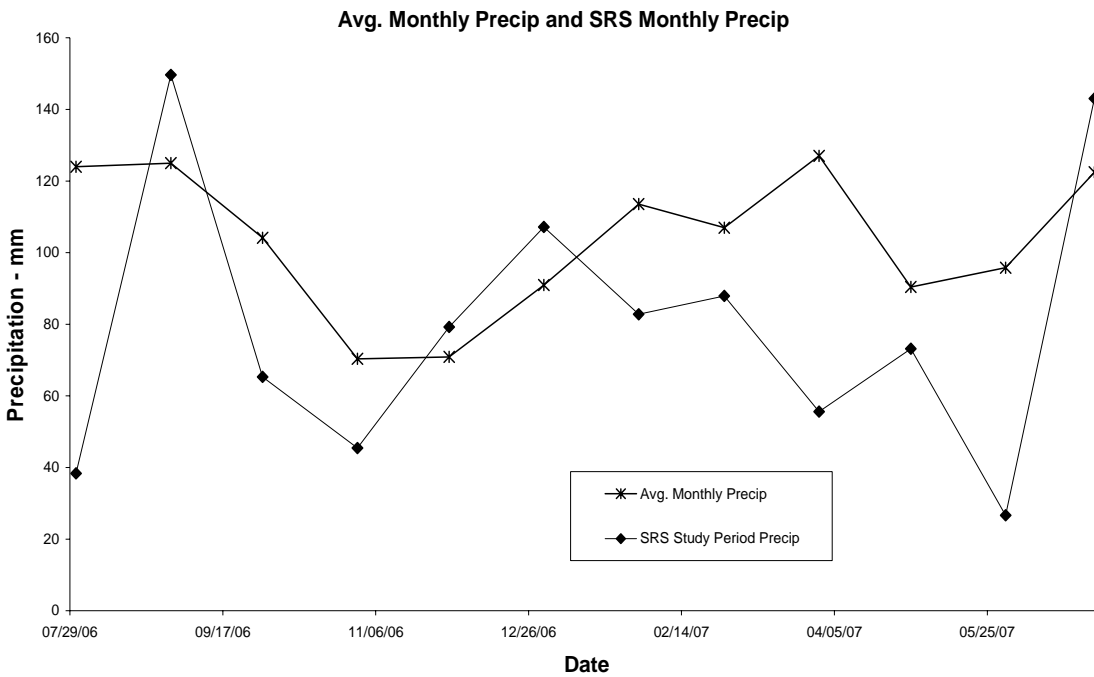


Figure 22. Long Term Average Monthly Precipitation and SRS Monthly Precipitation.

From figure 22, it is clear that August, November and December 2006 as well as June 2007 are the only months that precipitation exceeds the monthly average, all other months are below average. Figure 23 presents the cumulative precipitation deviation from measured monthly average precipitation throughout the study period (7/31/2006 to 6/29/2007).

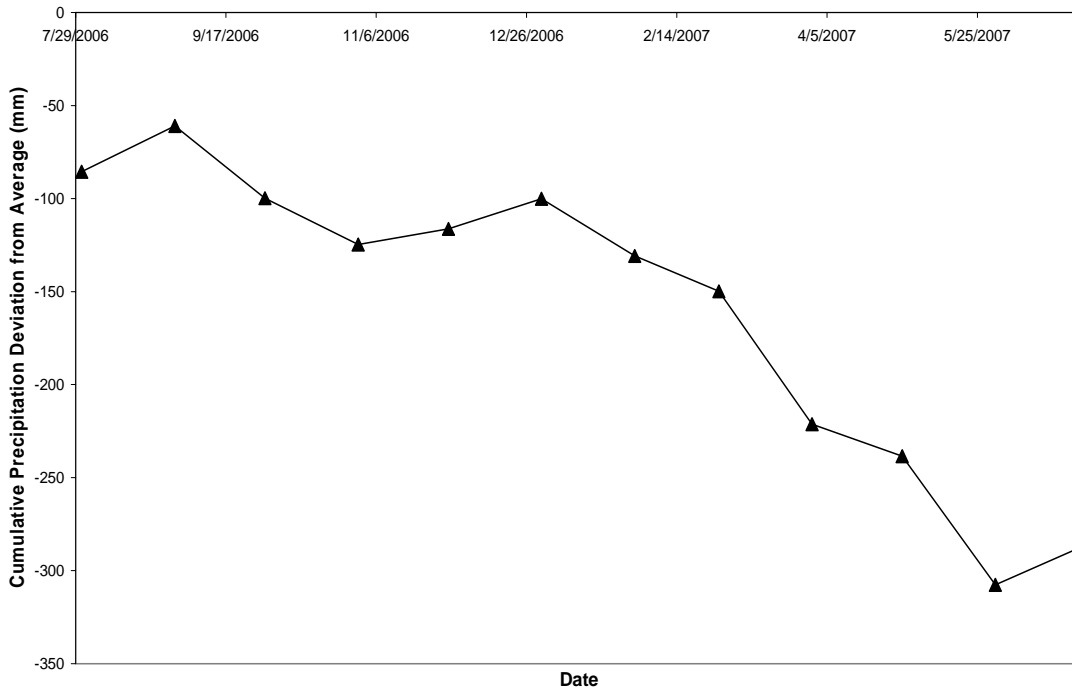


Figure 23. Cumulative Precipitation Deviation from Average.

Figures 24 to 37 present one year of data from the hillslope site, each figure is from a piezometer nest with all piezometers (A, IC and D), where elevation is the water surface elevation in (m) or total head (h) as related to discharge (Q) in liters per second (L/s). Other figures include a graph of the Alluvial floodplain piezometer (Alluvial FP) as related to Q, as well as individual perching events, at each piezometer nest.

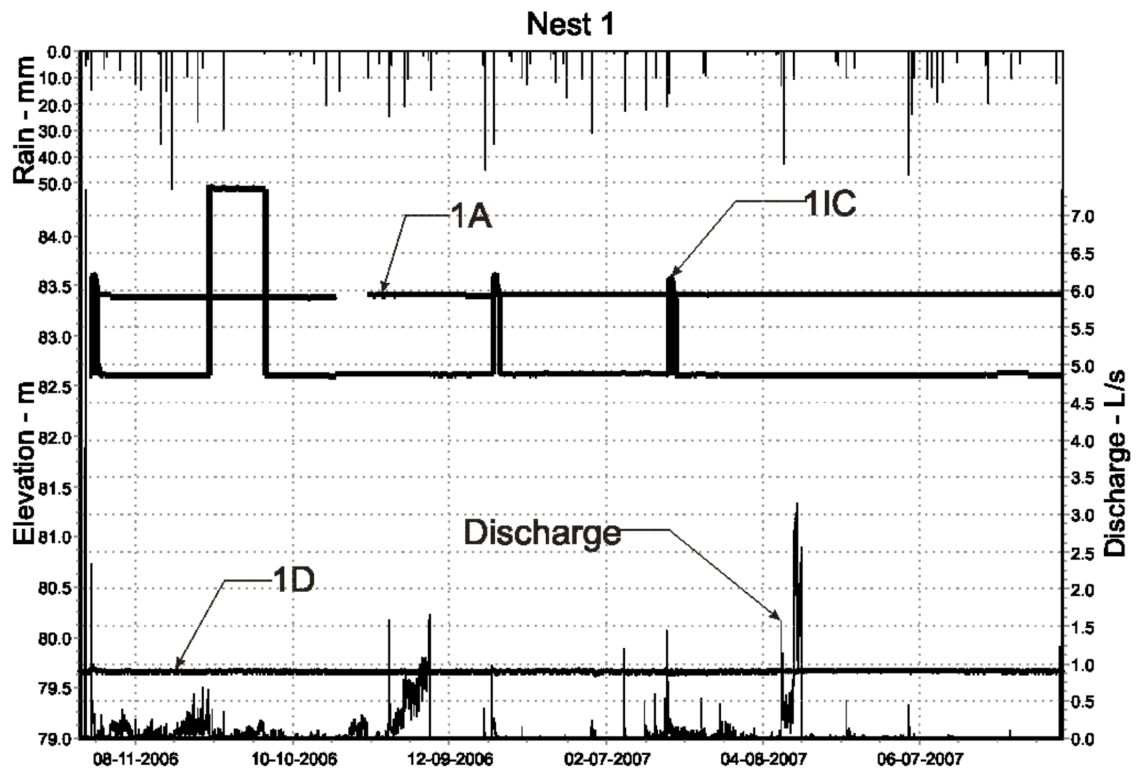


Figure 24. Graph of Piezometer Nest 1. Entire Study Period.

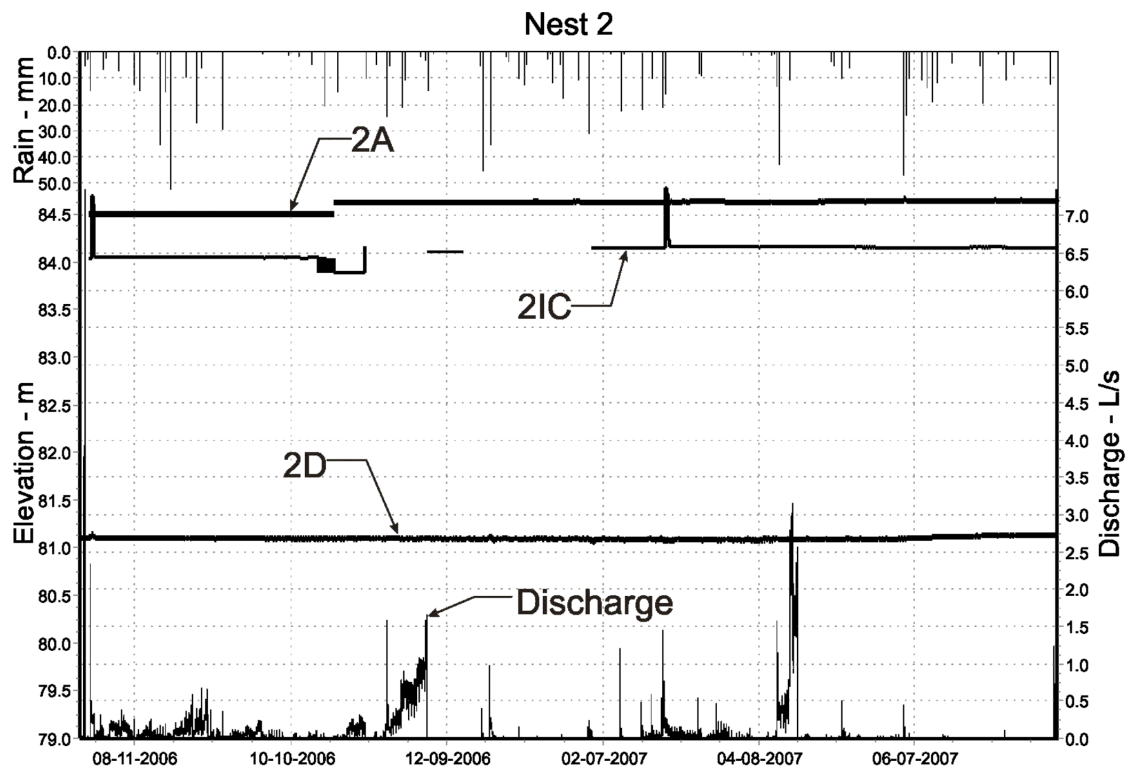


Figure 25. Graph of Piezometer Nest 2. Entire Study Period.

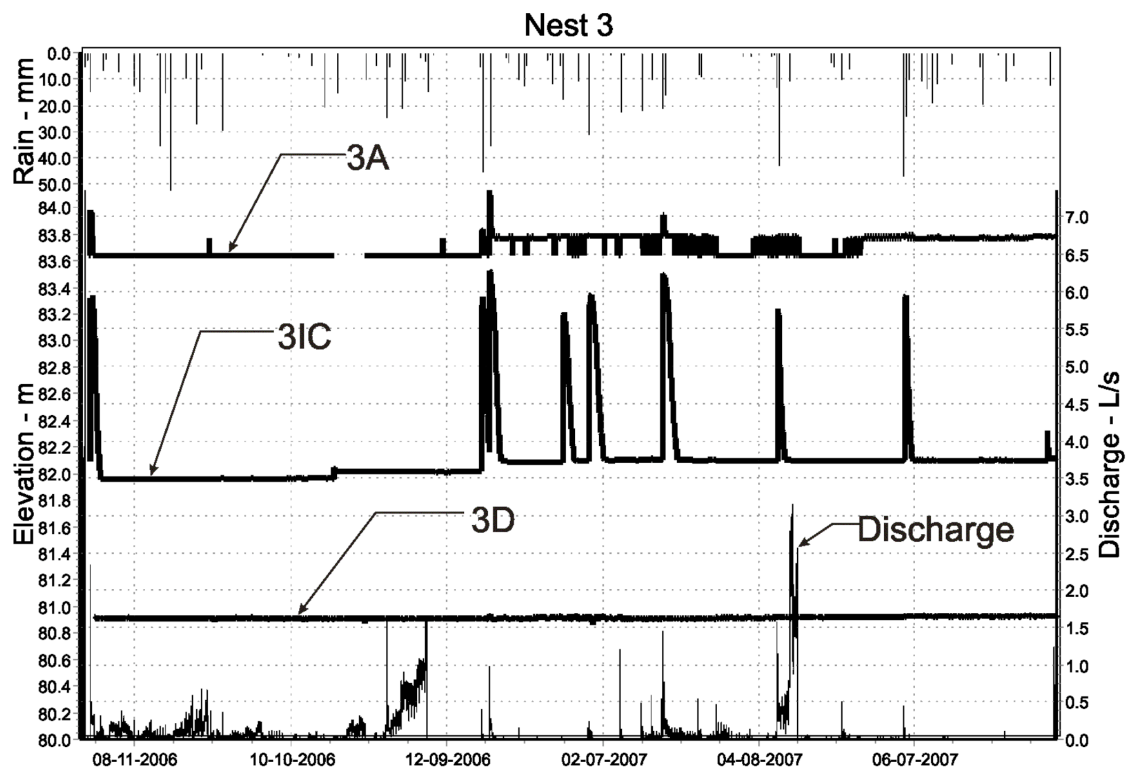


Figure 26. Graph of Piezometer Nest 3. Entire Study Period.

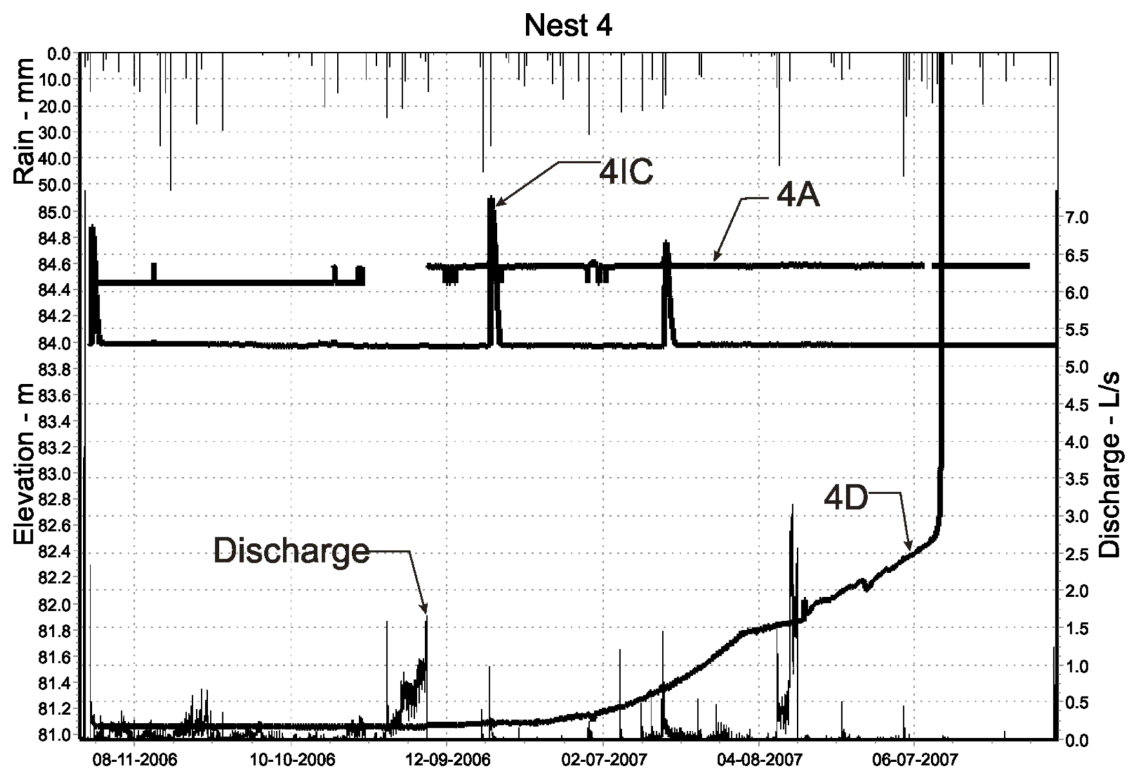


Figure 27. Graph of Piezometer Nest 4. Entire Study Period.

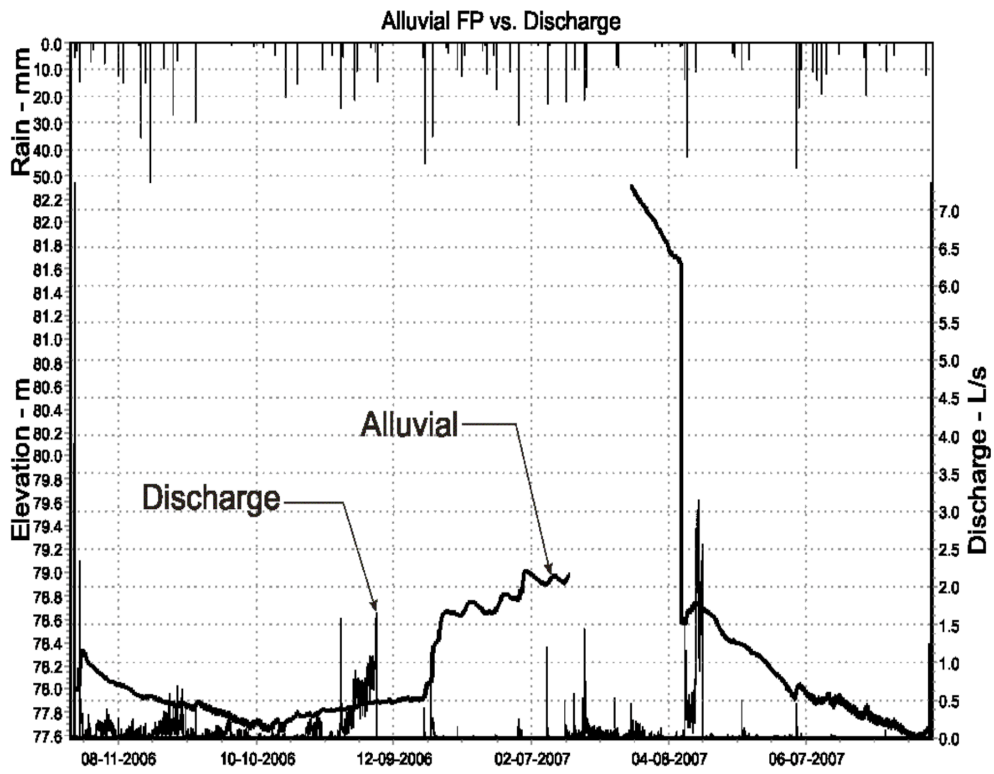


Figure 28. Alluvial Flood Plain Piezometer and Stream Discharge. Entire Study Period.

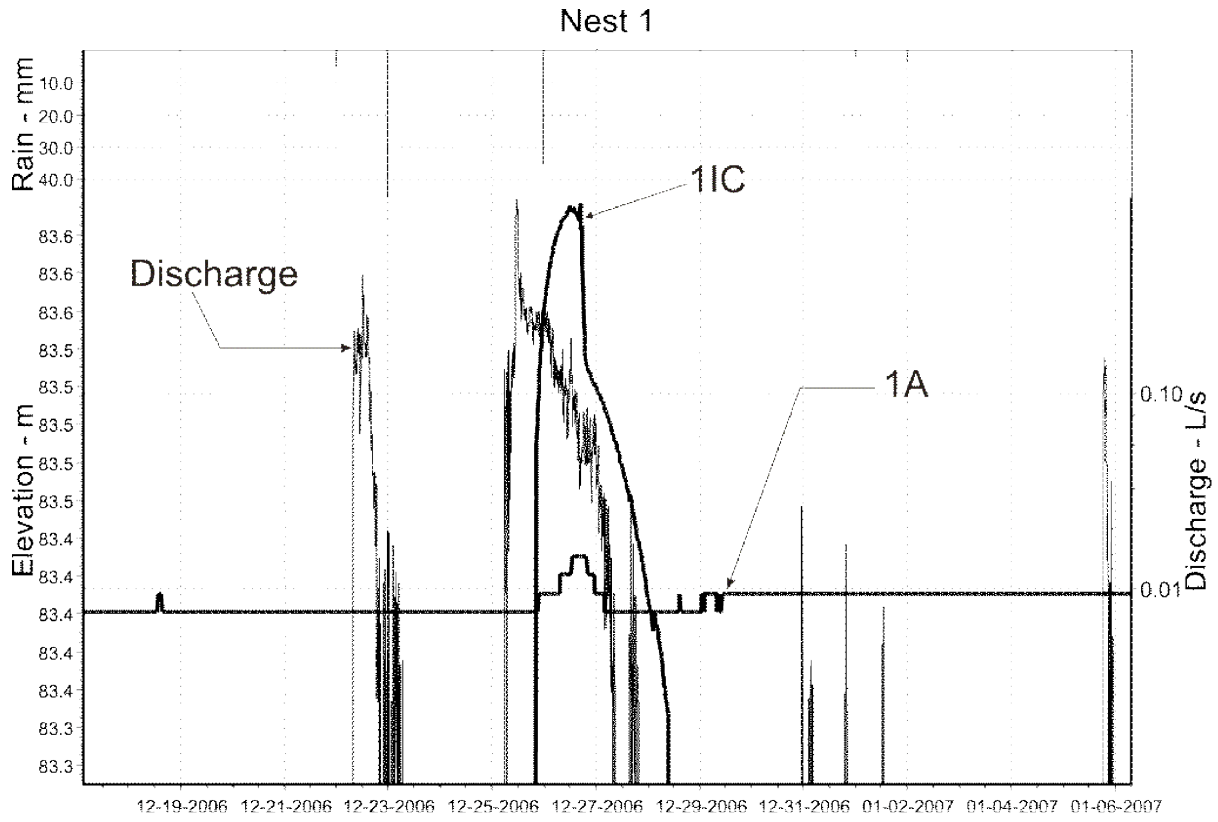


Figure 29. Piezometer Nest 1. 12/25/2006 Perching Event

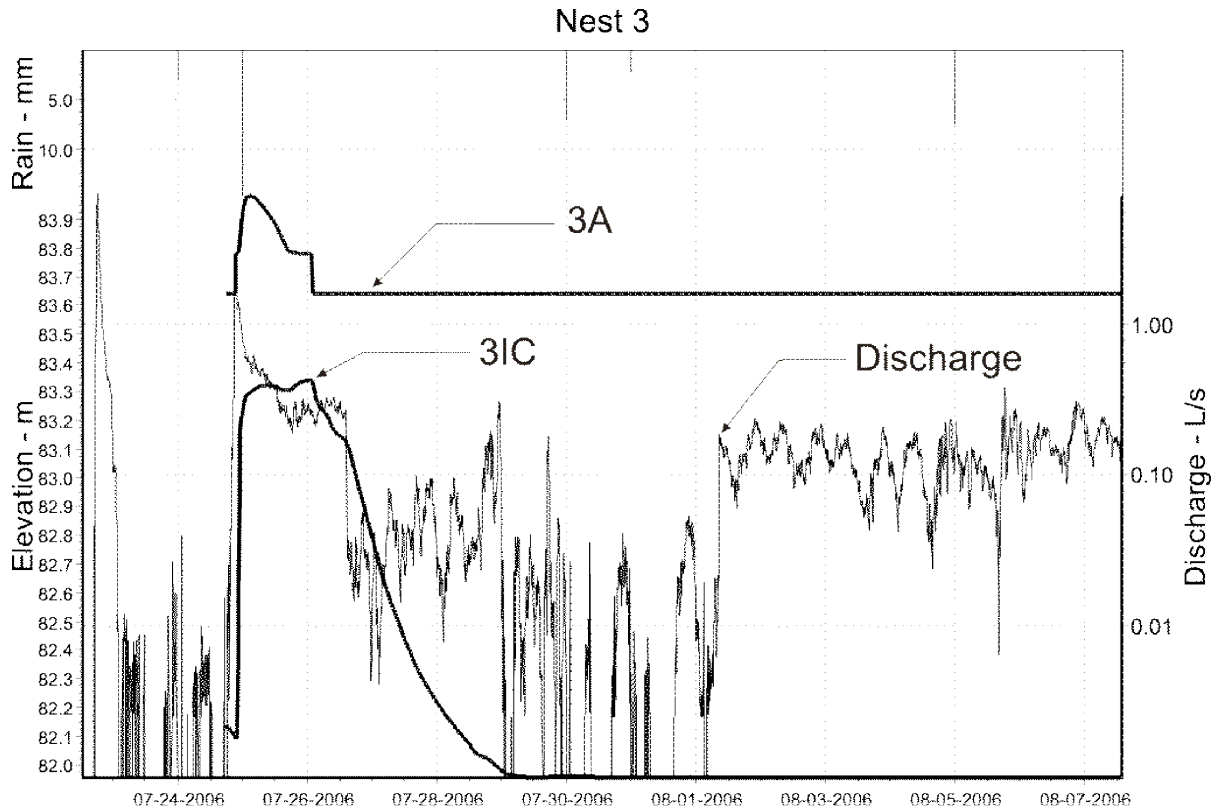


Figure 30. Piezometer Nest 3. 7/26/2006 Perching Event.

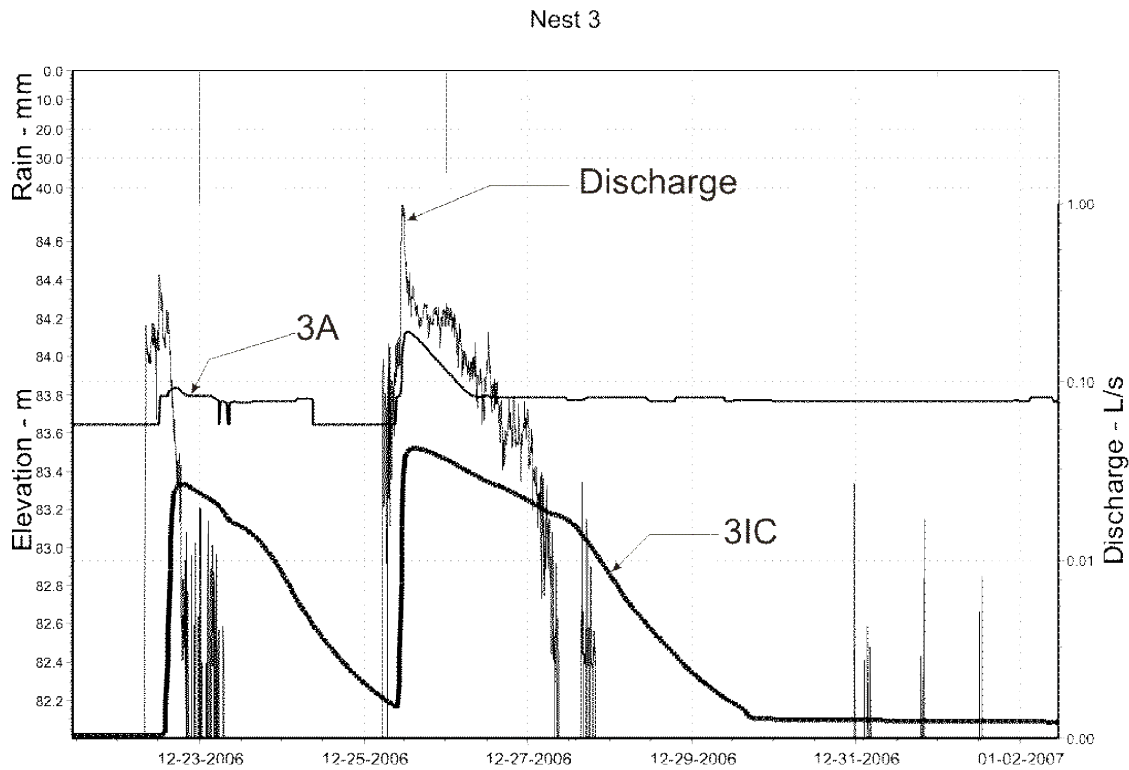


Figure 31. Piezometer Nest 3. 12/25/2006 Perching Event.

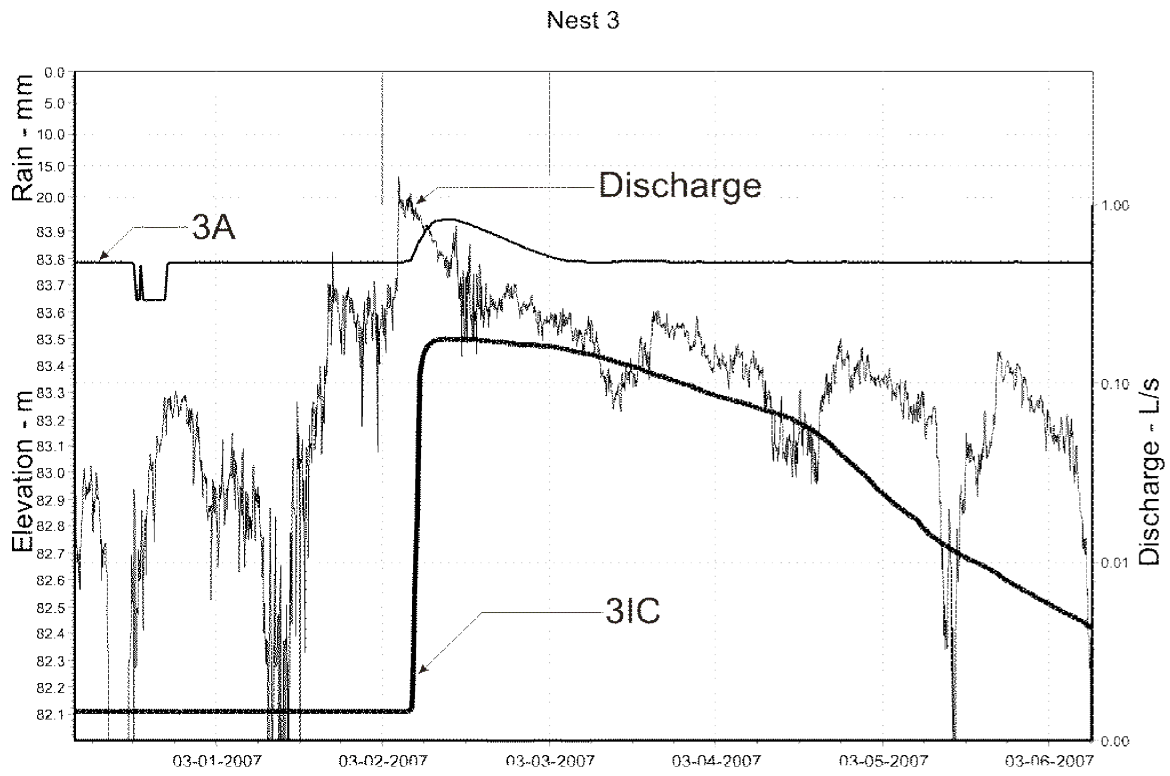


Figure 32. Piezometer Nest 3. 3/2/2007 Perching Event.

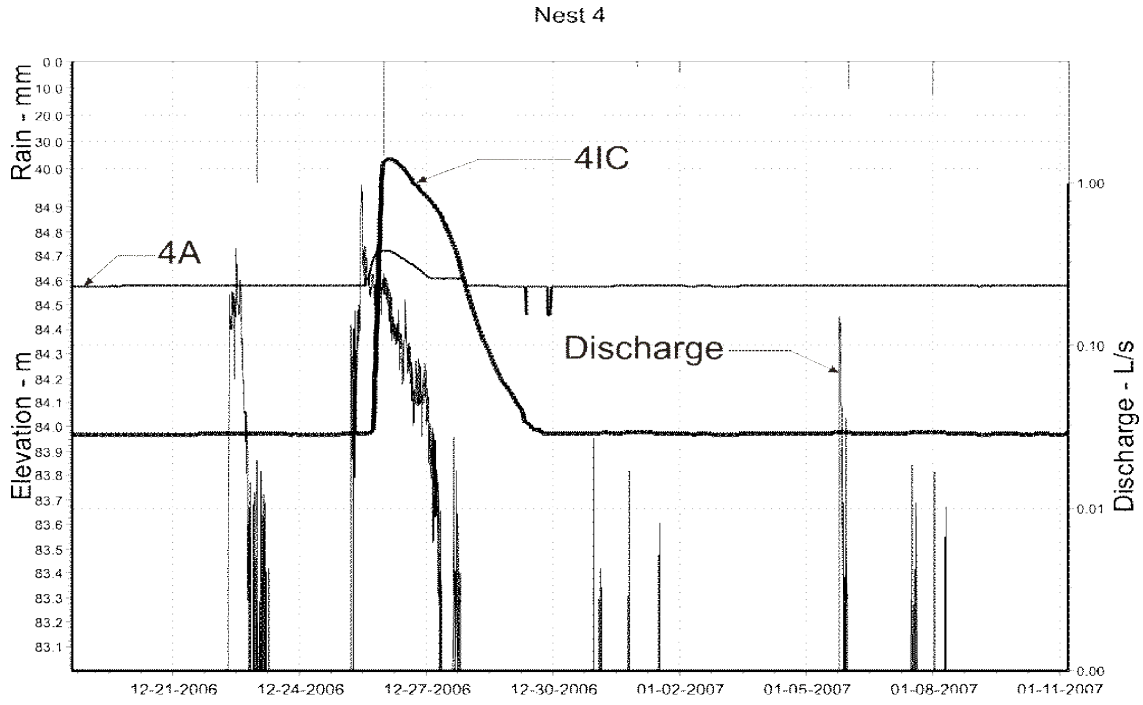


Figure 33. Piezometer Nest 4. 12/25/2006 Perching Event.

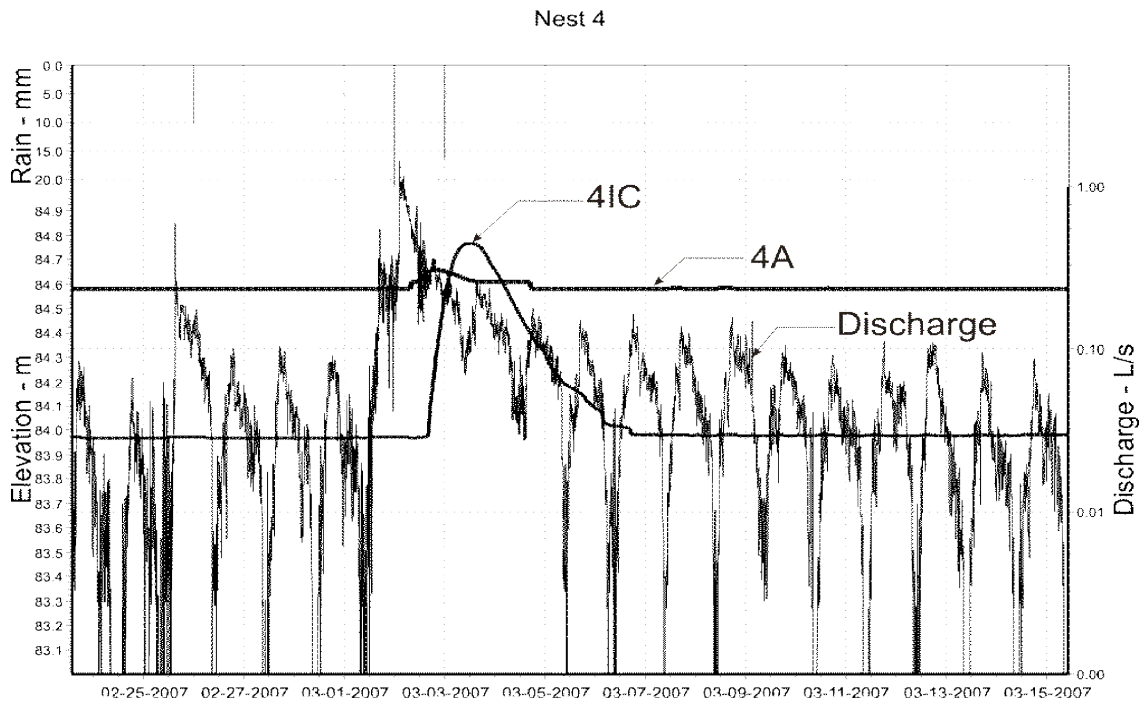


Figure 34. Piezometer Nest 4. 3/2/2007 Perching Event.

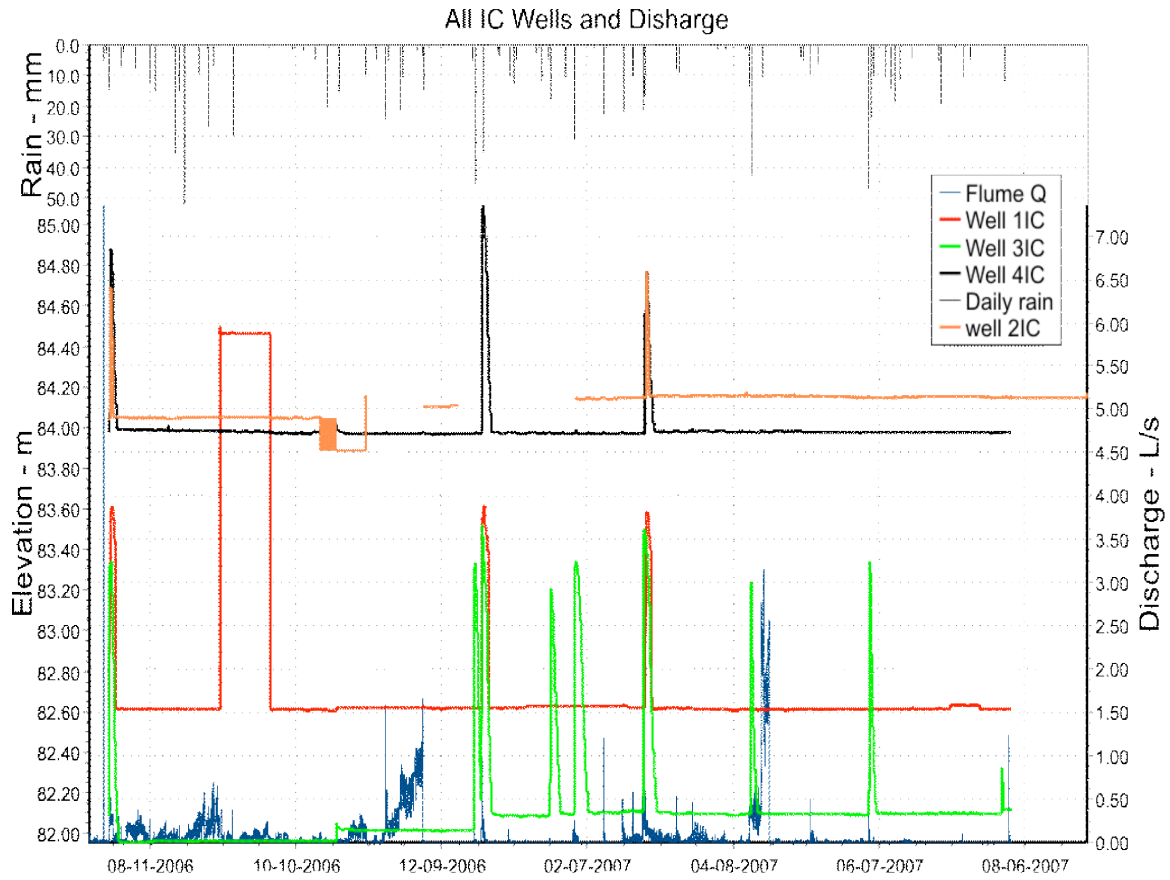


Figure 35. All IC Piezometers Perching Events. Entire Study Period.

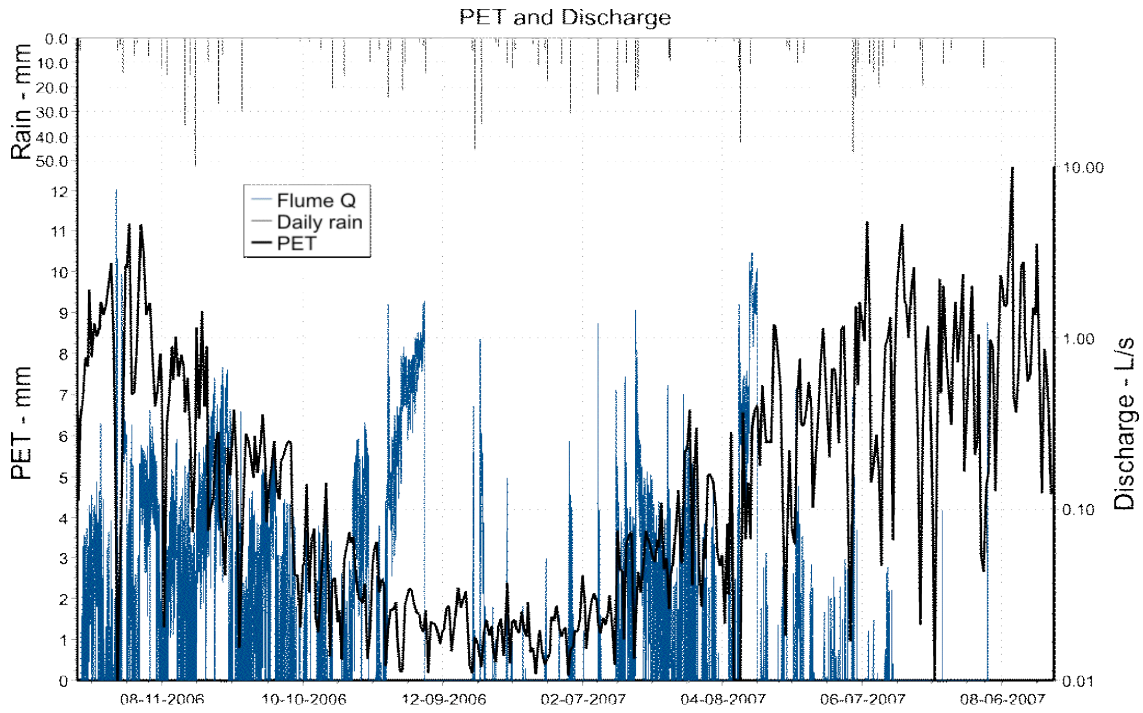


Figure 36. PET and Stream Q. Entire Study Period.

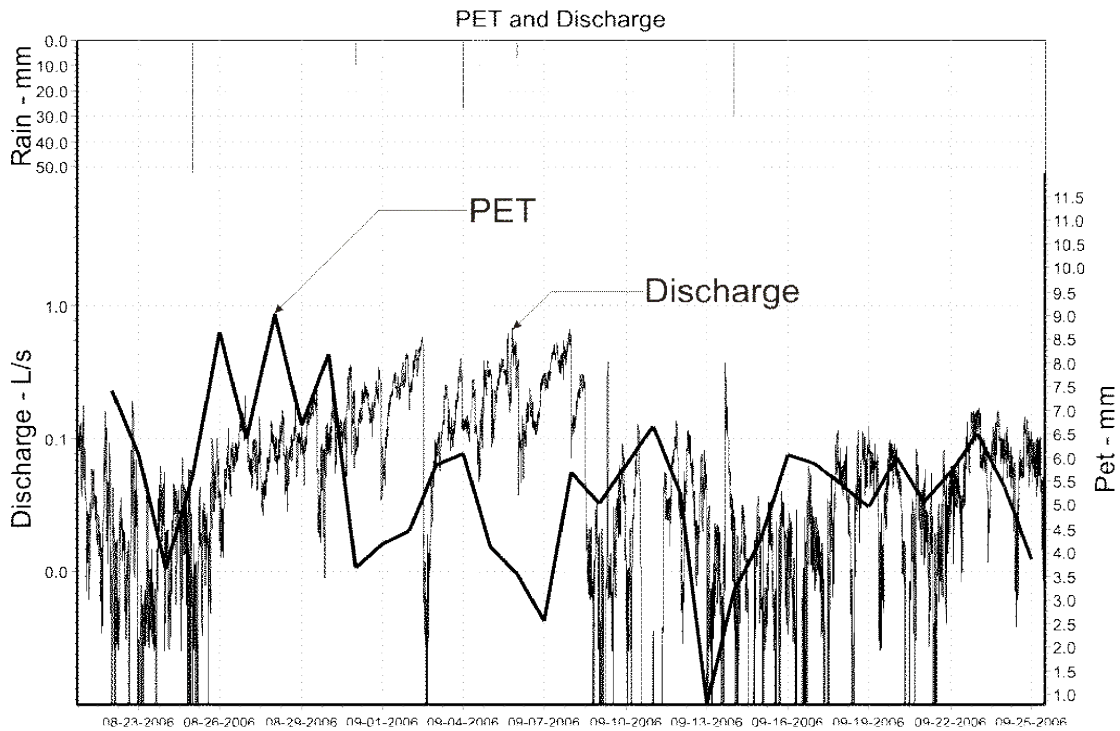


Figure 37. PET and Stream Q. 8/23/2006 to 9/25/2006.

All of the hydrologic graphs show missing data, this occurred either because a probe needed to be removed to be sent off for service, or the probe malfunctioned during the period where no data exists. At nest one (Fig. 24), around 9/12/2006, the graph shows a large increase in water level where at the top a plateau of about 86 m of total head (elevation), this was a case of where the probe malfunctioned due to any number of reasons (low battery voltage, water chemistry, improper calibration or a large wind event causing the piezometer casing to come in contact with the vented Teflon cable of the probe. Another instance of probe malfunction was evidenced in piezometer 4D (Fig. 27), where the elevation begins to increase very sharply after 2/20/2007, while the drastic increase was shown at the aforementioned date, it can be ascertained that the probe (SOLINST level logger gold pressure transducer) was malfunctioning well before the drastic increase (around 2/07/2007).

Perching events were highly variable and were not consistent at each nest, while some nests had perching events on the same day and time, there did not appear to be a consistent trend (Fig's. 29-34). For example, nest two (Fig. 25) showed no perching events throughout the study period. It should be noted that the capacitance probes in piezometers 2A and 2IC were removed for about a two month period to be serviced at the manufacturer, this might of had an influence on the perching events at nest two, as the down time (12/10/2006 to 2/10/2007) corresponds to the perching event on or around 12/25/2006 with a duration of 4 days as shown at all nests except two.

The perching event of 12/25/2006 was the only event where all the remaining nests (one, three, and four) showed a simultaneous response in the above clay (A) piezometers (Fig's 24, 26, 27). An interesting note was during the event, none of the piezometric response matches up exactly with discharge (Q). While piezometers in nest three seem to be very close in terms of

peak Q and elevation, this was the only nest that shows this phenomena, where the other perching events at nest three (7/26/2006 to 7/27/2006 and 3/2/2007 to 3/3/2007) (Fig's. 30 and 32) are very close to matching peak Q and elevation, there was an offset of about a day.

The final perching event during the study period was on 3/2/2007 to 3/3/2007 or 3/5/2007 and was dependant on the nest in question (nest three ended 3/3/2007 (Fig. 32) while nest four (Fig. 34) ended 3/5/2007). The response in nests three (Fig. 32) and four (Fig. 34) were very similar, however, well 4IC showed a greater response than 4A, and consequently was greater than nest three. Perching instances of this occurrence were only shown in nests one (Fig. 29) and four (Fig. 33), where both nests showed this higher total head (h) in piezometer IC for the perching event of 12/25/2006. The other perching event where piezometer IC, h, was higher than piezometer A, h, was in nest four (Fig. 34) during the 3/2/2007 event. Also, throughout the study period, h, of the IC piezometers (Fig. 35) would be greater than h in the A piezometers on a rather consistent basis (Nests 1, 2 and 4), while nest three had many elevated h events in piezometer 3IC (Fig. 35).

It could be speculated that the elevated head response in most if not all IC piezometers (Fig. 35) (with 3IC as an exception, due to the increased occurrences of higher h throughout the study period) was due to ODYSSEY probe error. After extensively testing each ODYSSEY probe, where water levels were raised and lowered, and remained static at set increments, and water level was recorded on a separate log sheet and compared to probe readings at said time. Also, noting the occurrence of the elevated h events in all IC piezometers (Fig. 35), probe error can be ruled out.

Max-rise piezometers (MRp), showed little response throughout the period of record, the period of record of MRp data differs from the entire study period, as can be noted in Appendix E.

Data from MRp's in Appendix E, will show some perching events on 1/12/07, 2/2/07, and 2/23/07, as evidenced in the data tables. Other small perching events occurred as well, however, it should be noted the aforementioned perching dates, were the first time the investigator took data from the MRp's and could be considered bogus, but the data has been included to support smaller perching events shown in recording piezometers.

Stream discharge (Q) was very small over the study period, and fluctuated at a very specific interval (diurnal), Q was thought to be affected by potential evapotranspiration (PET), reviewing the graphic of PET and Q (Fig's. 36 and 37), it is very clear that Q increases with increases precipitation and as PET decreases.

4.3 Model Results:

Modeling results were highly variable and created much doubt as to whether or not the model could simulate how the hillslope behaved when compared to measured data (hydrologic, soil and climatic). Target simulation periods were considered to be one year (365 days), as this was used to compare model simulation results to measured data. If a model did not run for the entire duration it was considered non-valid. The large model domain, did not support any perching (perching in the model sense would be evidenced by a positive head above the argillic horizon), above the argillic, consequently positive head within the argillic was not noticed either. The large domain (380 m x 60 m) showed unsaturated conditions directly below the argillic for about 40 m, positive head within the argillic and unsaturated conditions below were shown in observed data. After much thought and manipulation of the model, it was determined that the model could not handle such a large domain, along with abrupt changes in Ks.

A new model domain was created where a slice of soil was taken out of the large domain to determine whether the major malfunction was attributed to domain size, or abrupt Ks changes. This model ran, but when changing Ks values an order of magnitude, the computation speed slowed dramatically and in some instances timed out before the model could simulate a complete period of record (365 days).

A third domain used to simulate the hillslope was 30 m long and 5 m deep with a no flow boundary directly below the argillic horizon. This final model domain showed some small and very transient perching events above the argillic horizon, which supports field measured data.

Chapter 5: Conclusion

Field sampling and laboratory PSD analysis results show that the subsurface horizon is in fact an argillic horizon. While the texture of this horizon varies from clay to sandy clay loam to sandy loam, in-situ Ks and hydrologic results indicate that this argillic layer can impede the percolation of water.

In-situ Ks data shows very clearly that the Ks of the argillic layer varies from one to three orders of magnitude lower than both the surface and mid horizon (sand) sampling sites. This alone is reason to believe that the subsurface argillic horizon has the potential to impede water flow and create what we now believe is a transient water table on top of the argillic horizon.

Several instances of perching or ponding on top of the argillic horizon were evidenced throughout the study period. Perching conditions were evidenced both on top of the argillic horizon as well as within the argillic horizon, shown by elevated, h , in each horizon. While perching events were relatively few on top of the argillic horizon, the duration was long enough to sustain stream discharge at higher levels while perching occurred. Throughout the study period there appeared to be many more increases in h , within the argillic horizon than above. This could be due to what is known as a “loading effect” described by Rasmussen and Mote, 2007. Where infiltrating water exerts a force on water in storage of a specific hydrologic unit (in this case the argillic horizon), eliciting a response within the unit creating an increase in h , of the unit.

Model results were rather inconclusive with respect to the large domain and slice section of soil. However, the small scale model of the hillslope with a no flow boundary (Appendix F),

did show perching above and within the argillic horizon. The model simulations have led to the belief that HYDRUS 2-D is not numerically capable to compute large abrupt differences in K_s (where horizons change one or more orders of magnitude i.e. sand with a K_s of 6 m/day and an argillic horizon with a K_s of 0.01 m/day).

Much more experimentation is needed to fully characterize this watershed, however, with the small data-set provided by this study, several conclusions can be drawn. First and foremost the argillic horizon does act as an impediment to the downward flow of water, also the argillic horizon can create saturated conditions above leading to a transient water table. The transient nature of this water table could be an artifact of the warm winter and drought conditions which prevailed during most of the study period. Also, since the argillic horizon does impede downward flow of water, the influence of the argillic horizon could eventually lead to conditions necessary to create interflow at the site. HYDRUS 2-D should not be used for a hillslope with such heterogeneities and anisotropy in soil conditions combined with a large domain.

Further investigation should focus on the aspects necessary to determine whether or not interflow occurs at the site. Such aspects include but are not limited to: soil moisture monitoring equipment (such as TDR), geochemical investigations (to separate stream flow into fractions such as deep groundwater flow, shallow groundwater flow i.e. interflow, and precipitation).

Chapter 6: Recommendations for Continued Investigation

It is the intention of this section to give insight to what we believe would be helpful in future investigations of this project. It should be noted, the program used to create the graphs for all nest, discharge, and climate data were created using a program called “Slope Commander”, it was written by John Dowd, and can be obtained from his ftp site:

<ftp://128.192.40.45/pub/jdowd/>, and selecting ‘Setup_SC1014.exe’ or higher.

With respect to field data first, it would be ideal to use similar data-loggers (i.e. Campbell Scientific CR-10x) with similar programs to extract data. This will enable a uniform data set.

When measuring stream flow or deep groundwater use a differential pressure transducer to account for fluctuations in barometric pressure, thus negating the need to post barometric pressure corrections when using an absolute gage. Also if a pressure transducer is not necessary to measure stream flow, use another type of measuring device such as a bubbler or float type recorder.

After data has been extracted from each data logger, reset the all data loggers ensure that all loggers start at the same time, this helps with uniform data logging with respect to time and will reduce the amount of headache during data processing. Also, data from a specific data logger should be named with the same convention each time, for example, if extracting data from a piezometer, name the file after the piezometer and the date data was collected, this ensures uniform file names when processing data.

All data loggers should be recalibrated yearly, if not every other year. Another recording piezometer nest should be installed near the flume, as well as across the hillslope to further detail shallow subsurface water table dynamics. Future nest installations should include an upper

boundary and “low” point positions as can be shown in the “Argillic Topography”, “Depth to Argillic”, and “Surface Topography” maps, these installations should be done after the soil and water table of the hillslope has been further characterized. Future piezometer installations should be done with a mechanical device to ensure bore holes are straight, and due to the number of piezometer installations, should lessen the amount of human induced error.

Soil moisture should be measured at the hillslope with time domain reflectometry (TDR) or an equivalent measurement should be made in order to accurately assess soil moisture dynamics within the hillslope. Again, the soils and water table of the hillslope should be further characterized with respect to the variability of the subsurface topography of the argillic horizon, this can be done with GPR (ground penetrating radar GPR (soils) and resistivity (water table), or an equivalent method of each). Across the hillslope, more soil samples should be taken, to define the soils better and possibly characterize different depositional events and parent material distributions within soil horizons and across the entire hillslope.

Future studies should obtain more soil hydraulic information both in-situ (K_s) and laboratory (moisture release, PSD, etc.) to better detail the fine differences in soil hydraulic properties within the argillic horizon and the soil profile as a whole.

Finally, a new model platform should be used to accurately describe and simulate the entire hillslope. While HYDRUS 2-D worked at a smaller scale, the end goal is to simulate a larger domain (entire hillslope) with field observed values of K_s , climate, stream flow, and ground water data, as well as “design storm” or long term records of precipitation on the order of ten to one hundred years worth.

Literature Cited

- Anderson, M.G. and T.P. Burt. 1990. Process Studies in Hillslope Hydrology. Wiley. *In* Keinzler, P.M. and Naef, Felix. In Press. Subsurface storm flow formation at different hillslopes and implications for the 'old water paradox.' Hydrol. Process. (in press) doi: 10.1002/hyp.6687.
- Beven, K.J. 2001. How far can we go in distributed hydrological modeling? *In* Germann, P.F. and Michael Zimmerman. 2005. Directions of preferential flow in a hillslope soil. Quasi-steady flow. Hydrol. Process. 19:887-899, doi:10.1002/hyp.1506.
- Braun, E. L. 1950. Deciduous forests of eastern North America. Hafner Press. New York. 596 p. *In* Jones, S. M., D. H. Van Lear, and S. K. Cox. 1984. A vegetation-landform classification of forest sites within the upper Coastal Plain of South Carolina. Bull. Of The Torrey Bot. Club. Vol. 111 No. 3 pp. 349-360.
- Collings, G. H. and P.H. Montgomery. 1957. Land resource areas in South Carolina. Circular 112. Ag. Exp. Sta., Clemson Agricultural College, Clemson, South Carolina. *In* Jones, S. M., D. H. Van Lear, and S. K. Cox. 1984. A vegetation-landform classification of forest sites within the upper Coastal Plain of South Carolina. Bull. Of The Torrey Bot. Club. Vol. 111 No. 3 pp. 349-360.
- Cooke, C.W. 1936. Geology of the coastal plain of South Carolina. Geologic Survey Bulletin 867. U.S. Dept. Interior, Washington, DC. *In* Jones, S. M., D. H. Van Lear, and S. K. Cox. 1984. A vegetation-landform classification of forest sites within the upper Coastal Plain of South Carolina. Bull. Of The Torrey Bot. Club. Vol. 111 No. 3 pp. 349-360.
- Dingman, S. L. 1994. Physical Hydrology. Prentice-Hall, Inc. 575p.
- Freer, J., J. McDonnell, K.J. Beven, D. Brammer, D. Burns, R.P. Hooper and C. Kendall. 1997. Topographic controls on subsurface stormflow at the hillslope scale for two hydrologically distinct small catchments. Hydrol. Processes 11: 1347-1352.
- Freeze, R.A. 1972. Role of subsurface flow in generating surface runoff -2. Upstream source areas. Water Resour. Res. 8(5):1272-1283. *In* Keinzler, P.M. and Naef, Felix. In Press. Subsurface storm flow formation at different hillslopes and implications for the 'old water paradox.' Hydrol. Process. (in press) doi: 10.1002/hyp.6687.
- Flügel, W.-A., 1993. Untersuchungen zum Problem des Interflow. Heidelberger Geographische Arbeiten 56, 275. *In* Flügel, W.-A. and R. E. Smith. 1999. Integrated process studies and modeling simulations of hillslope hydrology and interflow dynamics using the HILLS model. Environ. Modelling & Software 14:153-160.

- Flügel, W.-A. and R. E. Smith. 1999. Integrated process studies and modeling simulations of hillslope hydrology and interflow dynamics using the HILLS model. *Environ. Modelling & Software* 14:153-160.
- Germann, P.F. and Michael Zimmerman. 2005. Directions of preferential flow in a hillslope soil. Quasi-steady flow. *Hydrol. Process.* 19:887-899, doi:10.1002/hyp.1506.
- Hewlett, J.D. and A.R. Hibbert 1963. Moisture and energy conditions within a sloping soil mass during drainage. *J. of Geophysical Research.* 68(4):1081-1087.
- Hewlett, J.D. and A.R. Hibbert, 1967. Factors affecting the response of small watersheds to precipitation in humid areas. In *International Symposium on Forest Hydrology*, Sopper WE, Lull HW (eds). Pergamon: Oxford, 275-290. In Keinzler, P.M. and Naef, Felix. In Press. Subsurface storm flow formation at different hillslopes and implications for the 'old water paradox.' *Hydrol. Process.* (in press) doi: 10.1002/hyp.6687.
- Horton, R.E. 1933. The role of infiltration in the hydrologic cycle. *Transactions of the American Geophysical Union.* 14:446-460.
- Hutchinson, D.G. and R.D. Moore. 2000. Throughflow variability on a forested hillslope underlain by compacted glacial till. *Hydrol. Process.* 14, 1751-1766.
- Jones, J.A.A. and L.J. Connelly. 2002. A semi-distributed simulation model for natural pipeflow. *Journal of Hydrology* 262: 28-49. In Keinzler, P.M. and Naef, Felix. In Press. Subsurface storm flow formation at different hillslopes and implications for the 'old water paradox.' *Hydrol. Process.* (in press) doi: 10.1002/hyp.6687.
- Jones, S. M., D. H. Van Lear, and S. K. Cox. 1981. Major forest community types of the Savannah River Plant, National Environmental Research Park Program, U.S. Dept. Energy SRO-NERP-9. In Jones, S. M., D. H. Van Lear, and S. K. Cox. 1984. A vegetation-landform classification of forest sites within the upper Coastal Plain of South Carolina. *Bull. Of The Torrey Bot. Club.* Vol. 111 No. 3 pp. 349-360.
- Jones, S. M., D. H. Van Lear, and S. K. Cox. 1984. A vegetation-landform classification of forest sites within the upper Coastal Plain of South Carolina. *Bull. Of The Torrey Bot. Club.* Vol. 111 No. 3 pp. 349-360.
- Kirkby, M.J. 1976. 'Hydrograph modeling strategies'. In Freer, J., J. McDonnell, K.J. Beven, D. Brammer, D. Burns, R.P. Hooper and C. Kendall. 1997. Topographic controls on subsurface stormflow at the hillslope scale for two hydrologically distinct small catchments. *Hydrol. Processes* 11: 1347-1352.
- Kirkby, M.J. (Ed.). 1991. *Hillslope Hydrology.* John Wiley and Sons.
- McDonnell, J.J. 1990. A rationale for old water discharge through macropores in a steep, humid catchment. *Water Resour. Res.* 26(11):2821-2832.

- McDonnell, J.J., Ian F. Owens, and M.K. Stewart. 1991. A case study of shallow flow paths in a steep zero-order basin. *Water Resour. Bulletin.* 27(4):679-685.
- Mosley, M.P. 1979. Streamflow generation in a forested watershed. *Water Resour. Res.* 15:795-806. *In* McDonnell, J.J., Ian F. Owens, and M.K. Stewart. 1991. A case study of shallow flow paths in a steep zero-order basin. *Water Resour. Bulletin.* 27(4):679-685.
- Newman, B.D., A. R. Campbell, B.P. Wilcox. 1998. Lateral subsurface flow pathways in a semiarid ponderosa pine hillslope. *Water Resour. Res.*, 34, 98WR02684.
- Nieber, J.L. and M. F. Walter. 1981. Two-dimensional soil moisture flow in a sloping rectangular region: experimental and numerical studies. *Water Resour. Res.* 17(6): 1722-1730.
- Ragan, R.M. 1967. An experimental investigation of partial area contributions. *In* Hydrological aspects of the Utilization of Water. Int'l Assoc. of Scientific Hydrology (IAHS). Publ. No. 76, pp. 275-290.
- Rasmussen T.C., T.L. Mote. 2007. Monitoring surface and subsurface water storage using confined aquifer water levels at the Savannah River Site, USA”, *Vadose Zone Journal*, 6(2):327-335.
- Retter, M., P. Kienzler, and P.F. Germann. 2006. Vectors of subsurface stormflow in a layered hillslope during runoff initiation. *Hydrol. Earth Syst. Sci.* 10:309-320.
- Rodhe, A. 1987. The origin of streamwater traced by Oxygen-18. Uppsala Univ., Dept. of Phys. Geog., Div., Hydrol., Report Series A41. *In* McDonnell, J.J., Ian F. Owens, and M.K. Stewart. 1991. A case study of shallow flow paths in a steep zero-order basin. *Water Resour. Bulletin.* 27(4):679-685.
- Rogers, V.A. 1990. Soil Survey of Savannah River Plant area, parts of Aiken, Barnwell, and Allendale counties, South Carolina. USDA, Soil Cons. Serv., Washington, DC.
- Shaw, J.N., D.D. Bosch, L.T. West, C.C. Truman, D.E. Radcliffe. 2001. Lateral flow in loamy to sandy Kandiuults of the Upper Coastal Plain of Georgia (USA). *Geoderma* (99)1-25.
- Sherrer, S. 1997. Abflussbildung bei Starkniederschlagen. Identifikation von Abflussprozessen mittles kunstlicher Niederschläge. *Mitteilungen der VAW*, Nr. 147, Zurich. *In* Keinzler, P.M. and Naef, Felix. In Press. Subsurface storm flow formation at different hillslopes and implications for the ‘old water paradox.’ *Hydrol. Process.* (in press) doi: 10.1002/hyp.6687.
- Tromp-van Meerveld, H.J. and J.J. McDonnell. 2006. Threshold relations in subsurface stormflow: 1. A 147-storm analysis of the Panola hillslope. *Water Resour. Res.*, 42, W02411, doi:10.1029/2004WR003778.

- Tromp-van Meerveld, H.J. and J.J. McDonnell. 2006. Threshold relations in subsurface stormflow: 2. The fill and spill hypothesis. *Water Resour. Res.*, 42, W02411, doi:10.1029/2004WR003800.
- Tsuboyama, Yoshio, Roy C. Sidle, Shoji Noguchi, Shigeki Murakami and Toshio Shimizu. 2000. A zero order basin- its contribution to catchment hydrology and internal hydrologic processes. *Hydrol. Process.* 14, 387-401.
- Ward, A.D. and S. W. Trimble. 2004. *Environmental Hydrology*, 2nd Edition. CRC Press LLC. Lewis Publishers. 475p.
- Weiler, M. and McDonnell J.J., Tromp-van Meerveld I., and Uchida, T. 2006. Subsurface stormflow. In *Encyclopedia of Hydrological Sciences*, Volume 3, Part 10, Anderson, M.G. and J.J. McDonnell (eds). Wiley. In Keinzler, P.M. and Naef, Felix. In Press. Subsurface storm flow formation at different hillslopes and implications for the 'old water paradox.' *Hydrol. Process.* (in press) doi: 10.1002/hyp.6687.
- Weyman, D.R. 1973. Measurement of the downslope flow in a soil. *J. Hydrol.* 20:267-288.
- Zaslavsky, D. and A.S. Rogowski. 1969. Hydrologic and morphological implications of Anisotropy and infiltration in soil profile development. *Soil Sci. Soc. Amer. Proc.* 33: 594-599.
- Zaslavsky and G. Sinai 1981a. Surface Hydrology IV- Flow in Sloping, layered soil. *Journal of Hydraulics Division, ASCE.* Vol. 107, No.HY1, Proc. Paper 15961. pp.53-64.
- Zaslavsky and G. Sinai 1981b. Surface Hydrology V- In-surface transient flow. *Journal of Hydraulics Division, ASCE.* Vol. 107, No.HY1, Proc. Paper 15961. pp.65-93.

Appendix A

Piezometer Notes

Nest 1

Piezometer 1A

Soil Texture	Depth cm	Notes
Sand	39.4	
Sand	70.5	
Sand	99.7	
Sand	114.9	Hit some river gravel
Sand/Sandy Loam	131.4	Starting to see some mottles of clay
Clay	147.3	

Piezometer 1 IC

Soil Texture	Depth cm	Notes
Sand	0-38.1	
Sand	76.2	
Sand	121.9	Hit river gravel
Clay	135.3	Top of clay layer
Clay	259.1	Bottom of piezometer

Piezometer 1 D

Soil Texture	Depth cm	Notes
Sand	0-38.1	
Sand	104.1	Hit river gravel
Loamy Sand	129.5	
Clay	152.4	Top of clay layer
Loam/Loamy Sand	414.0	Noticed purple color to clay
Sand/Loamy Sand	459.7	Sand had distinct purple color
Sand/Loam	530.9	Sand/loam seemed to be very moist almost saturated; borehole stopped here due to fear of collapse

Nest 2

Piezometer 2A

Soil Texture	Depth cm	Notes
Sand	0-86.4	
Sand	91.4	Hit river gravel
Loam	137.2	
Clay/Loamy Clay	144.8	Back filled hole with 68.6 cm Sand & 76.2 cm Bentonite

Piezometer 2 IC

Soil Texture	Depth cm	Notes
Sand	0-38.1	
Sand	76.2	
Sand	91.4	Hit river gravel
Loam/Clay	144.8	
Clay	167.6	Clay had white mottles (Kaolin)
Clay	180.3	Clay had white mottles (Kaolin)
Clay	218.4	Clay had distinguished purple color/mottling

Piezometer 2D

Soil Texture	Depth cm	Notes
Sand	0-38.1	
Sand	53.3	Hit river gravel
Loam/Sand	144.8	Soil had loamy texture & light color
Clay	152.4	Top of clay layer
Sand/Loam	444.5	Bottom of borehole

Nest 3

Piezometer 3A

Soil Texture	Depth cm	Notes
Sand/ Sandy Loam	0-38.1	
Sand	68.6	Hit river gravel
Clay/Loamy Clay	111.8	Backfilled with 81.3 cm Sand & 35.6 cm Bentonite

Piezometer 3 IC

Soil Texture	Depth cm	Notes
Loamy Sand	0-38.1	Sand was moist and had distinct loamy texture
Loamy Sand	76.2	Sand was moist and had distinct loamy texture
Clay	106.7	Top of clay layer & hit river gravel
Clay	147.3	Clay had red brick/purple mottles
Clay	228.6	Tape measure dropped into bottom of borehole; Clay had Kaolin and purple mottles

Piezometer 3D

Soil Texture	Depth cm	Notes
Sand	0-22.9	
Loam	33.0	Hit river gravel
Clay	121.9	Top of clay layer; purple soil
Clay/loam	256.5	Hit some sort of saprolite/quartz material
Rock/sand	289.6	Auger was completely torqued out and could dig any deeper.

Nest 4

Piezometer 4A

Soil Texture	Depth cm	Notes
Sand	0-38.1	
Sandy Loam	76.2	
Clay	121.9	Backfilled w/ 76.2 cm Sand & 45.7 cm Bentonite

Piezometer 4 IC

Soil Texture	Depth cm	Notes
Sand	0-15	
Loamy Sand	30	Began to see red/loamy clay
Clay/Loamy Clay	49	Top of clay layer
Clay	86	Bottom of borehole

Piezometer 4D

Soil Texture	Depth cm	Notes
Sand	0-38.1	
Clay	91.4	Top of clay layer
Loam	259.1	
Clay/loam	330.2	Soil had good structure
Clay/loam	365.8	Soil had good structure and mottling
Loam/sand	429.3	Sand w/ some clay/structure
Loam/sand	510.5	Bottom of borehole

Alluvial FP

Piezometer: Alluvial FP

Texture	Depth cm	Notes
Sand	20.3	
Sand	86.4	
Sand	165.1	Hit river gravel
Clay/Loam	182.9	Saw white/light purple color. Hit rocks and broke through tobacco road formation
Clay	195.6	Clay had some sand/sandy loam
Clay	203.2	Clay was very mottled w/ white, brown, and red colors
Clay	223.5	Bottom of auger bucket had pure white clayey material, (Kaolinite?)
Sandy Clay Loam	276.9	
Loamy Sand	289.6	Kaolinite & mottled deposits present
Kaolinite (mottled clay)	304.8	
Kaolinite	332.7	
Kaolinite	368.3	Gritty & moist
Clay	378.5	Kaolinite & increasing moisture content
Sandy Clay	386.1	Very gritty, very wet, hit river gravel
Sandy Clay	403.9	* Water table
Additional Notes		Backfilled borehole w/sand 281.9 cm and bentonite to the top. Ground to top of HIP = 123.5 cm.

Appendix B

Sand Column Particle Size Distribution

Particle Size Class	1 - 2 mm VCS	0.5 - 1 mm CS	0.25 - 0.5 mm MS	0.1 - 0.25 mm FS	0.05 - 0.1 mm VFS
Sample					
A	0.21	12.49	7.26	0.03	0.03
B	0.19	12.82	6.97	0.03	0.01
C	0.11	12.37	7.50	0.03	0.00
AVE.	0.17	12.56	7.24	0.03	0.01
%	0.85	62.80	36.22	0.15	0.07

Appendix C

Soil Descriptions

Location: SRS 1 (south end of trench)

Date: 7-13-07

Slope: 6% Shape: Linear Convex (on contour)

Climate: Humid Temperate

Landform: Coastal Plain

Geomorphic Surface: Upland

Hillslope component: Mid Backslope

Parent Material: Alluvium

Land Use: Forest/Ag.

Vegetation: Tree/Shrub

Classification: loamy, kaloinitic, thermic family of Arenic Kanhapludults; Ailey Series

Described by: Greco and West

Pedon Description: (colors are for moist soil unless otherwise stated)

A – 0 to 5 cm; brown (10YR 4/4) sand; weak fine granular structure; very friable; abrupt boundary.

E – 5 to 61 cm; light yellowish brown (10YR 6/4) sand; single grain structure; very friable; 1% 15 mm subround quartz rock fragments; abrupt boundary.

Bt1 – 61 to 84 cm; light brown (7.5YR 5/6) sandy clay loam; few fine distinct reddish brown (5YR 5/6) redox concentrations; weak medium subangular blocky structure; friable; gradual boundary.

Bt2 – 84 to 96 cm; light brown (10YR 5/6) sandy clay; many coarse prominent brown (2.5YR 4/6) redox concentrations; few fine light yellowish brown (10YR 6/4) redox depletions; moderate medium subangular blocky structure; clear boundary.

BC1 – 96 to 120 cm; brown (2.5YR 4/6) sandy clay loam; few medium light brownish yellow (10YR 7/4) and common medium prominent light brown (10YR 5/6) redox depletions; weak medium subangular blocky structure; firm; gradual boundary.

BC2 – 120 to 145+ cm; brown (2.5YR 4/6) sandy clay loam; common medium to coarse distinct pockets of dark reddish brown (10R 3/3) clay redox concentrations; weak medium subangular blocky structure; friable; 3% 8 mm quartz rock fragments.

Location: SRS 2 (3m SW Piezometer nest 3)

Date: 7-13-07

Slope: 4% Shape: linear linear Aspect: SW 260°

Climate: Humid Temperate

Landform: Coastal Plain

Geomorphic Surface: Upland

Hillslope component: Mid Backslope

Parent Material: Alluvium

Land Use: Forest/Ag.

Vegetation: Tree/Shrub

Classification: fine-loamy, kaolinitic, thermic family of Aquic Kandiodults; Goldsboro taxadjunct series

Described by: Greco and West

Pedon Description: (colors are for moist soil unless otherwise stated)

A – 0 to 15 cm; brown (10YR 4/4) loamy sand; weak fine granular structure; very friable; clear boundary.

BA – 15 to 41 cm; light brown (10YR 5/4) loamy sand; weak medium subangular blocky structure; friable; 3% 20-20 mm round rock fragments; clear boundary.

Bt1 – 41 to 74 cm; light brown (7.5YR 5/6) sandy clay loam; moderate medium subangular blocky structure; gradual boundary.

Bt2 – 74 to 137+ cm; light yellowish brown (10YR 5/6) clay; common medium prominent reddish brown (2.5YR 4/6) redox concentrations; few fine distinct light yellowish grey (10YR 7/2) redox depletions; weak medium subangular blocky structure; fine.

Location: SRS 3 (11.5m N of piezometer nest 2) Date: 7-13-07

Slope: 6% Shape: linear

Climate: Humid Temperate

Landform: Coastal Plain

Geomorphic Surface: Upland

Hillslope component: Mid Backslope

Parent Material: Alluvium

Land Use: Forest/Ag.

Vegetation: Tree/Shrub

Classification: loamy, kaolinitic, thermic, family of Grossarenic Kandiodults; Lucknow series

Described by: Greco and West

Pedon Description: (colors are for moist soil unless otherwise stated)

A- 0 to 20 cm; light brown (10YR 4/4) coarse sand; weak fine subangular blocky structure; clear boundary.

E1- 20 to 83 cm; pale brown (10YR 5/4) coarse loamy sand, single grain structure; very friable; gradual boundary.

E2- 83 to 100 cm; pale brown (10YR 5/4) coarse sand; single grain structure; very friable; 1% 20 mm quartz rock fragments; gradual boundary.

E3- 100 to 115 cm; light yellowish brown (10YR 5/6) coarse sand; single grained; very friable; 3% 20 mm round quartz rock fragments.

Bt1- 115 to 141 cm; reddish brown (2.5YR 5/6) coarse sandy loam; weak medium subangular blocky structure; friable; 2% 20mm quartz rock fragments; gradual boundary.

Bt2- 141 to 150+ cm; light yellowish brown (10YR 5/6) coarse sandy loam; few medium reddish brown (2.5YR 4/6) redox concentrations; few medium faint pale yellowish brown (10YR 6/4) redox depletions; weak medium subangular blocky structure.

Appendix D

Particle Size Distribution Pipette Method

1. Weigh 10.00 gm (9.998-10.002) soil into PSD Bottles of known weight. Duplicates should be done. If soil contains >2% organic matter, please see below.
2. Number aluminum weigh pans (one for each sample). Obtain weight of each aluminum pan and record. Add 10 gm (9.98-10.02) of soil sample to each aluminum pan add place in 105⁰ C oven overnight. Remove from oven in 24 hours. Obtain weight of each sample and record weight.
3. Add 5mL of 10% solution of sodium metaphosphate into each bottle.
4. Fill bottles approximately 1/2 full with DI water. Seal very tightly with stopper and place on shaker. Shaker holds 24 samples. Shake on low setting overnight.
5. Remove bottles from shaker. Rinse sides of bottle with DI water. Allow time for foam to disappear.
6. Bring volume of solution up to 400mL + bottle weight + soil weight. See tare reference chart for exact weight.
7. Place stirring bar in each of the bottles.
8. You are now ready for the timed portion of this procedure.
9. Line or arrange bottles in order as written on data sheet.
10. Place first two bottles on stirring plate. Start the two bottles stirring at the same time. After at least two minutes, place first bottle in water bath and place the third bottle on the stirring plate. Note the time at which the first bottle is placed in the water. After two minutes remove second bottle and place in the water bath. The fourth sample should be placed on stirring plate at this time. The bottles will be switched out every two minutes, with each bottle stirring approximately four minutes (except for the first bottle, which spins only two minutes or so).
11. Place pipette in ready position and have pre-weighed and numbered crucibles ready.
12. Measure the temperature of the tank water. Using Stokes Equation, determine sampling time (see temperature chart). Depth of sampling is 5 cm, which is pre-set on the pipette. Sampling will be done for 2 microns at an interval of 2 minutes.

13. Timer should still be running. You should pipette your first sample at the time given on the chart. From here, pipette samples every two minutes until finished. Sample collected in pipette should be dispensed into crucible and placed in 105⁰ C oven over night.

14. Remaining sample in bottles should be rinsed and sieved (300 mesh). Place collected sands in numbered 50mL beakers and place in oven to dry. This could take more than overnight for these to dry.

15. Remove crucibles from oven, place in desiccator until cool and then weigh each crucible. Use tweezers to handle each crucible when moving into desiccators and scale.

16. Remove sands from oven and allow to cool. Sands should be removed from beaker using small paintbrush and placed in a "nest of sieves" (aka sieve series). Shake for two minutes and weigh sample collected in each section of the sieve.

Organic Matter Removal (>2% Organic Matter)

1. Add DI water to each bottle. Water level should be just above soil.
2. Add 10 ml of 30% H₂O₂ to each bottle. Let stand overnight in hood beside water bath.
3. Place bottles in water baths, add 5 ml 30% H₂O₂ and heat to 80 degrees C. Don't let samples get dry. DO NOT leave water baths ON overnight.
4. The next day, add 5 ml 30% H₂O₂ and heat to 80 degrees C. Let bottles stay in bath for about 4 hours, then turn off the baths. Samples should be ready for shaking.
5. If you need to add more H₂O₂, add in 5 ml increments until all OM is burned off. Let samples stand at least 24 hours before shaking to avoid exploding samples.

Last updated 4/28/05 CMS

Appendix E

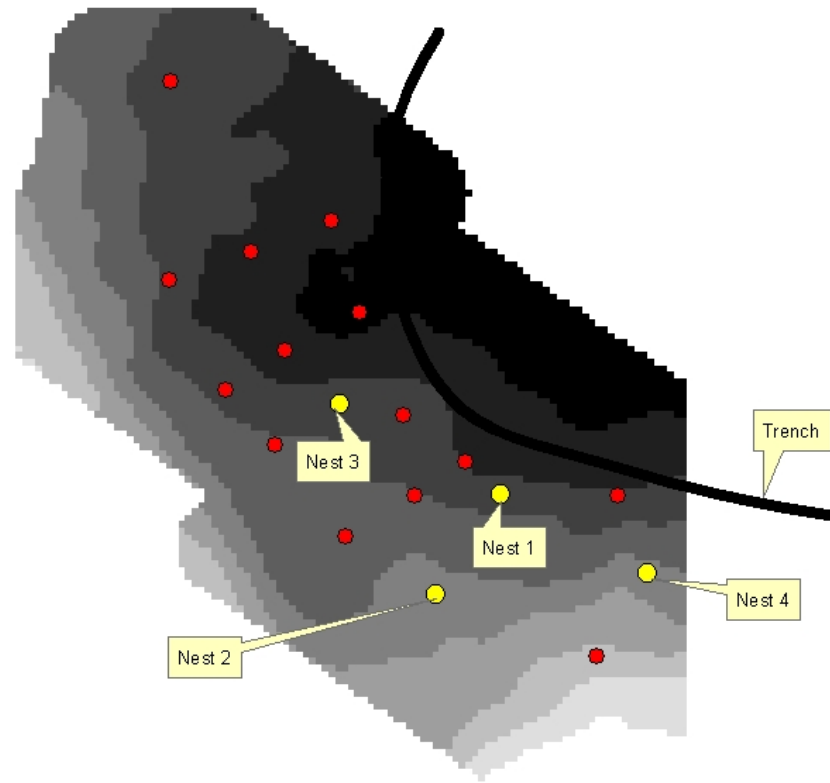
Maximum Rise Piezometer Data

Data from max rise piezometers as discussed in the materials and methods section are presented here. It should be noted that the piezometer ID, is the distance and aspect away from a specific piezometer nest (DISTANCE m, Aspect, Nest #), for instance 15MSW4, is 15 meters south west of piezometer nest 4. Max rise piezometer locations (red points) as well as recording piezometer nests (yellow points) are shown in the figure below. The piezometers are shown overlain the clay topographic map to give reference to low points in the argillic horizon. As discussed previously the first three dates that max rise piezometers were read, might be a little biased as it was the first time the author read them and the data is not considered to be valid, but is presented here as it was recorded. Data from max rise piezometers was considered valid if there was a concentric ring of cork dust around the inner PVC and or Kolor Kut paste either changed color or was not present along with the cork dust ring.

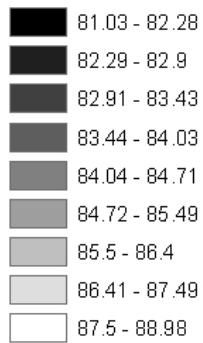
Piezometer ID	Date	WL cm	Date	WL cm	Date	WL cm	Date	WL cm
15MSW4	1/12/2007	189	2/2/2007	110	2/23/2007	63	3/22/2007	0
14MNW4	1/12/2007	211	2/2/2007	20	2/23/2007	11	3/22/2007	19
8.3MNW1	1/12/2007	235	2/2/2007	30	2/23/2007	19	3/22/2007	0
14MW1	1/12/2007	188	2/2/2007	89	2/23/2007	26	3/22/2007	19
20MS3	1/12/2007	194	2/2/2007	50	2/23/2007	4	3/22/2007	0
11.8MSW3	1/12/2007	122	2/2/2007	47	2/23/2007	2	3/22/2007	6
18MW3	1/12/2007	95	2/2/2007	100	2/23/2007	0	3/22/2007	4
11.8MNW3	1/12/2007	136	2/2/2007	122	2/23/2007	10	3/22/2007	0
28.5MNW3	1/12/2007	199	2/2/2007	190	2/23/2007	25	3/22/2007	0
32.5MNW3	1/12/2007	203	2/2/2007	202	2/23/2007	182	3/22/2007	9
56MNW3	1/12/2007	177	2/2/2007	168	2/23/2007	18	3/22/2007	0

Piezometer ID	Date	WL cm	Date	WL cm	Date	WL cm	Date	WL cm
15MSW4	4/13/2007	0	5/3/2007	0	5/18/2007	2	6/13/2007	2
14MNW4	4/13/2007	0	5/3/2007	0	5/18/2007	0	6/13/2007	2
8.3MNW1	4/13/2007	0	5/3/2007	0	5/18/2007	0	6/13/2007	1.6
14MW1	4/13/2007	0	5/3/2007	0	5/18/2007	0	6/13/2007	0
20MS3	4/13/2007	21.8	5/3/2007	0	5/18/2007	0	6/13/2007	0
11.8MSW3	4/13/2007	0	5/3/2007	0	5/18/2007	1	6/13/2007	0
18MW3	4/13/2007	2	5/3/2007	0	5/18/2007	0	6/13/2007	0
11.8MNW3	4/13/2007	0	5/3/2007	0	5/18/2007	0	6/13/2007	0
28.5MNW3	4/13/2007	0	5/3/2007	4	5/18/2007	0	6/13/2007	2
32.5MNW3	4/13/2007	0	5/3/2007	2	5/18/2007	3	6/13/2007	0
56MNW3	4/13/2007	0	5/3/2007	0	5/18/2007	0	6/13/2007	0

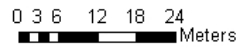
Piezometer ID	Date	WL cm	Date	WL cm
15MSW4	7/6/2007	0	7/31/2007	0
14MNW4	7/6/2007	0	7/31/2007	0
8.3MNW1	7/6/2007	0	7/31/2007	0
14MW1	7/6/2007	0	7/31/2007	2
20MS3	7/6/2007	0	7/31/2007	0
11.8MSW3	7/6/2007	0	7/31/2007	0
18MW3	7/6/2007	0	7/31/2007	0
11.8MNW3	7/6/2007	0	7/31/2007	0
28.5MNW3	7/6/2007	0	7/31/2007	0
32.5MNW3	7/6/2007	0	7/31/2007	0
56MNW3	7/6/2007	0	7/31/2007	0



Argillic Topograhly - m



- Max Rise Piezometer
- Piezometer Nest



Appendix F

HYDRUS Results

The first simulation for the hillslope modeling effort was named SRSNDMRATMobsexis_Base, and hereafter should be referred to as “base case”. The following images and tables are from HYDRUS 2-D output from the various model runs completed for the study. All domains will be labeled and noted as to what changed for each model (i.e. Base case, will correspond to field data with respect to field measured data, other models will change parameters or add parameters and will be accounted for in data tables, figures etc.). It should be noted that in some cases multiple model runs were completed using the same model domain, material distribution, boundary conditions, material conditions and time variable boundary conditions, in which case only one model domain will be shown, and parameter changes for the model run will be noted accordingly.

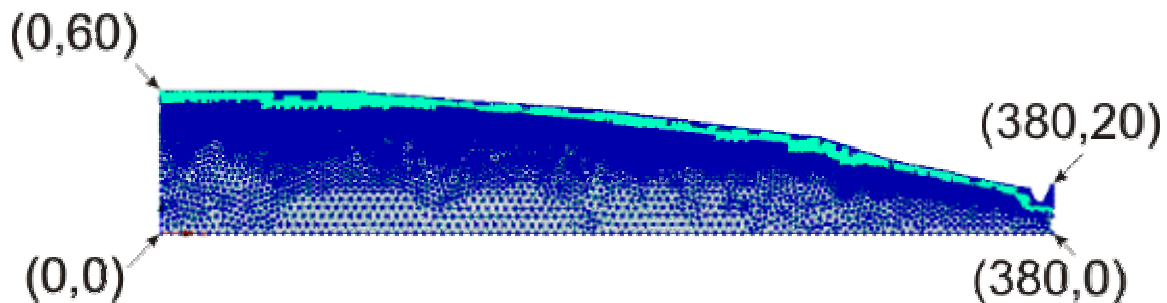


Figure 38. Material Distribution and Coordinates (x,z) in m, of the “Large” Model Domain.

The figure represents the entire hillslope from the summit (0,60) to the stream (380,20). The the dark blue points (nodes) are sand (Material 1), where the light blue nodes are the argillic (Sandy Clay Loam) (Material 2) horizon. The following table shows the soil hydraulic parameters HYDRUS 2-D used to compute soil moisture release as well as hydraulic head (h – m) throughout the entire model domain.

Table 17. HYDRUS 2-D Soil Hydraulic Parameters for “Large Model Base Case”.

Material	Qr	Qs	Alpha	N	Ks	I
1	0.053	0.3747	3.53	3.1798	6.4298	0.5
2	0.0633	0.3837	2.11	1.3298	0.1319	0.5

HYDRUS 2-D uses the van-Genuchten equation (from HYDRUS technical manual) (below) to calculate soil moisture release for 12 different soil textures.

$$\theta = \left\{ \theta_r + \frac{\theta_s - \theta_r}{\left(1 + |\alpha h|^n\right)^m} \right. \quad h < h_s ; \quad \theta_s \quad h \geq h_s$$

$$K(h) = K_s S_e^{0.5} \left[1 - \left(1 - S_e^{1/m}\right)^m \right]^2$$

Where:

θ_s - saturated water content [-]

θ_r - residual water content [-]

α, m, n - empirical parameters [1/L], [-],[-]

h_s – air entry value [L]

S_e – effective water content [-]

K_s – saturated hydraulic conductivity [L/T]

K_r – relative hydraulic conductivity [-]

$K_k(hk)$ – unsaturated hydraulic conductivity at pressure head hk [L/T]

The above equation comes from HYDRUS technical manual distributed with the software, the equation is derived from van Genuchten (1980).

Along with soil hydraulic parameters each model had set boundary conditions as outlined below, where “time-variable” boundary conditions were used to simulate a one year (365 day) period from observed field data (soil data was created using “Rosetta light” a function of the model along with in situ K_s data from SRS, climate data was used for the atmospheric boundary, where stage at the flume was used as a variable head boundary in the stream as shown in Figure 2 below). Also a no flow boundary was used along the sides and bottom as shown.

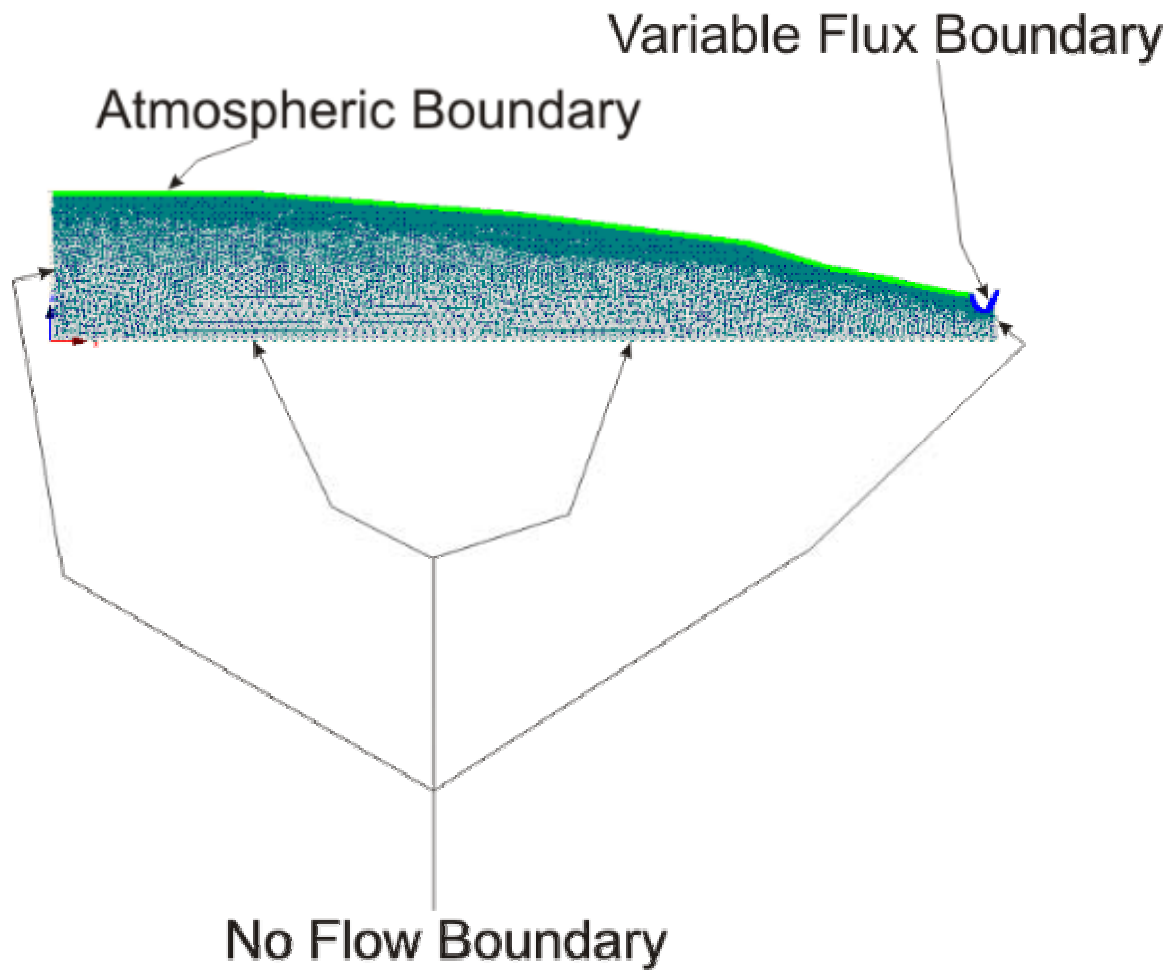


Figure 39. Boundary conditions used in “Large Model Domain”.

Once models were run, data from the model was extracted via observation nodes (Obs), which are placed in the model wherever the user desires. In this study Obs were placed above, in and well below the argillic horizon in order to observe pressure head and soil moisture dynamics at Obs, in Figure 3.

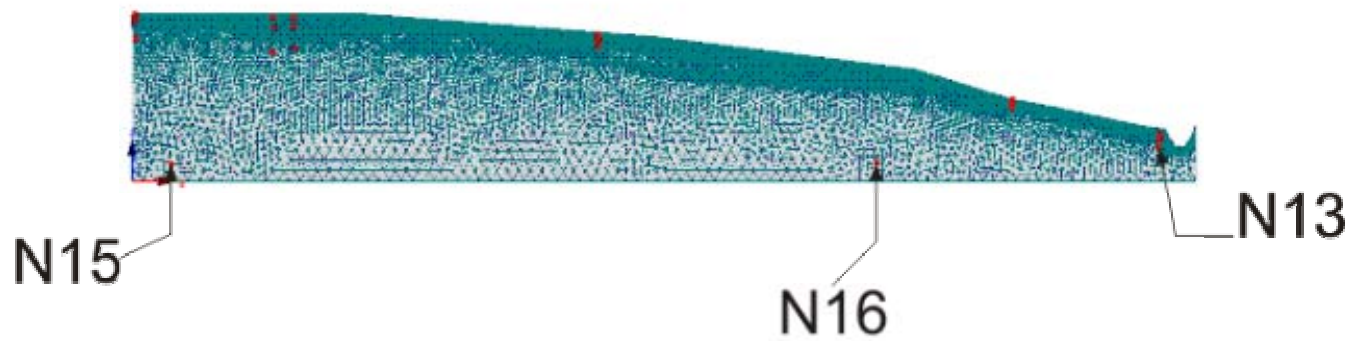


Figure 40. Observation nodes (red) of Large Model Domain.

Figure 3, shows all the observation nodes places throughout the model domain, where only three are numbered (N13, N15, and N16), these nodes correspond to positive pressure heads at some point in the model run. Consequently all these nodes are in what has been termed the saturated zone well below the argillic horizon. The following figure shows the positive pressure heads at day 148 in the model run.

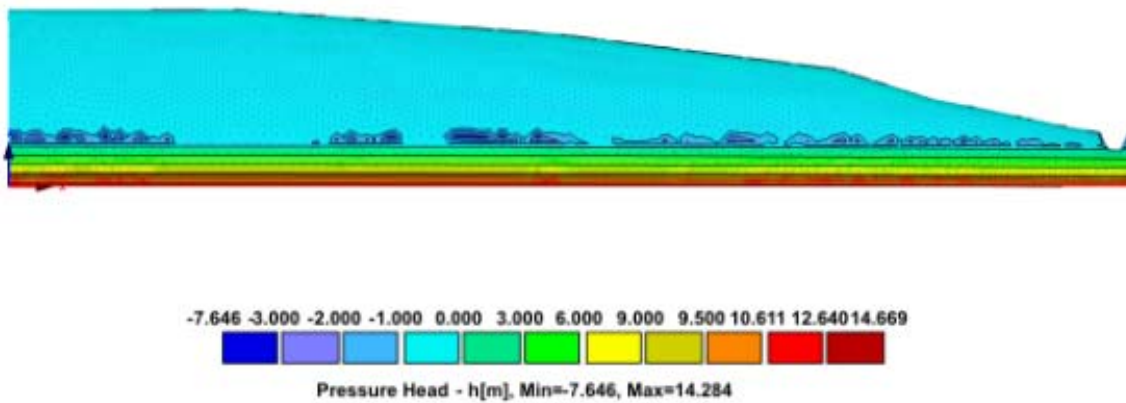


Figure 41. Pressure head distribution of “Base Case” Large model domain at day 148.

Also, water content at day 148 is shown (Figure 5), it should be noted that the argillic horizon is saturated (shown in red), and a large distance > 40 m below the argillic is unsaturated (shown in blue) while the soil does not become saturated (red) again until ~ 43 m below the argillic horizon.

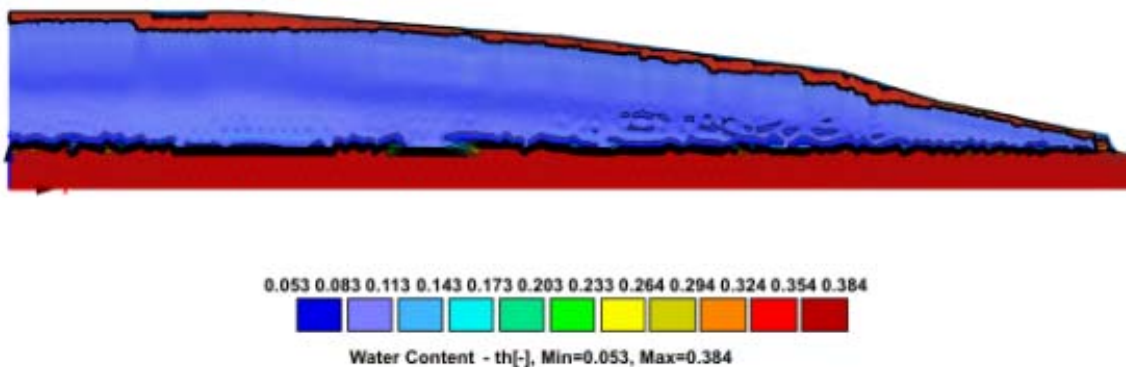


Figure 42. Water content of “Base Case Large Domain”.

The following graph is a HYDRUS output of pressure head vs. time showing only three instances of positive pressure throughout the simulation, these points are the aforementioned Obs in the model domain, it should be noted that none of the instances of positive head lie above or within the argillic horizon.

Observation Nodes: Pressure Heads

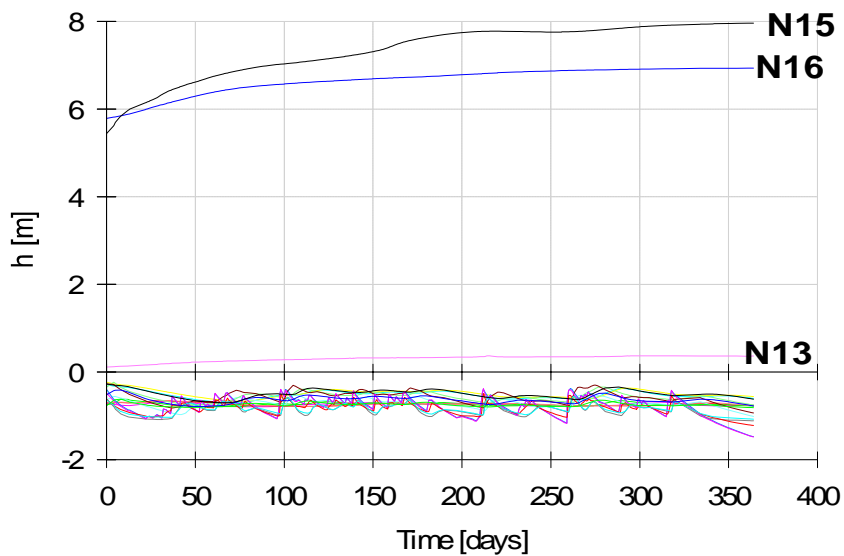


Figure 43. Graphical representation of pressure head from “Large Domain Base Case” simulation.

Observation Nodes: Water Content

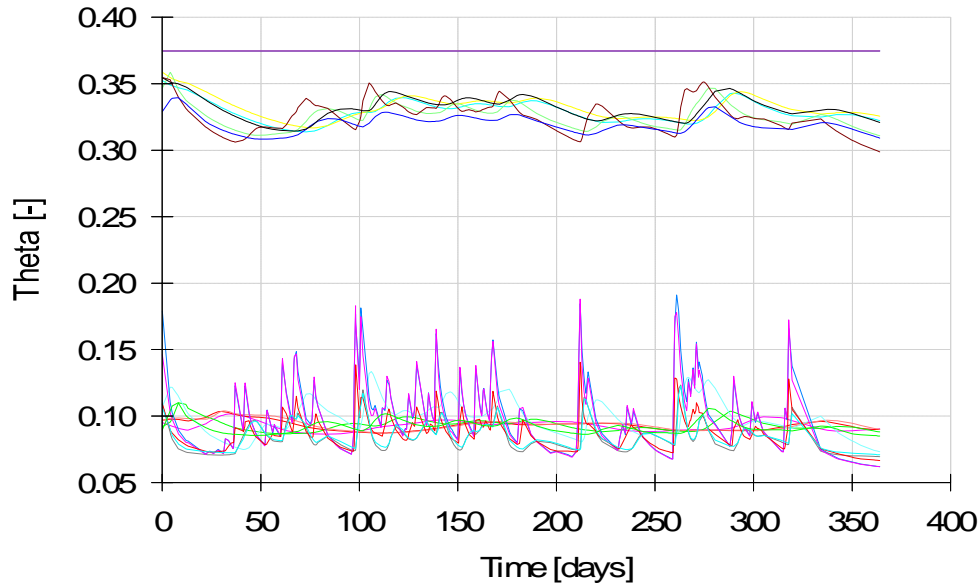


Figure 44. Graphical representation of water content from “Large Domain Base Case” simulation.

After discovering that the “base case” would not show the observed perching events or positive pressure heads it was decided to adjust the K_s of the argillic horizon to induce perching. The name given to this simulation was SRSNDRATMobsexis_3. SRSNDRATMobsexis_3, uses the same domain, material distribution, boundary conditions, and observation nodes as the base case. The only parameter changed was the K_s of the argillic horizon noted in the table below. The following table and graphics show the results and parameters used in this simulation.

Table 18. Soil hydraulic parameters of SRSNDRATMobsexis_3simulation.

Material	Qr	Qs	Alpha	n	Ks	l
1	0.053	0.3747	3.53	3.1798	6.4298	0.5
2	0.0633	0.3837	2.11	1.3298	0.04	0.5

Observation Nodes: Pressure Heads

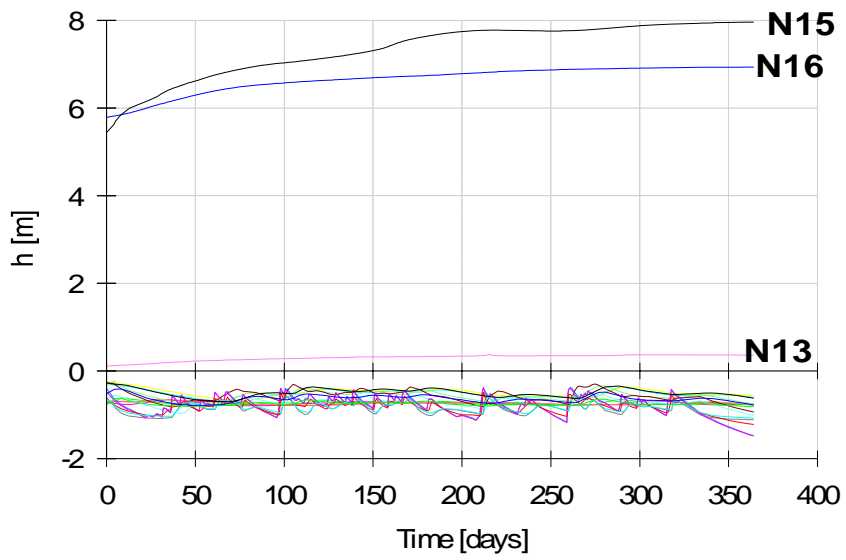


Figure 45. Graphical output of pressure head from SRSNDMRATMobsexis_3 simulation.

Observation Nodes: Water Content

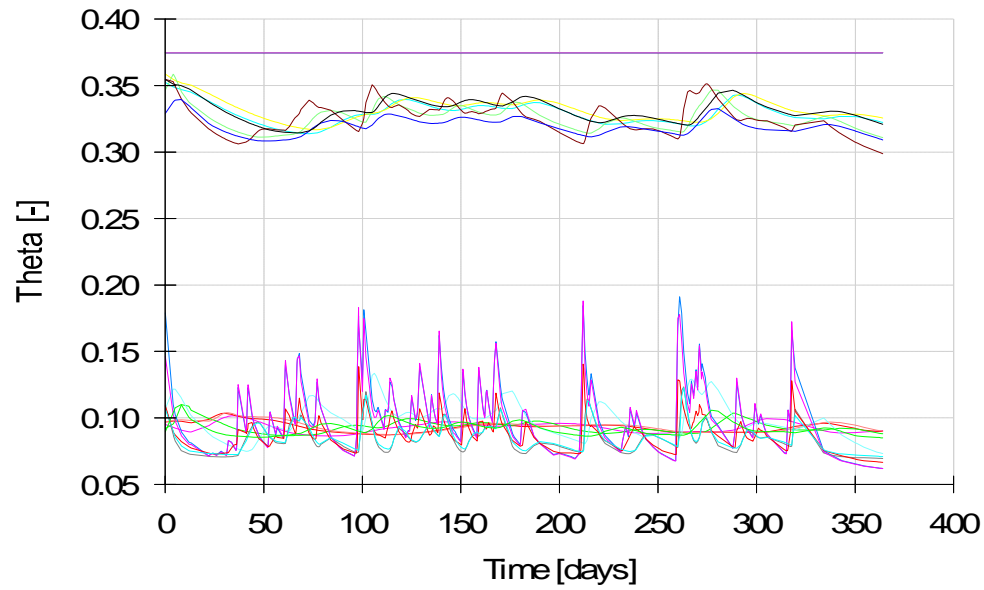


Figure 46. Graphical output of water content from SRSNDMRATMobsexis_3 simulation.

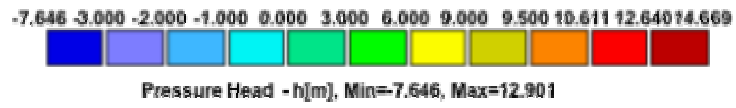
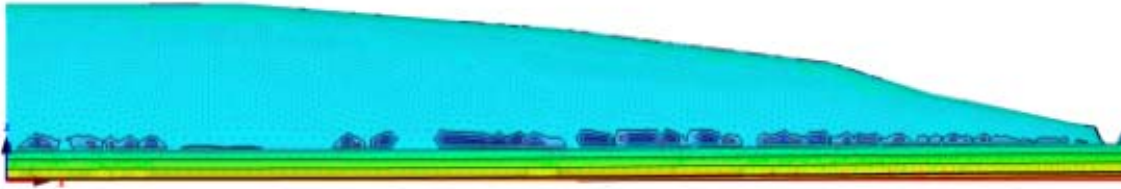


Figure 47. Graphic of pressure head from SRSNDMRATM_obsexis_3 simulation at day 148.

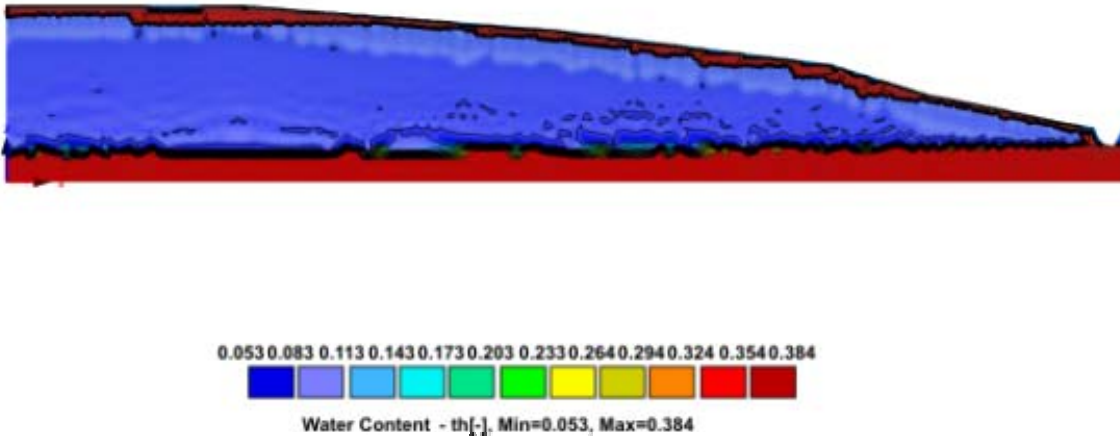


Figure 48. Graphic of water content from SRSNDMRATM_obsexis_3 simulation at day 148.

After reviewing the graphs and graphical output from each run, base case sand “obsexis_3” simulations it is clear that even lowering the Ks of the argillic two orders of magnitude would not create perching events above or in the argillic horizon. Therefore it was decided that the model domain was too large to account for such small scale variations in pressure head both within and above the argillic horizon.

A new model domain was created (SRS_smdom), to reason if domain size was the cause for the lack of a response (positive head above or within argillic horizon). This new domain is 2 m x 10 m (x,z), and the first simulation SRS_smdom_2 can be considered the base case.

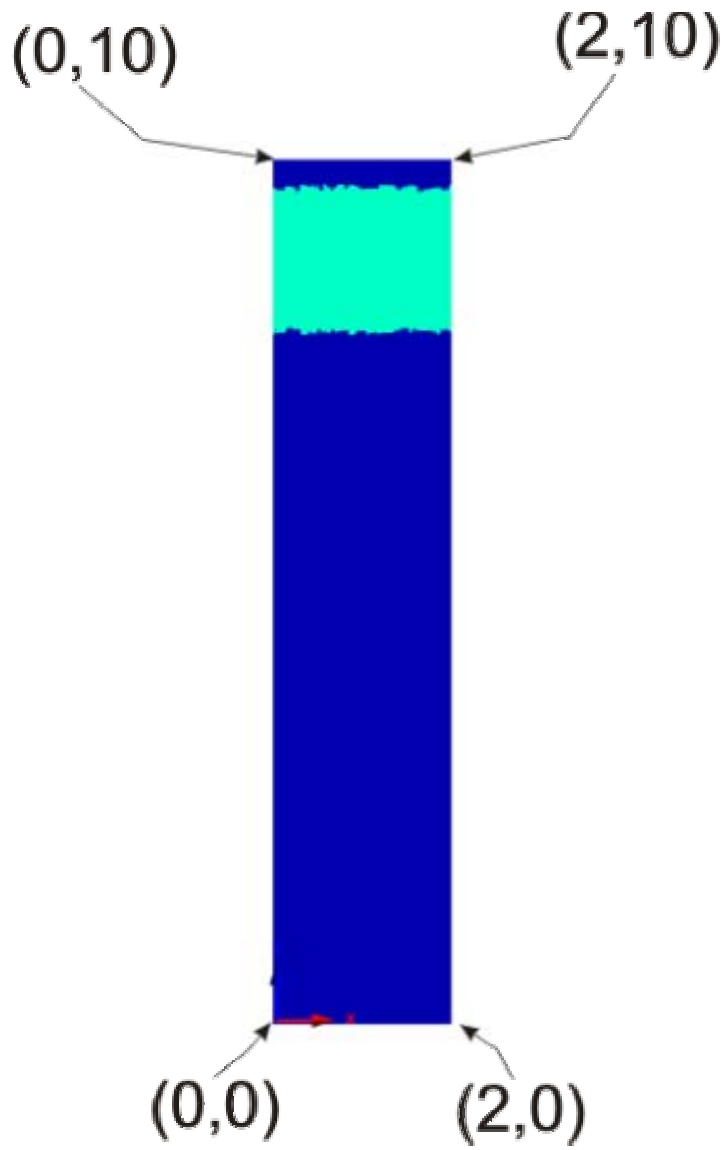


Figure 49. SRS_smdom domain and material distribution used for each simulation.

The base case for the small domain simulations used two materials shown above, where dark blue nodes are sand (Material 1) and light blue nodes are the argillic horizon (Material 2).

The soil hydraulic parameters are presented in the table below.

Table 19. Soil hydraulic parameters for small domain base case.

Material	Qr	Qs	Alpha	n	Ks	l
1	0.053	0.3747	3.53	3.1798	6.42979	0.5
2	0.0633	0.3837	2.11	1.3298	0.1319	0.5

The small domain (sm_dom) base case boundary conditions are presented on the next page, were uniform for each sm_dom simulation, using the same time variable atmospheric boundary condition on top, the model was able to simulate inputs from precipitation and outputs from potential evapotranspiration (PET), both of which were measured in the field. Along the sides of the model domain were no flow boundaries and at the bottom was a constant head boundary of 1 m, to allow for positive pressure heads and saturated conditions to build at the bottom of the boundary.

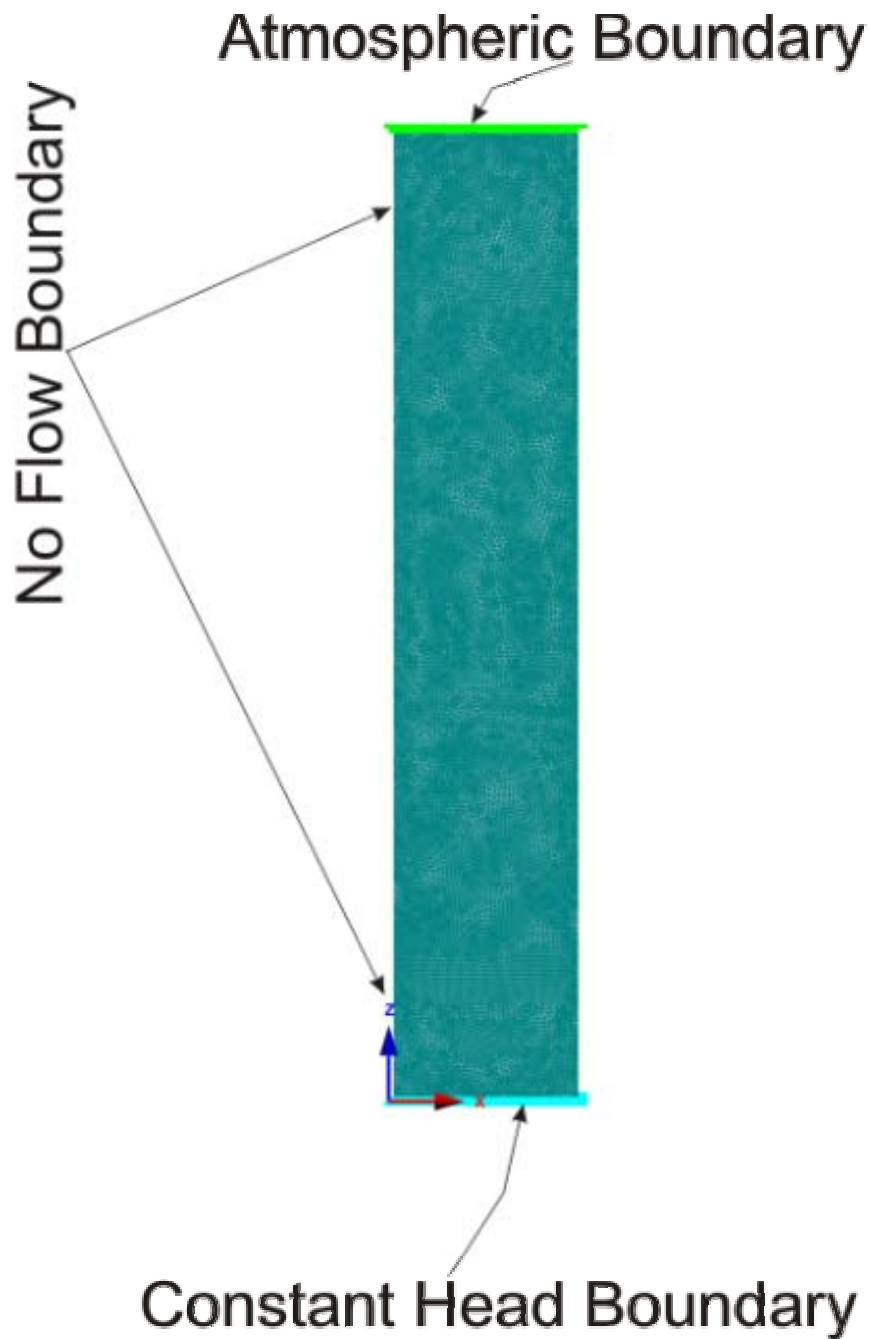


Figure 50. Graphic of small domain boundary conditions.

Pressure head and water content was recorded for each simulation via observation nodes, the following graphic illustrates the positions of each node with respect to the domain and material distribution for each model run.



Figure 51. Graphic of sm_dom observation nodes (red).

Observation Nodes: Pressure Heads

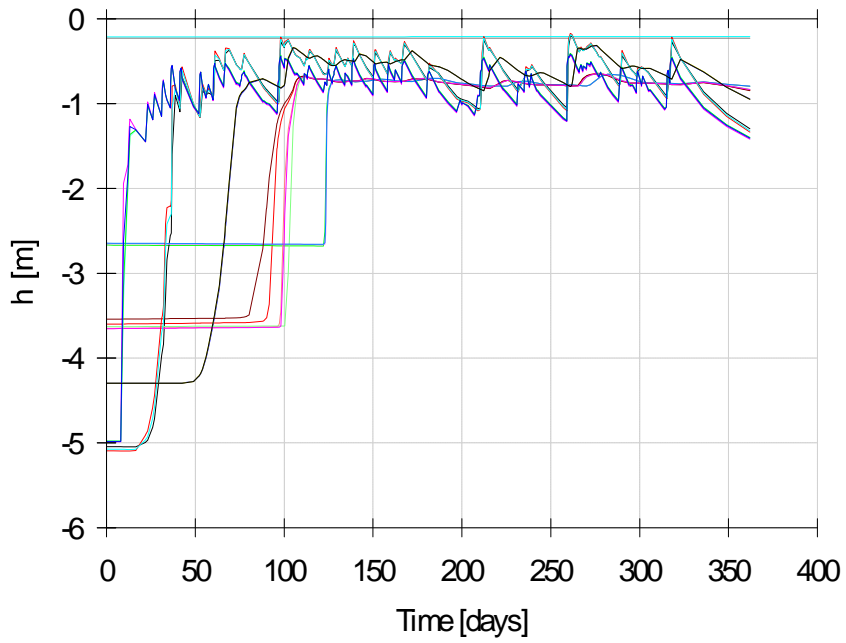


Figure 52. HYDRUS graph output of pressure head vs. time at each observation node from base case.

Observation Nodes: Water Content

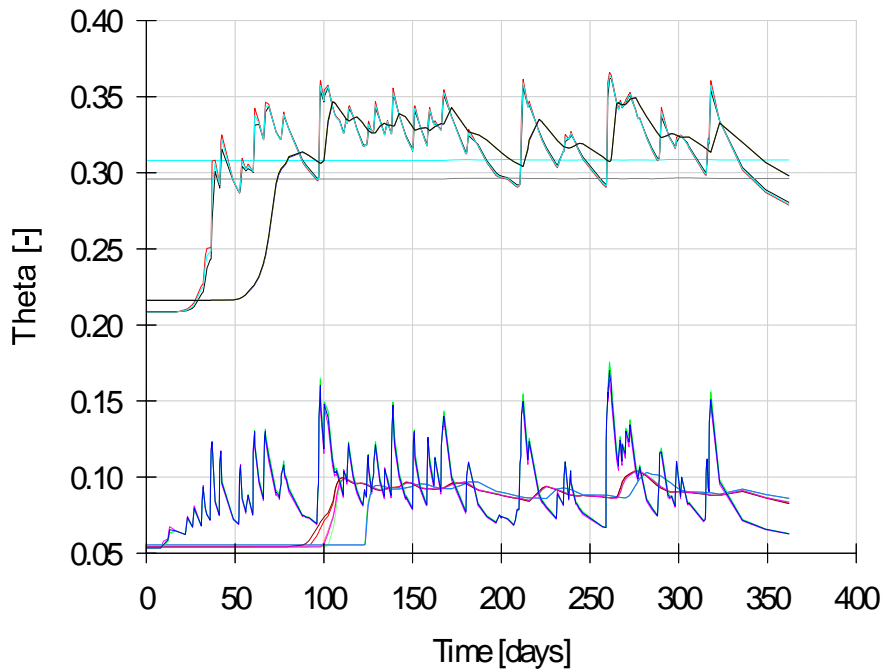


Figure 53. HYDRUS graph output from base case for each observation node.

It was deemed unnecessary to incorporate HYDRUS graphical displays of either pressure head or water content as, there were no instances of positive pressure head throughout the simulation, and water content is similar to the large domain results where saturated or near saturated conditions only exist within the argillic horizon. Thus new model simulations were done to try and force the model to create perching conditions above or within the argillic horizon. The following graphs and tables are from model simulations that represent these forcing conditions.

The first manipulation of parameters SRS_smdom_4, hereafter known as forcing condition one (FC1), used an unrealistic value for the sand Ks, as shown in the table below.

Table 20. Soil hydraulic parameters used for FC1 simulation.

Material	Qr	Qs	Alpha	n	Ks	l
1	0.053	0.3747	3.53	3.1798	600.43	0.5
2	0.0633	0.3837	2.11	1.3298	0.1319	0.5

Even with increasing the Ks of the sand two orders of magnitude larger to try and recreate kinematic or pressure wave propagation effect, still no positive heads could be created in the simulation, shown in Figure 17. Figure 18, water content from all observation nodes in FC1 is almost identical to the water content from the base case (Fig. 16). This indicates that even with a large Ks difference water is still not being forced to or into the argillic layer at a quick enough rate to create ponding within or on top of the argillic horizon.

Observation Nodes: Pressure Heads

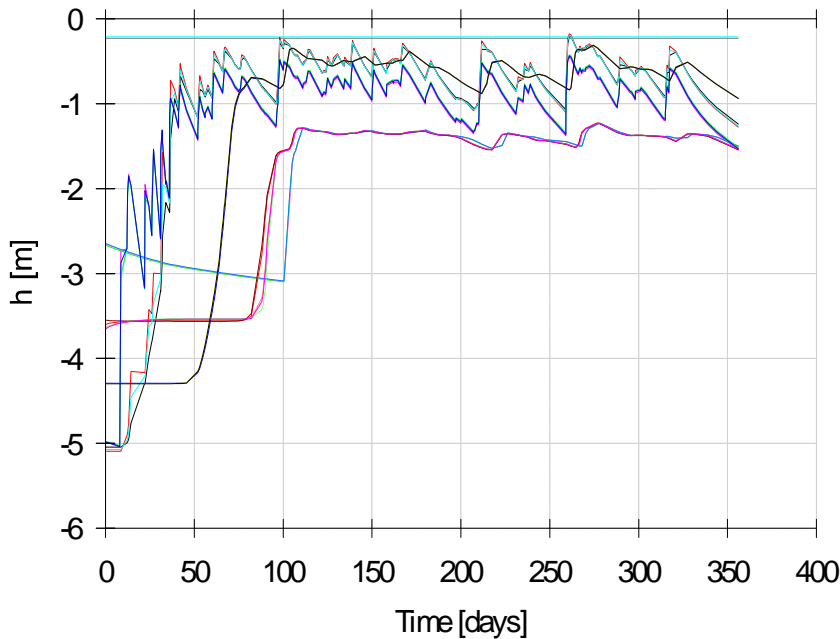


Figure 54. HYDRUS graphical output of pressure head from all FC1 observation nodes.

Observation Nodes: Water Content

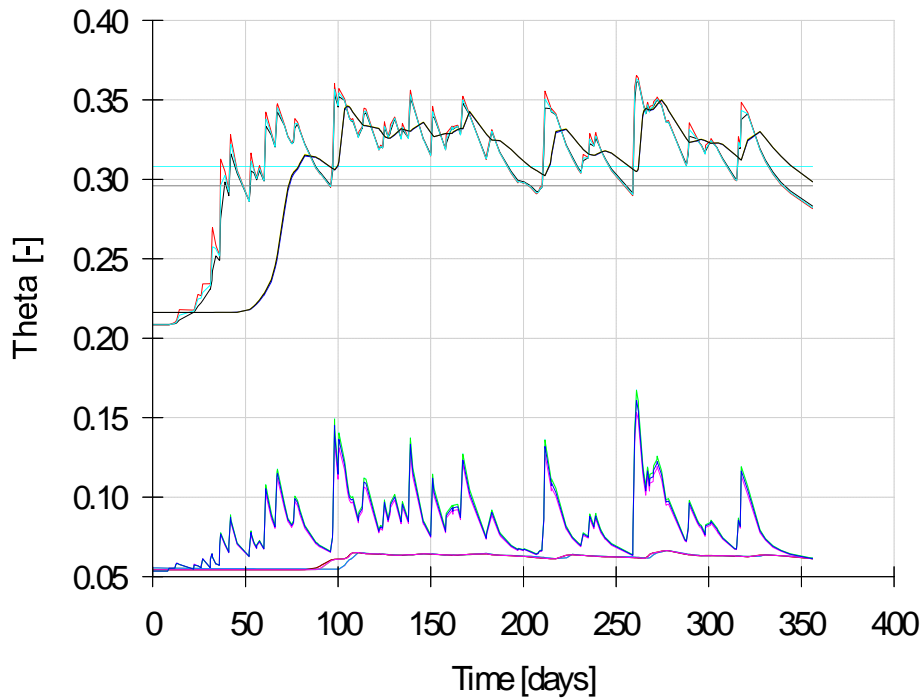


Figure 55. HYDRUS graphical output of water content from all FC1 observation nodes.

Another model run using the small domain SRS_smdom_7 (known hereafter as FC2) utilizes three soil materials, which “grade” down to very low Ks below the argillic. The intention of using three soil layers was to try and simulate the effects of a BC horizon or a capillary barrier below the argillic horizon that could have impeded the vertical flow of water out of the argillic and allowed the positive pressure heads exhibited in the measured data. Table 5, shows the soil hydraulic parameters used in this simulation, and figure 19 shows the material distribution, while figures 20 and 21 show pressure head and water content from each observation node.

Table 21. Soil hydraulic parameters used in FC2.

Material	Qr	Qs	Alpha	n	Ks	I
1	0.053	0.3747	3.53	3.1798	600.43	0.5
2	0.0633	0.3837	2.11	1.3298	0.1319	0.5
3	0.0485	0.3904	3.47	1.7466	0.01	0.5

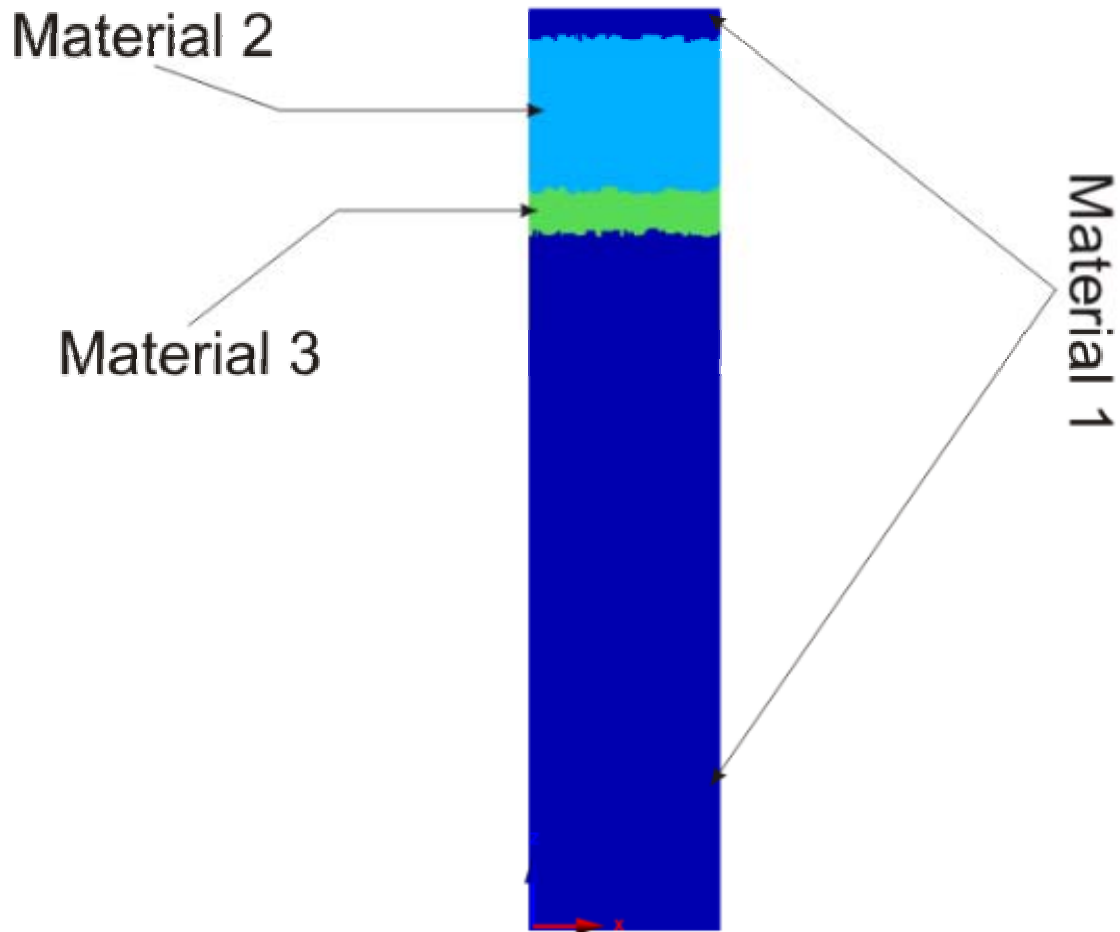


Figure 56. Material distribution from FC2.

Observation Nodes: Pressure Heads

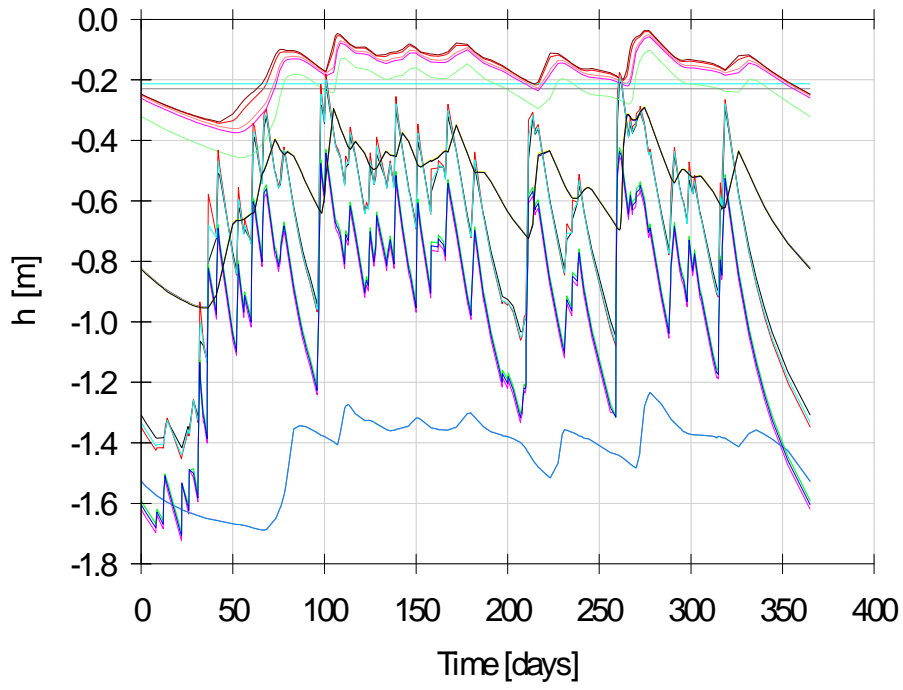


Figure 57. HYDRUS graph of pressure head vs. time at all observation nodes from FC2.

Observation Nodes: Water Content

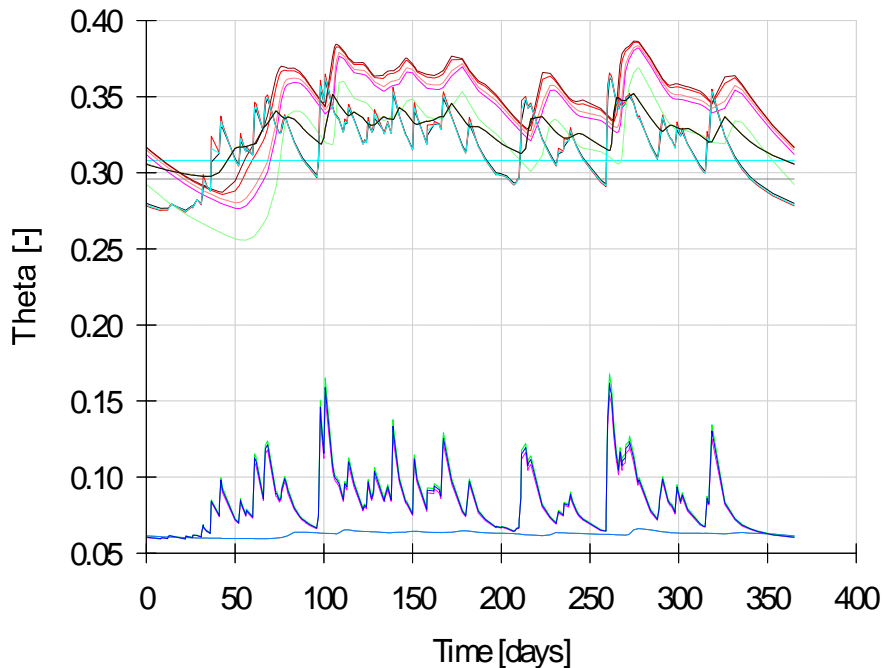


Figure 58. HYDRUS graph of water content vs. time at all observation nodes from FC2.

Results from FC2 are still very similar to FC1, where there are no instances of positive head above or within the argillic horizon, thus a new model was created, named SRS_smdom_7b2 (FC3), using the same boundary conditions, observation nodes, and domain as base case, FC 1 and 2. The difference was the number of materials and thickness of material 4 (BC layer), material 1 is sand, 2 a transition from sand to argillic, and material 3 is the argillic horizon. FC3 soil hydraulic parameters are presented in table 6, material distribution in figure 22, pressure head vs. time in figure 23. This model only ran for about 28 days until it timed out and could not longer simulate with the given conditions (fig. 23).

Table 22. Soil hydraulic parameters used in FC3 simulation.

Material	Qr	Qs	Alpha	n	Ks	l
1	0.053	0.3747	3.53	3.1798	6.4298	0.5
2	0.0387	0.387	2.67	1.4484	0.3825	0.5
3	0.0633	0.3837	2.11	1.3298	0.1319	0.5
4	0.0792	0.4418	1.58	1.4145	0.00818	0.5

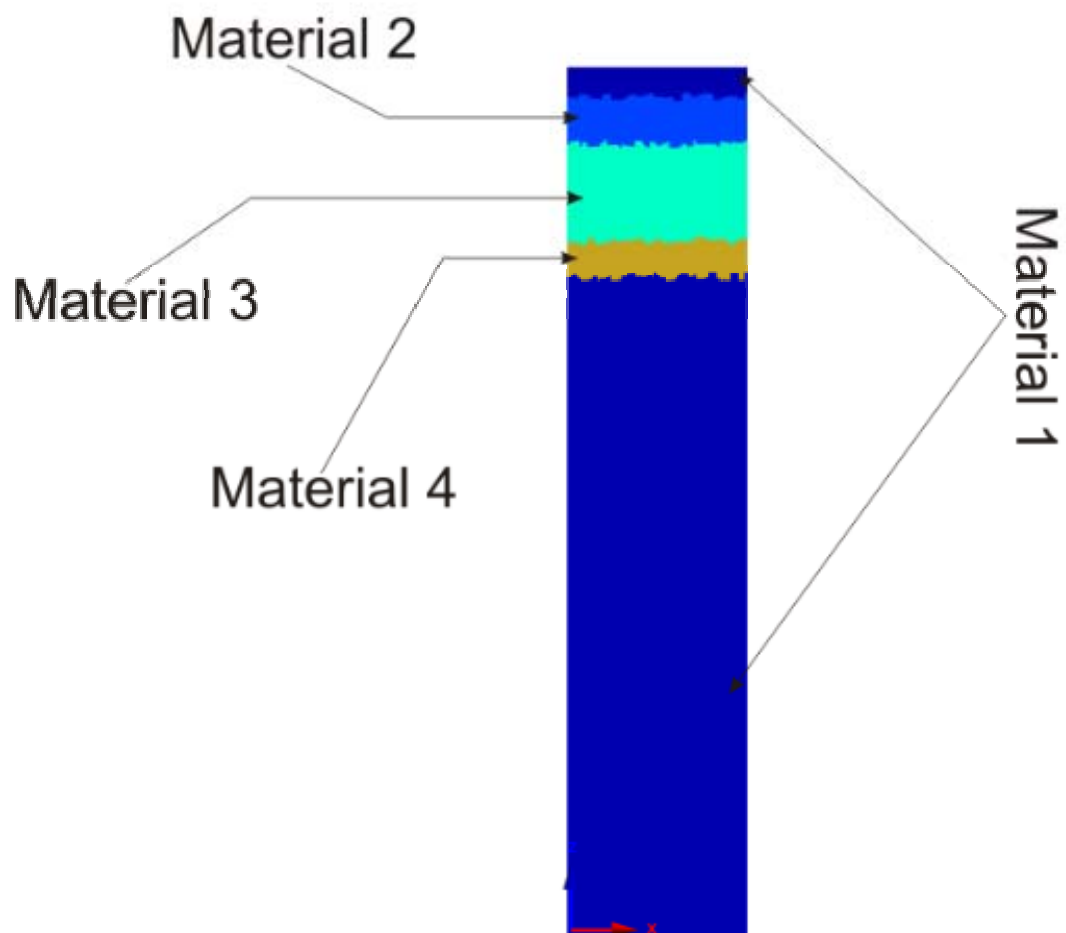


Figure 59. Material distribution from FC 3 simulation.

Observation Nodes: Pressure Heads

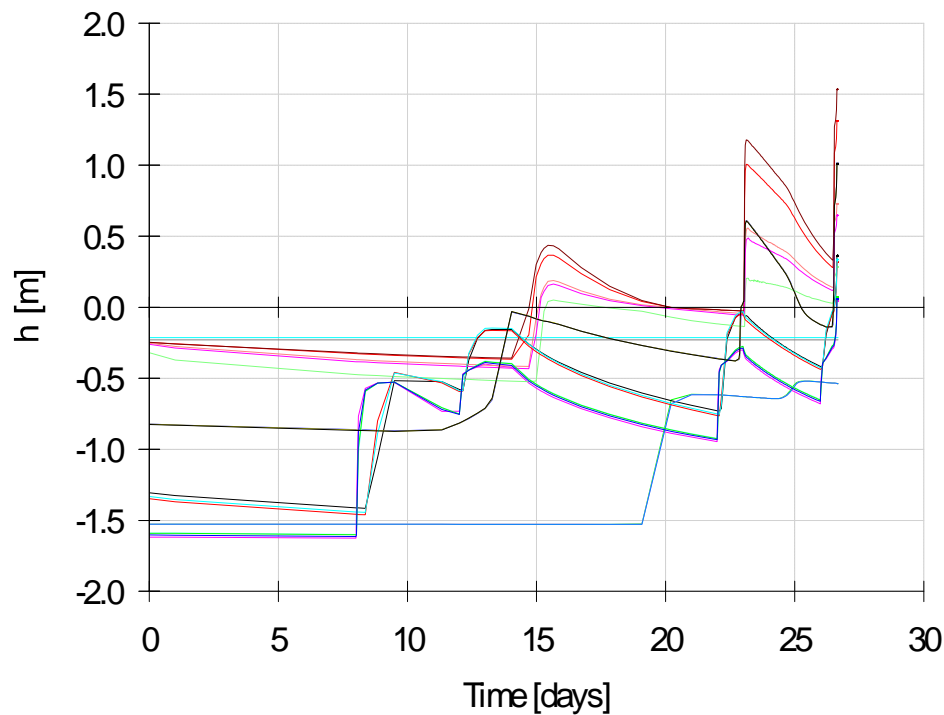


Figure 60. HYDRUS graphical output of pressure head vs. time for all observation nodes in FC3 simulation.

As can be noted the model only ran for about 28 days, notice there are positive heads, however, the model was not considered valid as it only ran for 28 days. This simulation (FC 3) was included to show that only with a small domain and very unrealistic or non-observed conditions would positive pressures build up anywhere in this model.

A final model domain (SRS_NoFloArg) was developed, where a no flow boundary was placed directly below the argillic horizon. It was after many model simulations and manipulations to existing models that this thought occurred, also it was through many hours of conversation with others well versed in hydrologic modeling that this domain was created and is not the creation of the author. SRSNoFloArg_3 was considered the base case, and for this

discussion will be further known as “NoFlo Base Case”. Figure 24, shows the model domain with (x,z) coordinates in m and 2 materials, where the dark blue is material 1 sand and the light blue is the argillic horizon material 2 and fig. 25 shows the boundary conditions used for each simulation. Table 7, shows the soil hydraulic parameters used in all SRSNoFlo argillic horizon simulations. The only parameter changed in these simulations was the geometry of the argillic horizon, thus with the geometry change of the material distribution an observation node rearrangement proved necessary to capture pressure head and water content dynamics for each simulation. Figure 26 shows the observation nodes throughout the model domain where each node that recorded a positive pressure head is located (Node #), and Figure 27, is a graphical representation of each node exhibiting positive pressure heads, and it should be noted that two nodes (1 and 12) show a positive pressure head above the argillic horizon while the remaining nodes show positive pressure head within the argillic horizon.

Table 23. Soil hydraulic parameters for all SRSNoFloArg simulations.

Material	Qr	Qs	Alpha	N	Ks	I
1	0.053	0.3747	3.53	3.1798	6.4298	0.5
2	0.0633	0.3837	2.11	1.3298	0.1319	0.5

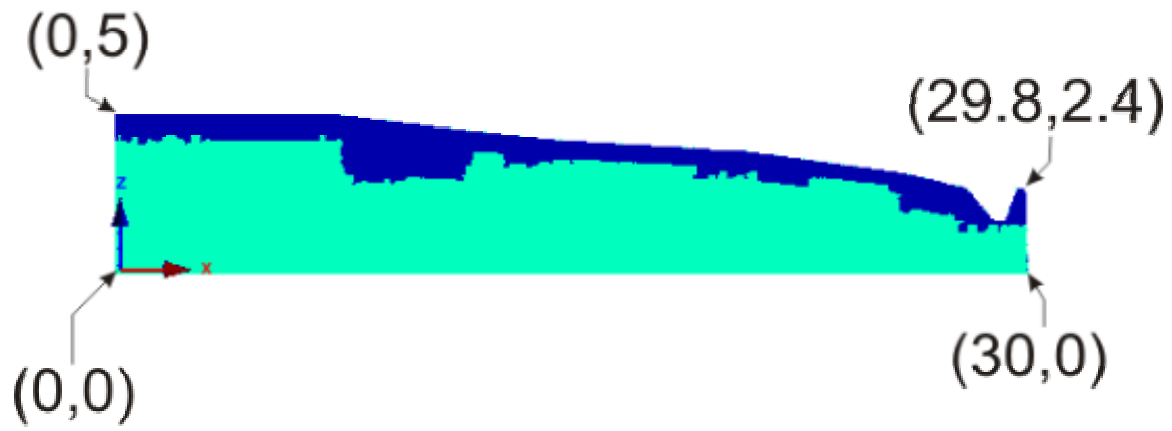


Figure 61. SRS_NoFloArg_3 model domain.

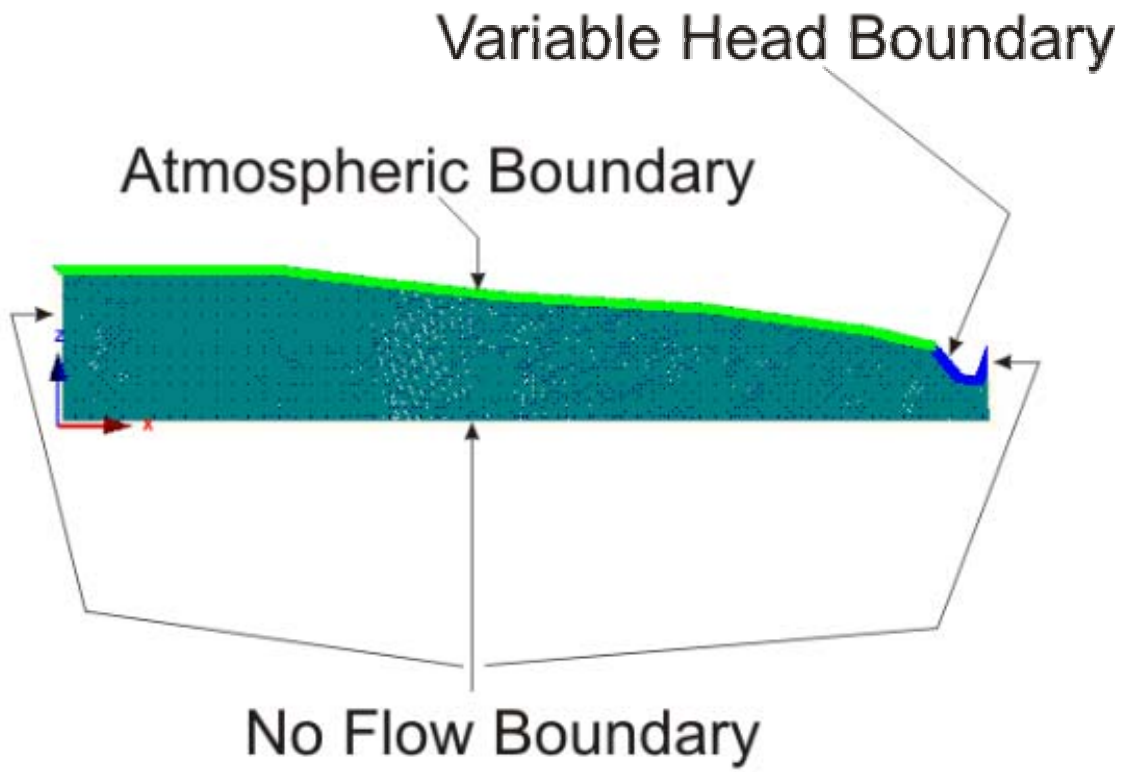


Figure 62. SRSNoFloArg boundary conditions.

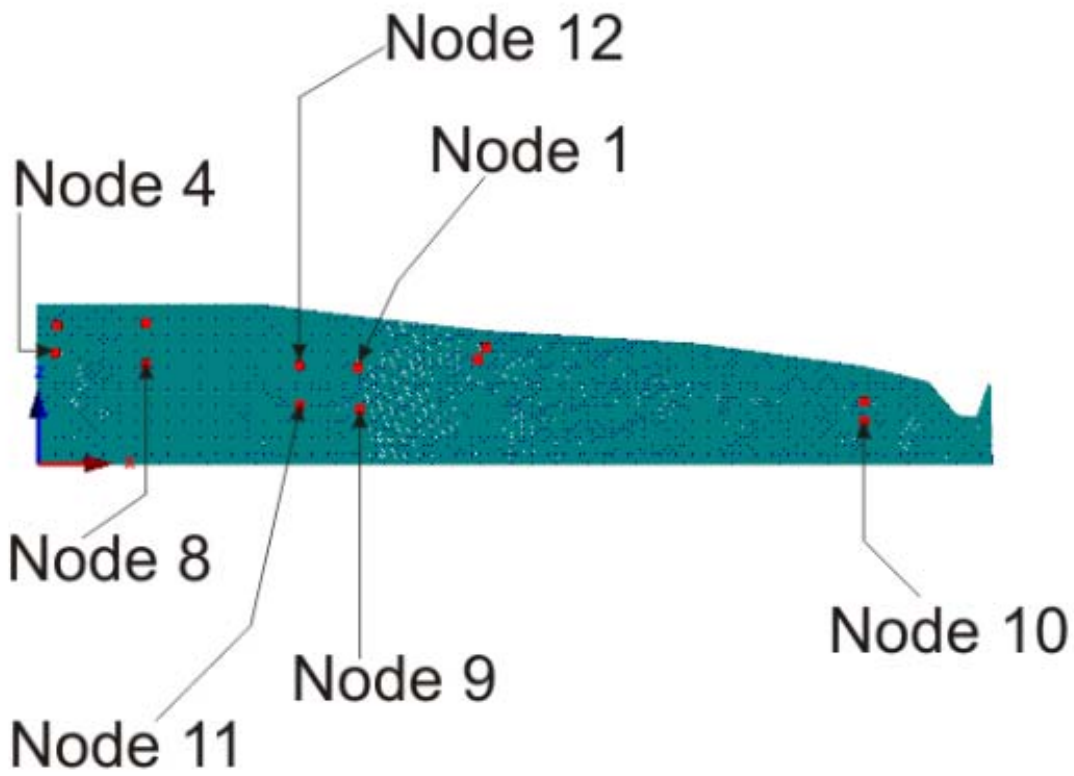


Figure 63. NoFlo Base Case observation nodes, each node where positive pressure was simulated is indicated.

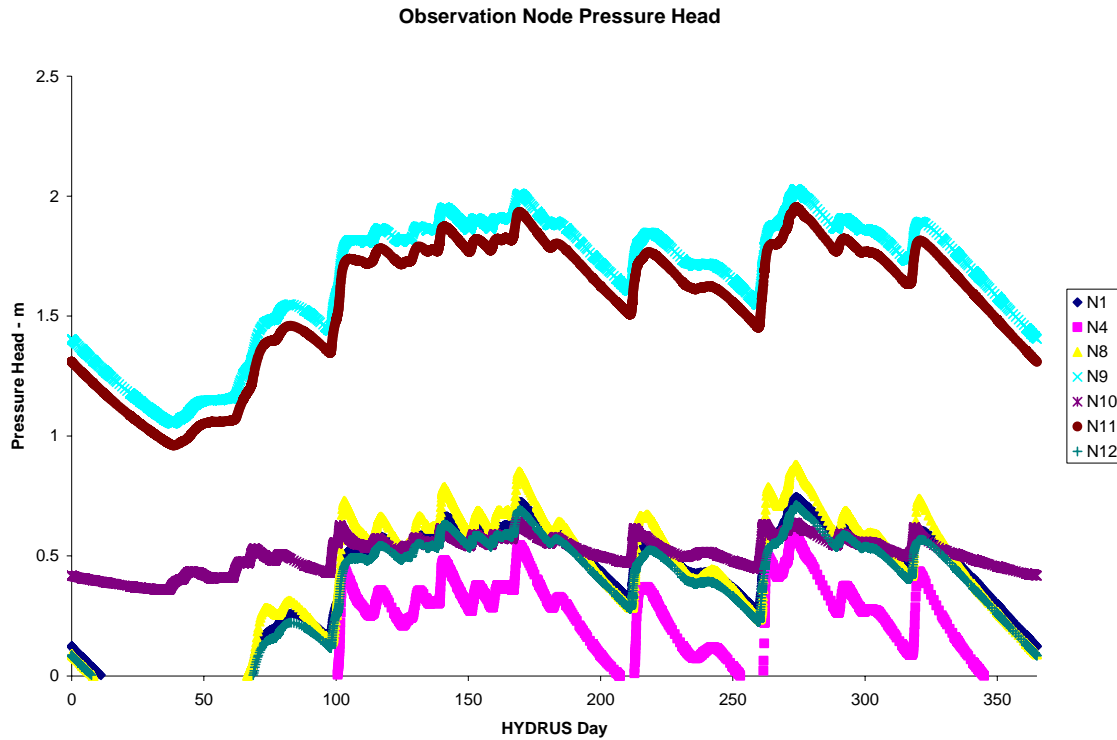


Figure 64. Graphic of positive pressure heads from NoFloArg Base Case simulation at specified nodes.

To rule out the rather large “low” point in the argillic horizon (Fig. 24) contributing to the positive pressure head above the argillic horizon, two other simulations were completed, one with an adjusted argillic geometry (Fig. 28)(SRSNoFloArg_3_adjarg) and a simulation with a relatively linear argillic horizon (SRSNoFloArg_3_lineararg) (Fig. 30) were used to compare said assumptions. Each simulation with differing argillic horizons had new observation nodes to correspond to the changes in the argillic geometry (Figs. 29 and 31, where nodes needed to be placed above the argillic). Figures 32 and 33, show the results from SRSNoFloArg_3_adjarg and SRSNoFloArg_3_lineararg, where positive pressure heads were shown both above and within the argillic horizon.

A final note on the model runs with a no flow boundary beneath the argillic horizon is that the argillic horizon geometry change did affect positive pressure head locations as was to be expected, however, it did not negate positive pressure head build up in the argillic horizon or above. This no flow boundary was imposed as stated before after much deliberation, as well as noting that throughout the study period, none of the piezometer nests showed a hydraulic response (positive pressure head) below the argillic, as measured by “deep” piezometers. Therefore, it was a logical and reasonable assumption to include in the model.



Figure 65. SRSNoFloArg_3_adjarg simulation model domain.

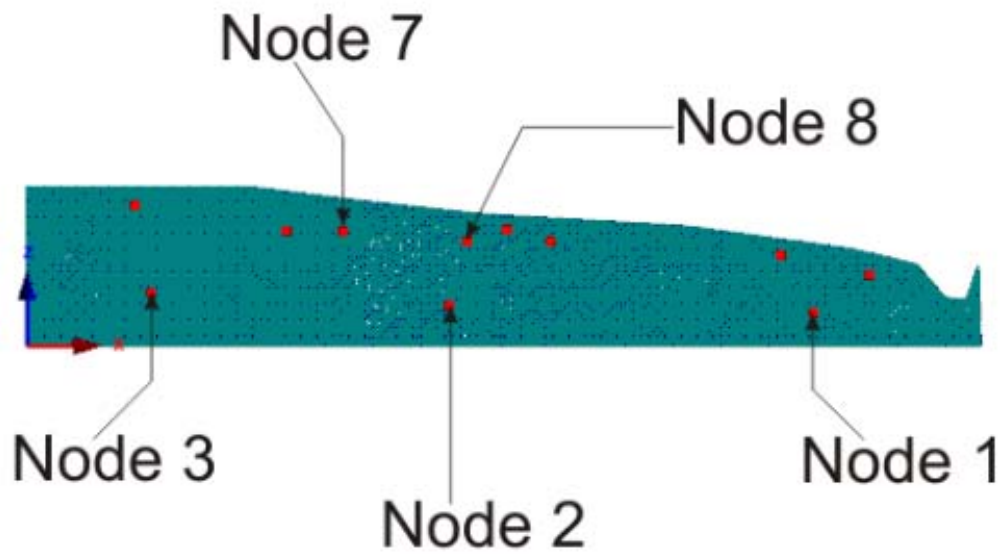


Figure 66. SRSNoFloArg_3_adjarg observation nodes, nodes recording positive head are labeled.



Figure 67. SRSNoFloArg_3_lineararg material distribution and model domain.

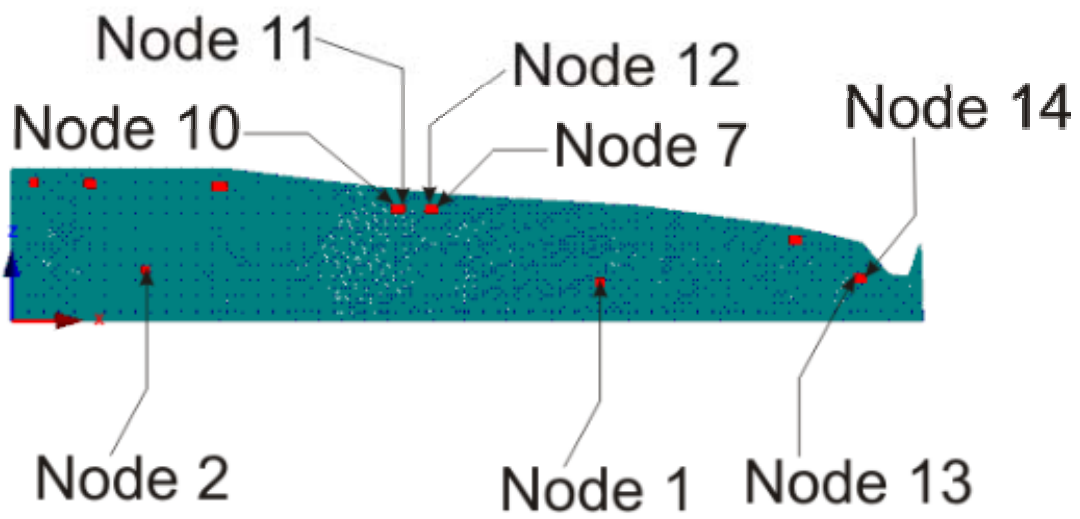


Figure 68. SRSNoFloArg_3_lineararg observation node, each labeled node recorded positive pressure heads.

Observation Nodes: Pressure Heads

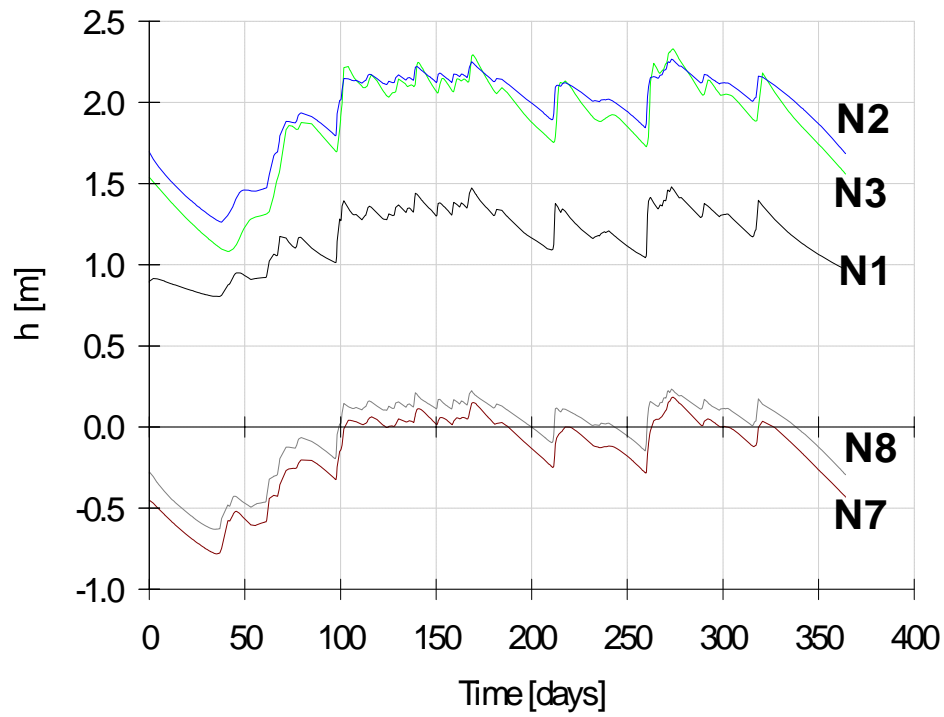


Figure 69. HYDRUS graphical from SRSNoFloArg_3_argadj, output of pressure head vs. time, each labeled node showed positive pressure heads as shown.

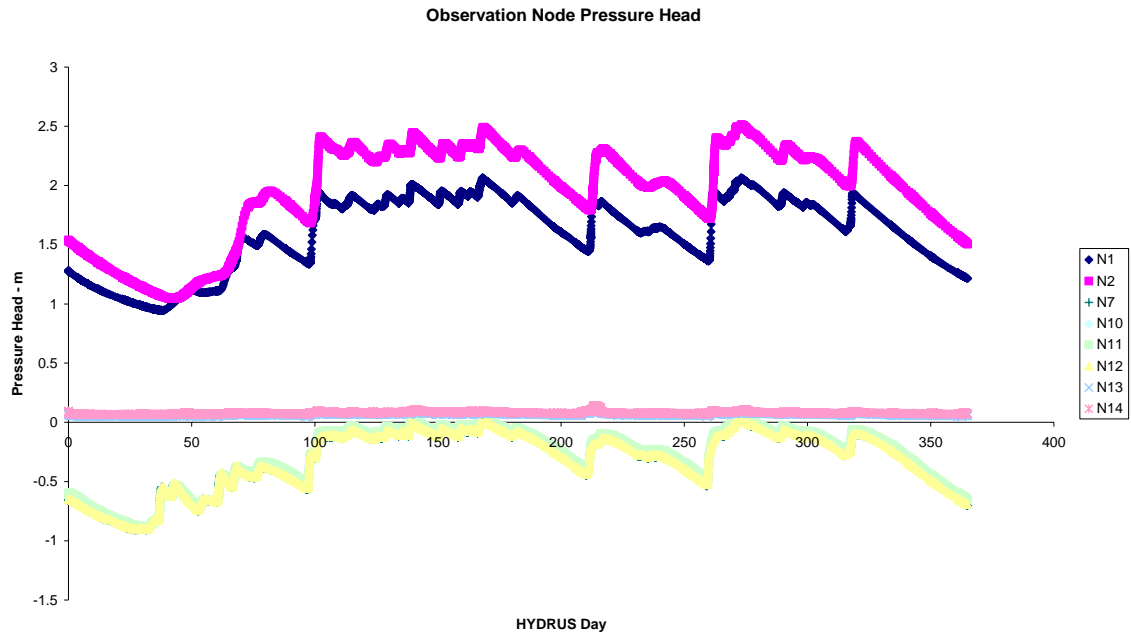


Figure 70. SRSNoFloArg_3_lineararg simulation nodes showing positive pressure heads.